Università degli Studi di Catania

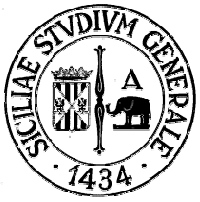

Dottorato di Ricerca in Scienze dei Materiali

XXV Ciclo

R. M. Gabriella Milazzo

ELECTROLESS SILVER DEPOSITION ON (100) AND (111) SILICON WAFERS, FABRICATION OF NANOWIRES AND NANOPILLARS BY ASSISTED ETCHING

Tutor: Prof. E. Rimini
Prof.ssa M.G. Grimaldi
Supervisor: Dr. G. D'Arrigo

Coordinatore: Prof. A. Licciardello

Tesi per il conseguimento del titolo

"In small proportions we just beauties see,
And in short measures life may perfect be"

Ben Jonson

CONTENT

INTRODUCTION

The nanoscience is the study of objects with sizes ranging from a few tenths to one hundreds of nanometers, and nanotechnology deals with the manipulation of nanomaterials to fabricate devices.

Low-dimensional nanomaterials are of particular interest because they exhibit anisotropic and dimension-tunable properties, both of which are important attributes in nanodevice application [1, 3]. Silicon is the mainstay of semiconductor industry and nanostructures such as quantum dots (SiQDs) [4], nanocrystals (SiNCs) [5], porous Si (por Si) [6], Si Nanopillars (SiNPs) [7] and Si nanowires (SiNWs) [8] exhibit interesting properties that are very different from their bulk counterparts [9]: a diameter-dependent bandgap, very high density electronic states, an increased surface-to-volume ratio, an enhanced exciton binding energy, enhanced thermoelectric properties and increased surface scattering for electrons and phonons.

SiNSs are very interesting for application in electronic and photonic devices [10], sensors [11], energy harvesting devices [12], and solar cells [13, 15].

For these reasons, the field of SiNWs synthesis represents an exciting and rapidly expanding research area.

The VLS (Vapor Liquid Solid) method [9], the main growth technique for SiNWs, was proposed by Wagner and Ellis in the mid 1960s and is the key mechanism for silicon wire growth. It relies on the dissolution of gaseous reactants into nanoscaled liquid droplets of metal, followed by nucleation and growth of single crystalline rods in one direction.

When Au, for example, is deposited on a silicon substrate, and this substrate is heated, small liquid Au-Si alloy droplets will form on the

substrate surface. When the substrate is exposed to a gaseous silicon precursor, the droplets become supersaturated with Si until silicon freezes out at the silicon droplet interface. The continuation of this process leads to the wire's growth.

So the globule at the wire tip must be involved in the growth by acting "as a preferred sink for the arriving Si atoms or, perhaps more likely, as a catalyst for the chemical processes involved" [16].

High temperature, hazardous silicon precursors, complex equipment and other rigorous conditions are often required. Moreover the usually adopted growth techniques yield disordered entanglements of nanowires, hampering subsequent experimental characterization and potential applications.

Hence the accurately controlled fabrication of ordered SiNW arrays with the desirable axial orientation using simpler and quicker ways is very desirable and of great importance.

Metal Assisted chemical Etching (MAcE) [17] has been exploited in the last decades as an alternative method for silicon manufacturing thanks to its desirable features. It allows the fabrication of various Si nanostructures with electrical properties directly inherited from the bulk silicon substrate. They are robust and they do not peel off from the substrate. The process could be accomplished in a chemical lab without expensive equipment. MAcE is essentially a wet etching method to produce anisotropic high aspect ratio semiconductor micro and nanostructures without incurring in lattice damage. It has been employed to fabricate Si, Si/Ge [18] and GaAs [19] nanostructures potentially useful in fields ranging from solar energy conversion, thermal power conversion, energy storage and chemical and biological sensing.

The process requires the deposition of a noble metal film on the silicon substrate (by Electroless Metal Deposition, evaporation, physical deposition, etc.). The metal, thanks to its catalytic activity, will locally assist the oxidation of Silicon in oxidative solutions. Hydrofluoridric Acid plays an important role in the whole reaction because it etches the oxidized silicon,

allowing the metal dipping and so the nanostructures' generation.
In spite of the simplicity of experimental apparatus and of the high quality of the obtained nanowires, a detailed theoretical description of MAcE is still missing.
Several factors affect the fabrication of SiNWs, e.g., the doping level and type, the substrate orientation, the temperature, the etchant composition.
In addition, the control of position and size of metal agglomerates is an important goal to achieve since the spatial distribution and the diameter of nanowires depend on them. Considerable efforts have been done to solve this question (Nanosphere Lithography, Anodic Aluminum Oxide Mask, Interference Lithography etc. have been employed as masking techniques for metal deposition).
In this thesis, the noble metal mesh has been achieved electrolessy, through immersion of silicon in a solution containing Ag^+ and Hydrofluoridric Acid. This method is very simple and inexpensive but in general doesn't allow an accurate metal positioning. In this work numerous efforts have been done to understand the mechanism responsible for Ag^+ nucleation and growth on Si.
In Chapter I, after an overview on the general aspects of MAcE, an investigation on the early stages of silver deposition is presented.
In Chapter II, the mechanism of electroless deposition is presented on both (100) and (111) oriented Si wafers.
By means of a substrate patterned with etching in alkaline solutions, it will be shown that when the two surfaces are contiguous, a self selective mechanism for deposition could be achieved.
It results form a complex combination of non homogeneous surface bond density, variations in the kind of Hydrogen-terminations and mass transport effects
As a result, deposition is enhanced on convex surfaces, where silver is in the form of large clusters and on (100) oriented areas and nearly inhibited on concave surfaces.
In Chapter III, the strong influence of metal morphology on the etching

direction is presented. It will be shown that when silver clusters are small and well separated, etching is not normal to the surface but it proceeds along the [001] directions for both orientations under investigation.
On the other side, large and interconnected particles sink always along the normal to the surface.
In addition, by scaling the pattern obtained with etching in alkaline solutions, an enhancement of the self selective behavior for metal cluster's nucleation and growth occurred. The non uniform silver particles' density and size in the micro regions gave rise, after etching, to the fabrication of an ordered array of Si Nanopillars, 600nm in size.

CHAPTER 1

PHENOMENOLOGY OF METAL ASSISTED ETCHING OF SILICON

The first demonstration of Metal Assisted chemical Etching (MAcE) of Si was reported in 1997. Porous Si was fabricated by etching a Si substrate Aluminum covered in a solution composed of HF, HNO_3 (Nitric Acid) and H_2O. It was discovered that the incubation time to etch silicon decreased thanks to the presence of the metal film on the surface [20].
The method was first investigated in some details by Li and Bohn [17]. A thin layer of noble metal (e.g., Au, Pt, Ag), sputtered on silicon surface, catalyzed the etching in a mixed solution containing HF, H_2O_2 (Hydrogen Peroxide) and EtOH (Ethanol) by enhancing the silicon oxidation reaction. HF was needed to remove the silicon oxide.
It is a simple and inexpensive technique for the fabrication of porous silicon and it has been also employed in the nano-structuring of other semiconductors: Germanium [18], GaAs [19, 20], GaN [21]and SiC [22]

The overall process consists mainly in two steps:

1. Deposition of a noble metal that could be achieved by various method, e.g. evaporation, plating, sputtering, etc.;
2. Etching in a solution containing an oxidative agent (usually H_2O_2) and HF.

The noble metal should assume a discrete distribution on the substrate, e. g. in the form of NPs (Nano Particles), or ordered pattern. It enhances the oxidation process, by the oxidative agent, of silicon underneath it. The oxidized silicon is then removed by HF. The substrate in contact with the metal is etched, generating holes whose conglomeration produces the nanostructures. Their shape and size are determined by the metal mesh features [23]. The process is depicted in fig. 1.1. Various metal configurations are reported: isolated or interconnected islands (a and c), metal films with holes (e and g) and metal pattern (i) together with the corresponding etched structures.

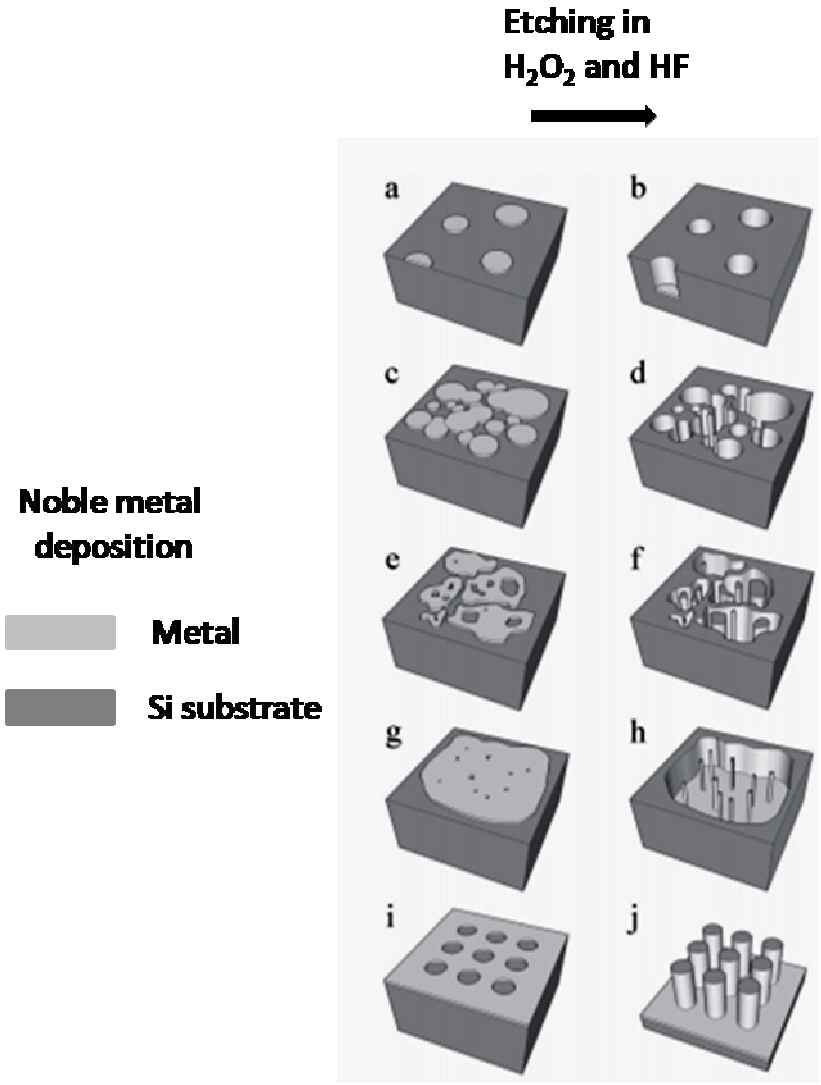

Fig.1. 1: A schematic representation of Metal Assisted chemical Etching of Si: (a-c-e-g) Si substrate partly covered with a metal film and (b-d-f-h) corresponding structures after etching of Si underneath. If the metal is an ordered pattern (i), ordered arrays of nanostructures are obtained (j).

The factors influencing MAcE of silicon are various: temperature, etching

solution, metal morphology. The substrate plays also an important role in both described steps. Its orientation and its starting surface morphology influence the metal deposition and so the subsequent etching directions.
In this chapter, I will give an overview on the general dynamics of the two aforementioned steps. A detailed description of dependences on the orientation and substrate morphology will be given in chapter 2 and 3 respectively.

1.1 Metal Deposition

1.1.1 General Concepts

Metal deposition could be realized in various ways, e.g., evaporation, sputtering, molecular beam epitaxy or, as in this work, via electrochemical processes.
The chemical deposition involves a reduction reaction with a charge transfer between the metal ion present in the solution and the substrate.
The metal deposition on silicon, in general, occurs with nucleation of metallic clusters, growth of them and coalescence, followed by thickening of the layer.
The substrate influences mainly the nucleation and coalescence steps.
The cluster formation by deposition of a metal onto a foreign substrate depends on the interaction energy between the adsorbed metal atom and the substrate and on the difference in interatomic spacing between the bulk metal phase and the crystalline substrate.
Three different modes of growth can be identified: layer by layer (Frank-van der Merwe growth), 2D layer deposition followed by the growth of 3D islands (Stranski-Krastanov growth) and 3D island formation (Volmer-Weber growth) [25-27]. The latter is the most frequent mode, due to the weak interaction energy between the adsorbed metal atom and the semiconductor.

1.1.2 Electroless Metal Deposition (EMD)

Electroless deposition is a simple method for the deposition of noble metals and it is usually utilized if there is no strict demand on the morphology of the resulting metal layer.

Electroless plating refers to the autocatalytic or chemical reduction of aqueous metal ions and subsequent plating onto a substrate. It is a widely used method to cover the surfaces with a variety of metals such as Cu, Ni, Au, Pt, etc [28].

Electroless Nichel offers unique properties including uniformity of the deposit in deep recesses, bores and blind holes. Electroless Copper deposition is generally applied to improve the lifetime and performance in a corrosive atmosphere and upon exposure to a harsh environment. Electroless gold is currently being used in the fabrication of semiconductors devices, tabs and chips.

The electroless deposition of metals on silicon from fluoride solutions has raised considerable interest, owing to its wide application in microelectronics. The working principle is the galvanic displacement reaction: the reduction of metal ions and the oxidation of Si atoms. Fluoride ions in solution help sustain the reaction by dissolving the silicon substrate as silicon hexafluoride, avoiding the formation of silicon oxide, thus exposing new silicon surface (fig. 1.2).

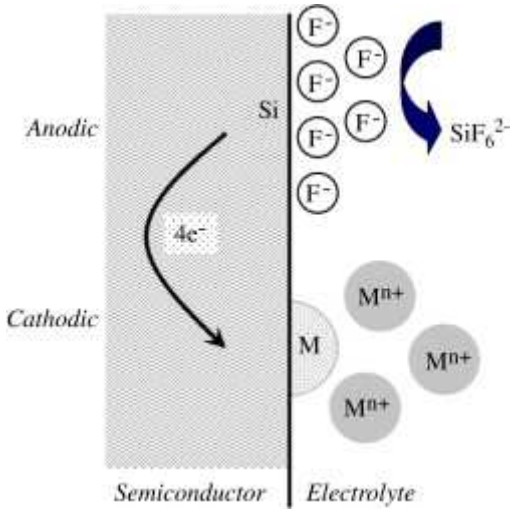

Fig.1. 2: Mechanism of Galvanic displacement of metals on silicon.

It is usually accepted that the metal ions coming in the proximity of the silicon surfaces, capture electrons from the valence band of silicon (holes injection) and deposit in the form of metallic nuclei [29].

The metal deposition in this work has been achieved electrolessly, by immersion of the silicon substrate in an aqueous solution containing 0.005M Silver Nitrate ($AgNO_3$) and 4.8M HF. The results of a detailed investigation on silver electroless deposition on silicon will be presented in the next paragraphs. Here I review the general concepts laying at the basis of the process.

1.1.3 Electroless Silver Deposition

Electroless silver deposition on a silicon surface from HF/$AgNO_3$ solution is based on the galvanic displacement reaction, in which two simultaneous processes occur at the silicon surface [30]:

(i) The cathodic reaction (reduction of Ag^+ ions) which produces metallic Ag deposits;

$$Ag^{+} + e_{VB}^{-} \rightarrow Ag^{0}(s)$$

Eq.1. 1

(ii) The anodic reaction (oxidation of silicon) during which the charges released by the oxidation of silicon atoms are transferred to the sites of silver deposition:

$$Si(s) + 2H_2O \rightarrow SiO_2 + 4H^{+} + 4e_{VB}^{-}$$
$$SiO_2 + 6HF \rightarrow H_2SiF_6 + 2H_2O$$

Eq.1. 2

As soon as Ag deposition begins, Ag^{+} ions in the vicinity of the silicon surface capture electrons from the valence band of Si, due to the relative positions of electrochemical potentials [31], (a schematic representation is reported in fig. 1.3) are deposited in the form of nanoscale metallic Ag nuclei.

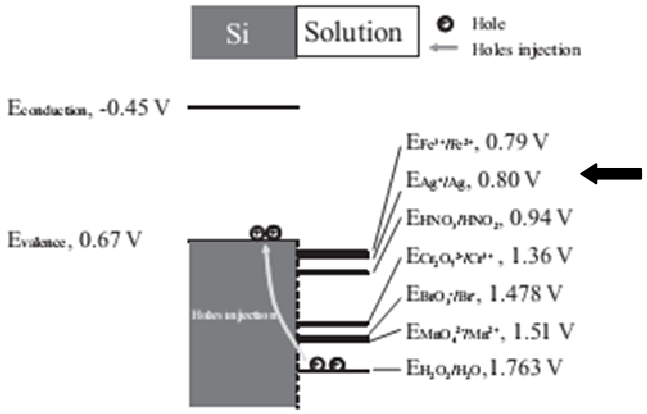

Fig.1. 3: Scheme of the potential relationship between bands in a Si substrate and standard potentials of various oxidants indicating that during silver electroless deposition holes are injected into the valence band.

The subsequent Ag^+ ions approaching the Si surface would be reduced preferentially on initial Ag nuclei sites rather than on bare silicon due to the relatively low-energy barrier for holes at the Ag/Si interface, i.e. the strong catalytic activity of silver for reaction [32].
The present deposition of Ag leads to the growth of silver nuclei by metal on metal deposition [33].
However the chemical reactions do not give us any information about nucleation and growth of Ag particles or Si dissolution [34]. The kinetic of wet catalytic deposition is hard to record and is thus still unclear to date, due to the difficulty of combining in situ HF-contained chemical etching of SiNWs and observation by a transmission electron microscope (TEM) or scanning electron microscope (SEM).
In addition, the charge transfer between Si and the noble metal would be heavily affected by the surface band bending of Si. Since the hole and the subsequent electron transfer for oxidation of Si occurs at the surface of the Si, the surface state of Si is of importance in exploring the etching mechanism [23]. Their influence is still under investigation [35-37].

1.1.4 Growth of Silver clusters on Silicon.

A large number of possible steps are involved in the electroless deposition of silver onto silicon. It has been speculated that, *after nucleation*, we have [38]:

(i) Diffusion of Ag^+ to the silver surface;
(ii) Discharge (after adsorption) of Ag^+ to give Silver on Silver;
(iii) F^- discharge and reaction at Si surface to give SiF_6^{-2};
(iv) Desorption of SiF_6^{2-};
(v) Diffusion of SiF_6^{2-} away from the surface.

Possible F^- diffusion limitation (i.e. removal of oxidized silicon) with the usual adopted etching solution is ignored, since HF concentration is higher

than the Ag^+ concentration (e.g in the present experiments [HF]/[$AgNO_3$] is about 10^3). It does however appear that the overall growth rate is diffusion controlled by silver species. This is based upon the observation that the silver deposition rate can be increased by a factor of about two by stirring the solution.

1.1.5 Investigation on Silver Nanoparticles (AgNPs) growth.

Silver deposition has been investigated in times ranging between 1s and 160s. The starting substrate was Si (100) (P doped ρ=3-5Ω·cm), it was cut in squares of 1cm in side and dipped in Diluited Hydrofluoridric Acid Solution (DHF, Hydrofluoridric Acid and Water 1:7). By this treatment, introduced to remove the native oxide, H-terminated surfaces were obtained. Deposition for times shorter than 5s was achieved by gradual immersion of sample in the deposition bath, as depicted in fig. 1.4

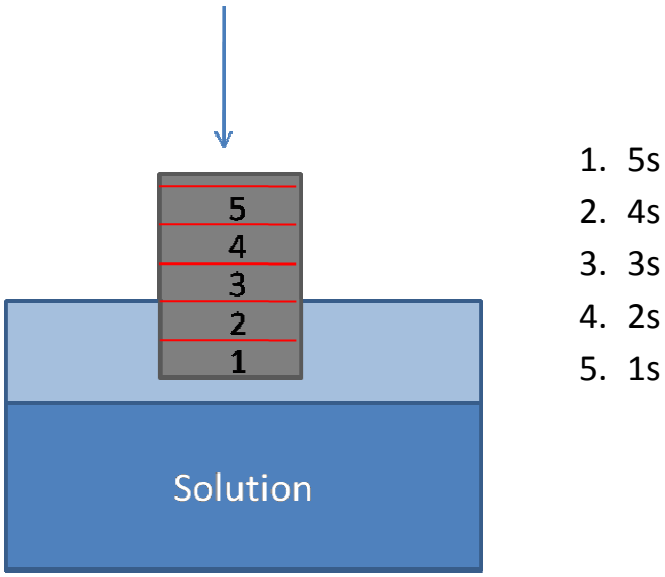

Fig.1. 4: Gradual immersion of sample in the plating solution.

The volume of plating solution was chosen to ensure a large reservoir for

Ag^+ ions (the adopted 50ml solution contains 1.5 x 10^{20}ions that could grow a continuous layer about few µm thick on squares samples of 1cm in side).
The as-deposited samples were analyzed with various techniques, in order to obtain a detailed description of silver evolution with time.

- *SEM (Scanning Electron Microscopy)*

These analyses allowed a direct evaluation of coverage and size distribution of the silver clusters. The magnification was chosen high enough to allow a clear observation of silver nanoparticles and the empty areas surrounding them.

- *Rutherford Backscattering Spectroscopy*

The samples were analyzed with RBS (Rutherford Backscattering Spectroscopy) of 2.0MeV He^+ ions to determine the amount of deposited Ag atoms (in terms of Ag atoms/cm^2) with time.

Some samples were also analyzed with cross section TEM (Transmission Electron Microscopy), to evaluate the height of silver clusters
The SEM micrographs of samples are reported in fig.1. 5. They show that just after 1s the formation of Ag islands has been accomplished. The early stages of deposition are characterized by fast nucleation and growth.
The corresponding RBS spectra are reported in fig. 1.6.

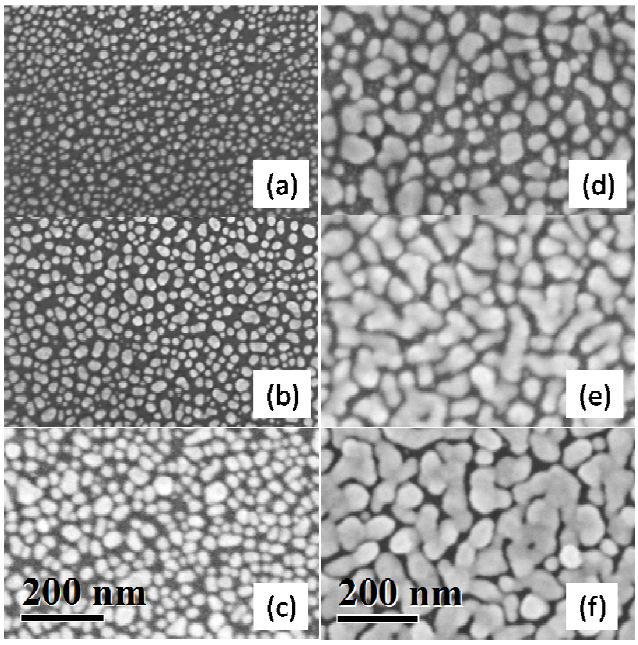

Fig.1. 5: SEM micrographs of samples immersed for (a) 1s; (b) 3s; (c) 5s; (d) 40s; (e) 120s and (f) 160s.

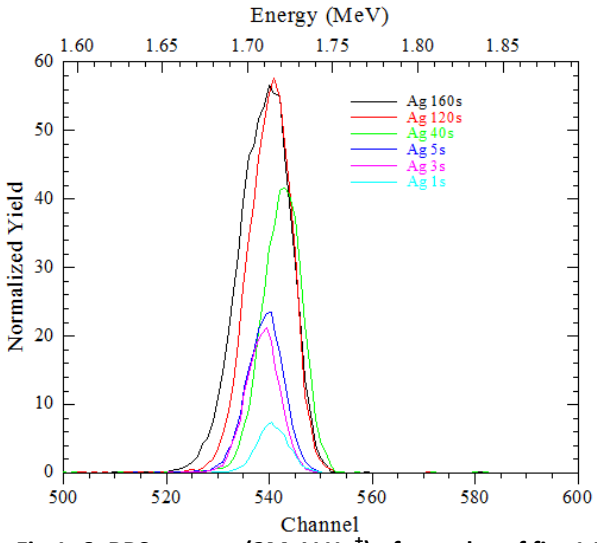

Fig.1. 6: RBS spectra (2MeV He^{+}) of samples of fig. 1.5.

In fig. 1.7 the evolution of surface atomic density, as calculated from RBS spectra, is reported.

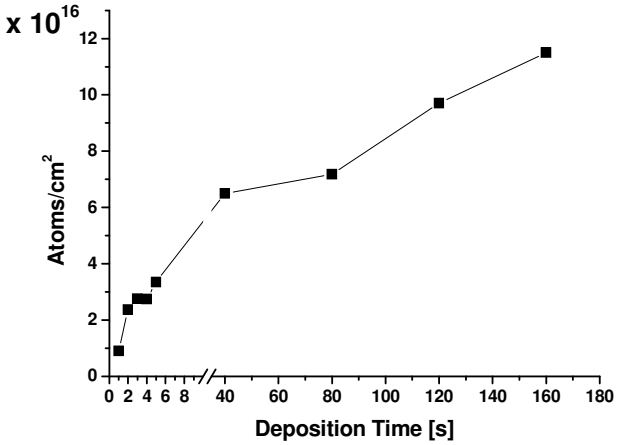

Fig.1. 7: Atomic surface density calculated from RBS spectra (2.0MeV He^+ ions).

Deposition is characterized by a fast initial step. The RBS spectra show that in the first two second the highest deposition rate is detected: from 0 to 2s it is about 10^{16} [atoms/(cm^2s)]. From 2s to 5s the deposition rate become one third of the previous value, about $3x10^{15}$ [atoms/(cm^2s)]. Then it continues to decrease and from 40s to 160s the variation is one order magnitude lower ($4x10^{14}$ [atoms/(cm^2s)]. So the deposition rate continuously slows down.
The corresponding nuclei density is reported in fig. 1.8.

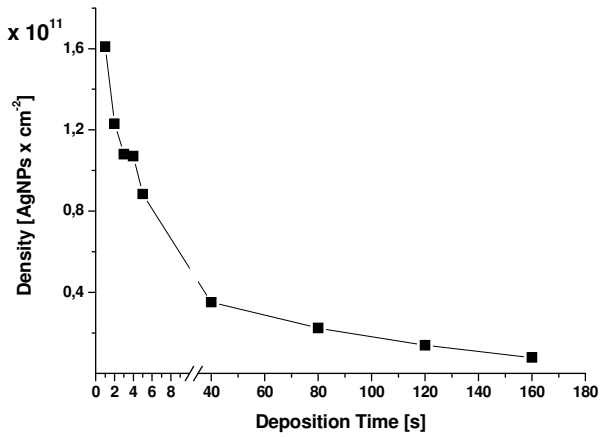

Fig.1. 8: Density of AgNPs as calculated for SEM micrographs elaboration.

During the first seconds (from 1s to 5s) it decreases of a factor 2, going from 1.6 x 10^{11} [nuclei/cm^{-2}] to 0.8 x 10^{11} [nuclei/cm^{-2}]. The higher value is found on sample deposited for 1s, probably after this time, the nucleation step has been already accomplished and coalescences take place. The analysis of the silver nuclei density with time indicated that the aggregation rate slows down too. From 1s to 5s, agglomeration of 3 clusters in 1 occurs (0.4 clusters/s are lost). From 5s to 40s a lower aggregation value (about 0.05 clusters/s) is calculated. For longer times, i.e. from 40s to 160, it further decreases. From the elaboration of SEM micrographs the variation of the clusters mean size with deposition time has been calculated, as reported in fig. 1.9.

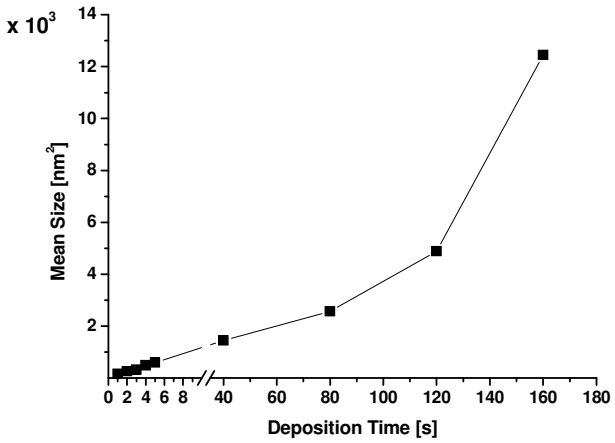

Fig.1. 9: Particle mean size vs deposition time

In fig. 1.10 the radius distributions for 1s and 2s deposited samples is reported.

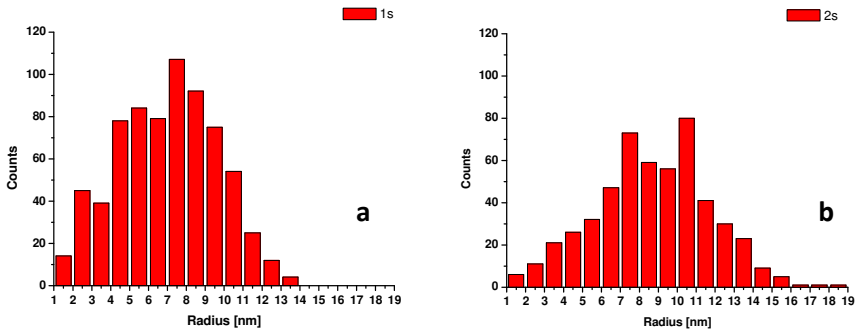

Fig.1. 10 Radius distribution for (a) 1s and (b) 2s immersion time.

The cluster thickness is reported in fig. 1.11. The trend indicates that in the first seconds a quick deposition occurs and the clusters grow both in thickness and in extension. Then when the deposition slows down, particles coalesce and their height grows slowly.

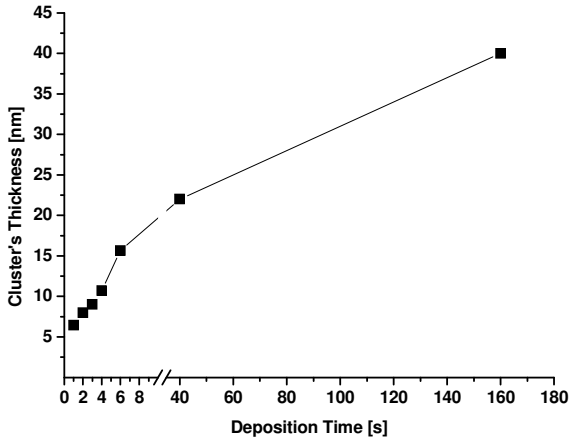

Fig.1. 11: Fig. 1.9 Evolution of mean thickness for particles with deposition time

The cross sections TEM of fig.1.12 indeed show the occurrence of grain boundaries in the long particles obtained after 160s deposition time (fig. 1.12 b), while those after 40s (fig. 1.12 a) have aspect ratio≅1 (i.e. are nearly round).

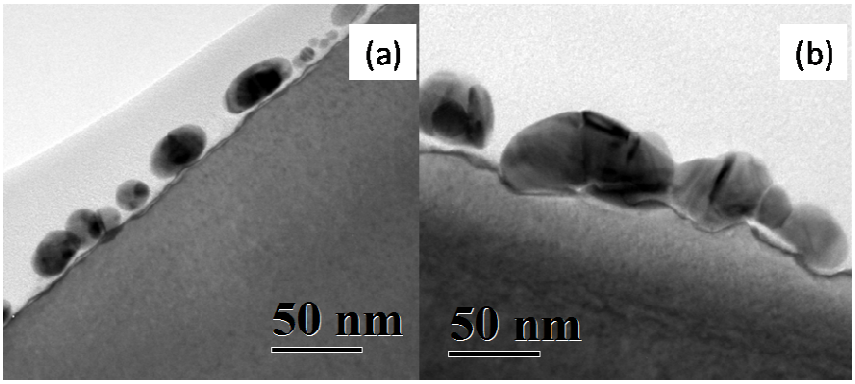

Fig.1. 12: Cross section TEM as samples deposited for (a) 40s and (b) 160s. In (b) many grain boundaries are detectable

As a result the covered area increases. (fig. 1.13)

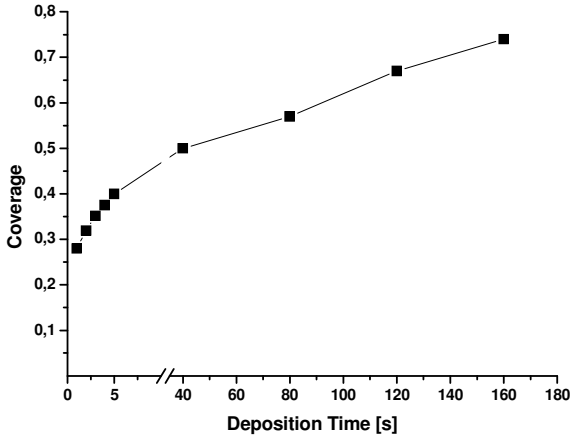

Fig.1. 13: Covered Area by AgNPs vs deposition time.

A detailed characterization about AgNPs generation and evolution was conducted by [39] on H-terminated (111) p-type Silicon.
The OCPt (Open Circuit Potential vs time) of deposition was acquired and the measured curve is reported in fig. 1.14.

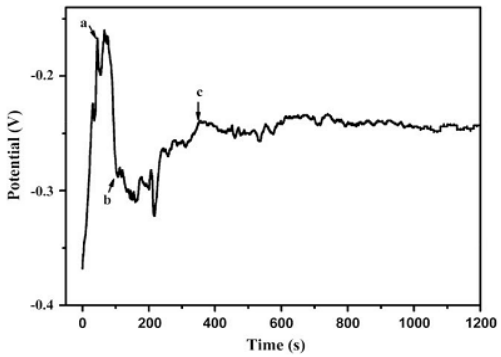

Fig.1. 14: Ocp-t curve by [39]. The electrolyte was 150mL of 1.0 M HF, 0.1 M $AgNO_3$ solution.

Therefore, at the early reaction time, the silver deposition is under the kinetic growth process and the amount of silver deposits increased. In between the points denoted b and c, the slowly increased. E_{OCP} with small fluctuations implies that a thermodynamic quasi-equilibrium or equilibrium condition might control the reaction. From c then, the unchanged E_{OCP} suggests that the reaction almost ceased. The time location of the aforementioned points depends on the experimental conditions (the volume and the Ag^+ concentration of plating solution much higher than those adopted for our experiments) but a clear trend could be identified. With prolonged deposition times (30min) dendritic structures have been observed, as reported in fig. 1.15.

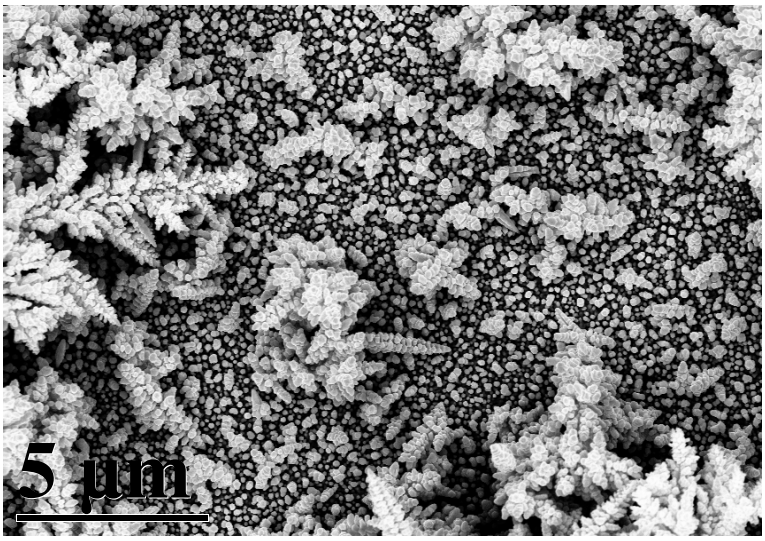

Fig.1. 15: Dendritic silver clusters achieved after 30min deposition.

Formation of silver dendrites should be considered within the framework of a diffusion limited aggregation model that involves cluster formation by adhesion of a particle via a random path to a selected seed and particle diffusion to stick to the growing structure. In the initial stage, high concentrations of silver salt lead to a reduction-nucleation-growth of silver nanoclusters on multiple locations to form a chain like network. As the

reaction continues, the salt concentration decreases and the growth is mainly driven by the reduced surface energy resulting in the formation of dendritic structures [40].

1.2 Silver Assisted chemical Etching

After the electroless deposition step, Metal Assisted chemical Etching is achieved by immersion of the as-deposited substrate in a solution containing H_2O_2 and HF. The involved reaction and the factors influencing it are reported in this section.

1.2.1 The system Ag-Si-H_2O_2-HF.

The silver assisted chemical etching proceeds according to the reactions (eq.1.3a-d). The reduction of H_2O_2 (eq.1.3a) occurs on the silver surface. Silicon is oxidized (eq.1.3b), due to injected holes and then etched by HF into H_2SiF_6 and SiF_4 (eq.1.3c-d) [41-43].

a. $H_2O_2 + 2H^+ + 2e^- \rightarrow 2H_2O$

b. $Si + 2H_2O + 4h^+ \rightarrow SiO_2 + 4H^+$

c. $SiO_2 + 6HF \rightarrow H_2SiF_6 + 2H_2O$

d. $SiO_2 + 4HF \rightarrow SiF_4(g) + 2H_2O$

Eq.1. 3

In order to dissolve Si, it is necessary that two conditions must be fulfilled:

(i) Electronics holes are available in the proximity of the etched region
(ii) A direct contact with the HF electrolyte exists.

Two half cell reactions that include cathode and anode reactions would be greatly enhanced at different sites on the metal particle surface. The side of Ag particle facing the etching solution would act as a cathode, which would catalyze H_2O_2 reduction, consuming H^+ and electrons in the process, while the other side of Ag particle facing the Si would function as the catalyst for Si oxidation, which would generate H^+ and electrons. A schematic representation is given in fig. 1.16 [44].

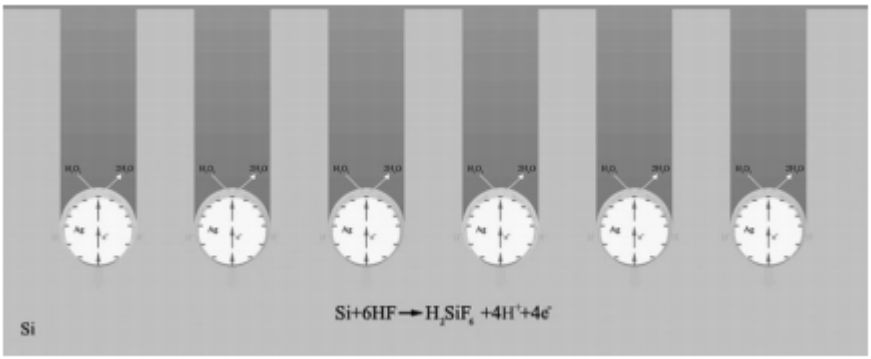

Fig.1. 16: A schematic representation of silver assisted etching a silicon through the reduction of H_2O_2 on the Ag particle facing the etching solution and removal of oxidized silicon. The process results in etching of nanopits in silicon.

So the catalythic Ag particles would act as a redox center: electrons are transferred from silicon to silver nanoparticles to reduce H_2O_2 on the surface of metal particles facing to the electrolyte. Meanwhile, the metal particles, thanks to HF action on silicon, etch nanopits down into the wafer. Such an electron cycle results in the formation of silicon nanowires arrays.

The electrochemical potential of H_2O_2 is much more positive than the valence band of Si, from the energy point of view; H_2O_2 can inject holes into the valence band of Si. Thus, a Si substrate subjected to HF/H_2O_2 solution should be etched [23].

The presence of a noble metal is necessary for fast etching of the Si substrate in solution with certain oxidants. Indeed, without any catalytic enhancement, the corresponding etch rate is below 10nm/h, thus very low

[45]. It increases substantially, when a metal particle or film is introduced into the system. In this case the oxidizing agent is reduced at the top side (not being in direct contact with the substrate) of the metal, and the resulting holes are injected into the Si beneath the metal particle. If the catalyst is present as an isolated particle, the electrolyte can easily penetrate the etching front under the metal.
In the case of extended metal film it is reasonable to expect that etching should have a different dynamics and particularly the diffusion of the byproducts will occur in a different way.

1.3 Mass transfer

Since the Si atoms are oxidized and dissolved at the interface between the noble metal and the Si substrate, the reagent and byproduct diffuse along the interface. This assumption is plausible for the specific case in which the etching is assisted by noble metal particles with small lateral size. The diffusion of the reagent and byproduct along the interface between the noble metal and the Si involves only a short distance and may be easily accomplished (fig.1.17 Model I). There is another model proposed in the literature.
That is, the Si atoms that are in contact with a noble metal are dissolved in the noble metal and then diffuse through the noble metal to the noble metal/solution interface where the silicon atoms are oxidized and etched away (fig. 1.17 Model II).
If the Si is covered with a noble metal with a relatively large lateral size (e.g., larger than 1 μm), lateral diffusion of the reactant and the byproduct along the interface of Si and the noble metal (Model I) is a long distance diffusion process, while diffusion of Si atoms through the metal involves a relatively short distance (Model II) (typically a few tens of nanometers).

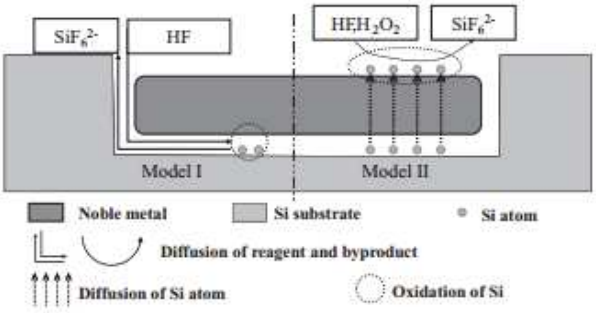

Fig.1. 17: Scheme of two possible diffusion models during metal assisted chemical etching. Model I: the reagent and byproduct diffuse along the interface between the noble metal and the wall of the etched structure. Model II: A Si atom is dissolved into noble metal and diffuses through noble metal and is the oxidized on the surface of the noble metal.

Recently together with model II, a new scenario is depicted for diffusion of by-product. It is reported in fig. 1.18.

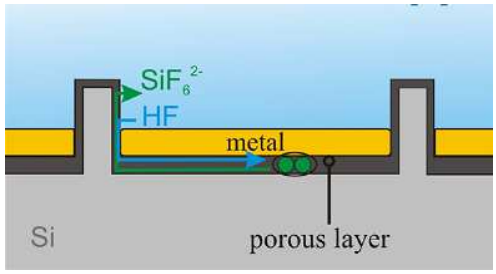

Fig.1. 18: Diffusion of reactants and byproduct during metal assisted etching [geyer]. through thin permeable channel formed at the Si/metal interface.

The oxidation of the Si surface proceeds at the interface of the metal and the Si substrate by forming a porous silicon layer that facilitates the diffusion of the reactants and the byproducts. Evidence was given by Geyer et al. [46]

Lee et al. observed that the etching rate of pores induced by an aggregation composed of a large number of Au particles was apparently larger than that induced by a single Au particle or an aggregation composed of two Au

particles. The faster etching rate was attributed to the larger cross-section of the pores, which enabled the efficient diffusion of HF, H_2O_2, and SiF_6^{-2} into or out of the etching front [47]. An efficient diffusion of agents and byproduct can also be achieved by stirring the etching solution.

1.4 Factors influencing MAcE

As explained in the previous paragraphs MAcE is influenced by various factors. Up to now a lot of efforts have been done to understand the process. The influence of temperature and illumination has been elucidated, that of the starting conditions of substrate (doping level and type, morphology, orientation) are still under debate and the reported data are also conflicting.

1.4.1 Temperature

Cheng et al. [48] systematically studied the relationship between the etching time and the lengths of Si nanowires etched at different temperatures (from 0C to 50C). A linear relationship between length of nanowire and etching time at all temperatures was confirmed. The etch rate was about 5µm/h at 0C, with increasing temperature up to 20C it grows to 20µm/h. At 50C an etch speed of 50µm/h was found. The results are reported in fig. 1.19

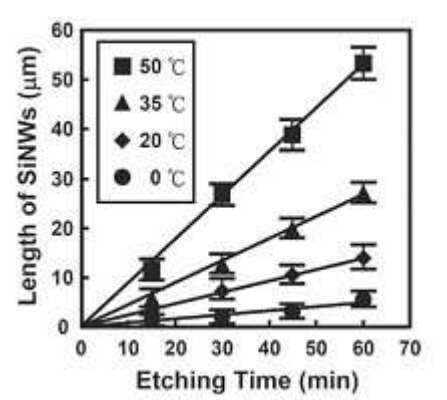

Fig.1. 19: Relationship between the length of SiNWs vs time and temperature [ref]

Temperature influences the etching process also indirectly. An effect of the employed solutions is that the process substantially lead to a heating of the etching solutions from initially room temperature to strongly elevated temperature of 70°C and above (depending on the used volumes of the solution). As reported in ref [49], depending on the etching solution, in the first 10min the temperature could be high (about 70°C); after 15min of reaction time it slowly decreases reaching room temperature after 1h. One of the possible explanations of this energy release during the etching procedure is the catalytic decomposition of H_2O_2 on Ag nanoparticles. So the etching process in acid atmosphere is a strongly exothermic process. It has been found that this thermal fluctuations are responsible for the observed change in the etching direction of (111)Si from the normal to the substrate, to the [001], but the crystallographic influence during MAcE will be discussed in detail in Chapter 2.

1.4.2 Illumination.

The influence of light during metal assisted etching has been investigated in the literature and, for the same etching times, the difference between

etching depths in the dark and under room light illumination was less than 5% for both p and n type substrates [23].
Illumination is not required for metal-assisted chemical etching of an n-type Si substrate. Indeed, the electrochemical potential of the oxidant (H_2O_2) is much more positive than the valence band of Si. Due to the catalytic activity of the noble metal, reduction of H_2O_2 is fast and copious and so, if the intensity of illumination is low (e.g., room light illumination), the number of photoexcited holes is much smaller than the number of holes injected from the reduction of H_2O_2 and no obvious difference in etching rate is observed. If the intensity of illumination is sufficiently high so that the concentration of photoexcited holes is comparable with or higher than the concentration of holes injected from H_2O_2, faster etching occurs (1.5 times higher about).

1.4.3 Doping type and level.

Several groups have reported on the effect of Si doping types and levels on the MAcE rate and the resulting silicon morphology. For highly doped Si wafers, etching conditions used for p and n Si wafers do not readily produce high aspect ratio solid nanowires arrays.
Qu et al. has reported a systematic study of MAcE on highly doped n-type Si wafer using Ag nanoparticles. By systematically tuning the H_2O_2 concentration in the etching solution, solid nonporous (low [H_2O_2]) and porous [higher [H_2O_2]) nanowires were obtained [50].
Cruz et al [51] attributed the formation of the porous structure in degenerately doped silicon to the diffusion of excess holes from the Si/Metal interface to the off-metal areas. The doping level do not produce any variation in the etch rate of SiNWs. This is clearly reported in fig. 1.20 where the SiNWs have been obtained with deposition for 160s in 0.005M $AgNO_3$, 4.8M HF and etching in 0.1M H_2O_2 and 4.8M HF (solid nanowires) for 30min. The images are referred to a n^{++} (100)Si (a) and to n^- (100)Si (b). The nanowires length is 10μm in both cases.

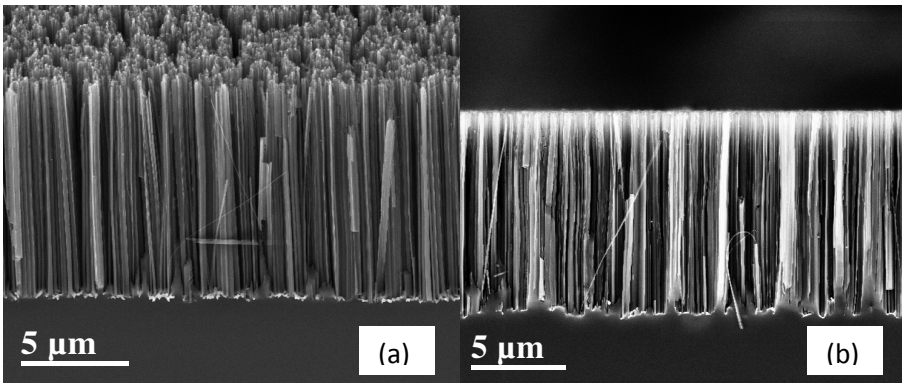

Fig.1. 20 SiNWs obtained from (a) n^{++} (100)Si and (b) n^{-} (100)Si. The wires' length is unchanged.

The potential applications of this etching technique are numerous but there is still a lack in the comprehension of the process, because of the impossibility to perform direct in situ measurements or observation. In addition the electrochemistry of the system is very complex and still under debate. Up to now there are only phenomenological models to explain the obtained data in the literature. As mentioned before, the role of the doping type and level is still under investigation. On the other side, the influence of temperature and illumination has been elucidated from an experimental point of view. The theory of Metal Assisted chemical Etching of Silicon still misses a detailed argumentation. However nanostructuring of silicon with this method is very useful and some masking techniques have been adopted to produce ordered arrays of nanowires.

1.5 Metal Patterning for MAcE applications.

Controlled fabrication of Si and Si-based nanostructure is essential for their application. MAcE allows fabrication of Si nanowires or pores with a controlled doping level, a partially controlled orientation and with a high aspect ratio. The control of position and size of metal agglomerates is an important goal to achieve since the spatial distribution and the diameter of

nanowires depend on them. Considerable efforts have been done to solve this question.

Patterned metal deposition is typically carried out with different methods, e.g., photolithography or Block Copolymer Lithography (BCP) combined with evaporation, electrodeposition or molecular beam epitaxy (MBE). Table1. 1 compares the advantages and disadvantages of the MAcE characteristic when a solid metal thin film mesh or a solution based metal is employed. The latter is simple and less expensive but there is a little control on the positioning of metal on silicon surface and also on its in plane extension. As a consequence the size and shape of the produced nanostructures are not uniform because they are strictly related to the metal clusters distribution. For example, $AgNO_3$ solution based MAcE of Si generates Si nanowires with diameters in the range of 20-300nm.

	Evaporated or sputtered metal catalyst	Solution based metal catalyst
Pattern size	Micro and nanoscale	Nanoscale only
Pattern size distribution	Uniform, determined by lithography	Random, large distribution
Pattern site control	Complete control	Not feasible
Patterned structure	Versatile	Interconnected network
Etching rate	Fast	Slow
Scalability	Good	Good
Cost	Relatively high	Low

Table 1. 1: A comparison between solid metal thin film pattern vs. solution based metal deposition. Usually EMD is employed when there is not a requirement of strict control over the produced feature size and shape.

In the following paragraphs an overview on the techniques employed up to now to pattern metal on silicon substrate for subsequent MAcE will be given.

1.5.1 Nanospheres lithography

Nanosphere lithography (NSL) is a powerful fabrication technique to

inexpensively produce nanoparticle arrays with controlled shape, size, and interparticle spacing. It makes use of nanospheres placed in a tightly packed array on a substrate, in order to create a mask for thin film deposition or etching. By removing the spheres, the remaining 2-D array on the substrate has triangular shaped nanostructures in a hexagonal pattern, often called a Fischer pattern [52].

In the experiments of Huang et al. [53] a self assembled monolayer of polystyrene sphere (PS) array was produced on silicon (see fig. 1.21). Their size reduction was achieved by a RIE (Reactive Ion Etching) process. Subsequently, a noble metal (silver) film was deposited by thermal evaporation through the PS mask. The process resulted, after removal of PS, in a continuous layer of noble metal with an ordered array of pores, whose diameter was strictly related to that of the RIE etched spheres (according to the recently developed techniques, it could range from 200nm to several micrometers). The patterned substrate was then etched in the etching solution containing HF and H_2O_2 and an ordered array of silicon nanowires was obtained.

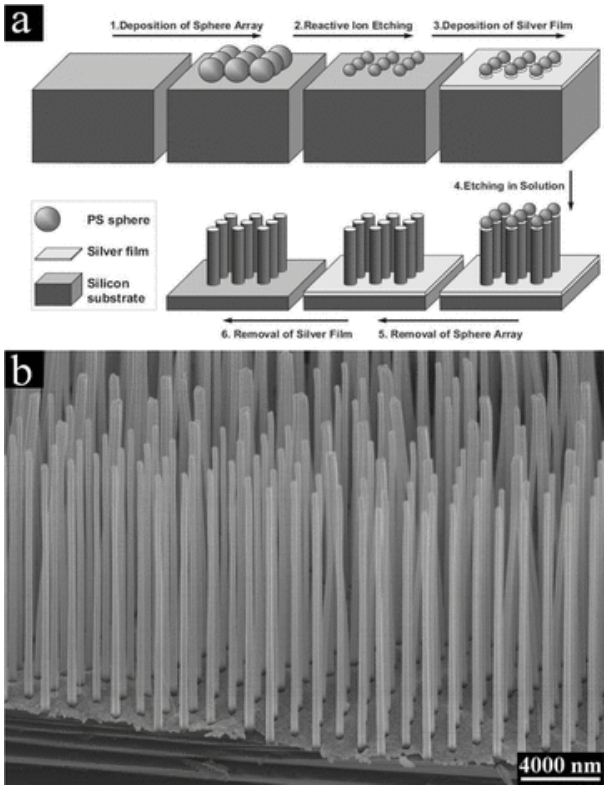

Fig.1. 21: (a) Scheme showing the processes in a method combining nanosphere lithography and metal-assisted chemical etching [50]: after the deposition of a nanospheres array and the diameter reduction, through a dry etching process, a noble metal film is sputtered on the substrate. The subsequent metal assisted etching generated an ordered array of silicon nanowires. (b) SEM image of Si nanowire arrays fabricated by the method combining nanosphere lithography and metal-assisted chemical etching.

In practice, it is difficult to assemble polymer spheres with diameters less than 200nm into a highly ordered monolayer array. In order to achieve Si nanowires with diameters less than 20nm, the mask must be obtained by reducing the diameter of spheres of much larger diameter. This process usually leads to an irregular shape of the remaining polymer and it is therefore not appropriate for the fabrication of Si Nanowires with well defined circular cross section. In addition, a limitation in the obtainable

metal pattern size is expected: it is difficult to successfully pattern a noble metal film with arrays of discrete holes if the typical thickness of the noble metal film is comparable to the height of the size reduced polymer mask. The nanosphere lithography method is usually limited to Si nanowires with diameter larger than 50nm.

1.5.2 AAO Mask Method

This method was proposed to overcome the limitations induced by nanosphere lithography. The masking material is the Anodic Aluminum Oxide (AAO) and is fabricated by anodization of aluminum. The process results in a thin Al_2O_3 foil containing pores of diameter from 10 to 350nm with a density ranging from $5x10^8$ pores per cm^2 to $3x10^{10}$ pores per cm^2 [54]. The pore size and pore density of the ultrathin AAO membranes (i.e., interpore distance) could be changed by varying the electrochemical parameters (e.g., voltage and electrolyte) of the anodization reaction of aluminum.
In the technique employed by Huang et al. [55], an ultrathin AAO membrane (thickness ≈300 nm, pore diameter ≈20 nm) was placed on a Si substrate via a solution-based transfer process. RIE was then performed to transfer the AAO membrane pattern to the wafer. In fig.1.22 the Si substrate after this step, with the etched pits, is reported.]

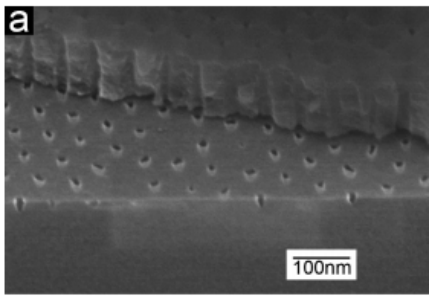

Fig.1. 22: Etched pits on silicon substrate from the experiments of [ref] after transfer of the AAO mask with RIE. The AAO mask is partially removed to show the pattern transfer.

The features of the AAO membrane were transferred onto the underlying Si substrate with a high degree of fidelity. After its removal, a thin layer of noble metal was deposited onto the patterned Si. It was characterized by a continuous film with holes corresponding to those on the substrate).
The side walls of the pores stayed uncovered while silver, at the bottom of each hole, exists as a discrete particle disconnected from the silver film on the surface of the silicon substrate.
By etching the metal-covered Si substrate in an etchant containing HF and H_2O_2, the substrate was transformed into Si nanowires (see fig. 1.23).

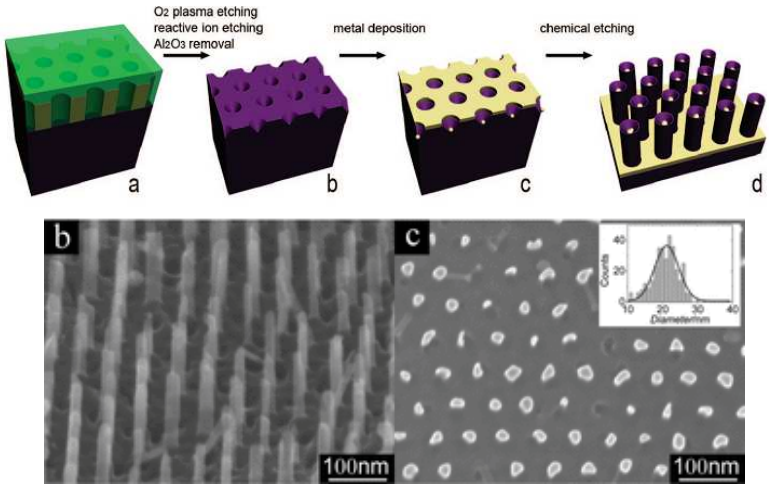

Fig.1. 23: Scheme showing the fabrication process of a method combining an AAO mask and metal-assisted chemical etching. (a-b-c-d) AAO membrane on silicon, dry etching for mask transfer, metal deposition and chemical etching. b) SEM of the obtained array of SiNWs and c) plan-view SEM images of vertical nanowires. Inset in (c) shows the regular diameter distribution of theSi nanowires.

Experimentally the etching rates are different for the metal mesh and the isolated metal particles that after etching are usually located in a thin porous layer at the top of each wire. It cannot be excluded some are lost from the top of the Si nanowire by non-vertical etching.

1.5.3 Interference Lithography Method

Another approach is that based on Interference Lithography (IL), developed by Choi et al.[57] The Si substrate is spin coated with a thick (about 400 nm) layer of photoresist. An IL system (a Lloyd's mirror type interference lithography setup with a 325 nm wavelength laser source) is employed for the exposure. After developing, oxygen plasma etching is employed to reduce the size of the remaining photoresist and to remove the residual unexposed photoresist. The substrate was then subjected to a metal (Au) deposition and to the assisted chemical etching, resulting in a perfectly ordered Si nanowires array (see fig. 1.24) with diameters of about 150nm. Recently the size of the obtained structures has been reduced to 60nm.

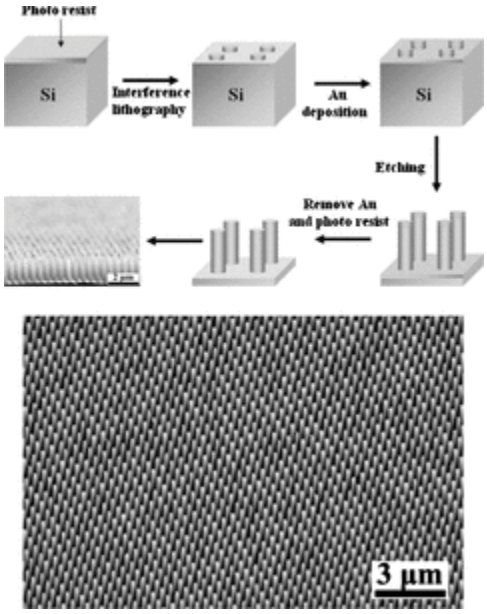

Fig.1. 24: Scheme showing the processes involved in a method combining interference lithography and metal-assisted chemical etching. The exposed photoresist is a mask for metal deposition. The corresponding SEM image of the well ordered resulting Si nanowires structure.

1.5.4 Block-Copolymer Mask Method

Chang et al. used block-copolymers as a mask to fabricate a metal mesh, creating high aspect ratio Si nanowires with diameters less than 20 nm. [58]. A thin layer of SiO_2 was evaporated on a Si substrate (see fig. 1.22). A diblock copolymer (polystyrene-block-ployferrocenyldimethylsilane PS-*b*-PFS), was then spin coated on the SiO_2/Si. Vacuum annealing was performed to achieve the micro-phase separation. The PS matrix was removed by oxygen plasma, leaving behind PFS as dot arrays on the SiO_2/Si substrate. The SiO_2 film was etched into pillars by RIE with the PFS dots acting as a mask.

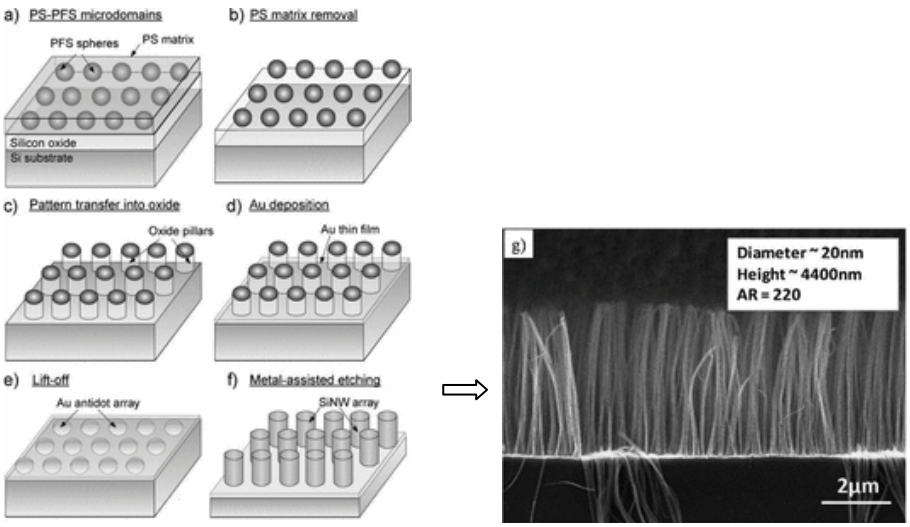

Fig. 1.22 Scheme showing the processes involved in a method combining block-copolymer mask and metal-assisted chemical etching.(a) PS-PFS micromembrane and microphases separation, (b) PS matrix removal and (c) mask transfer to SiO_2. (d) Metal deposition took place on the uncovered region. (e) After liftoff an ordered metal mesh was obtained with the subsequent etching (f) nanowires were obtained. (g) SEM image of Si nanowire array fabricated by a method combining a block-copolymer mask and metal-assisted chemical etching

Gold was deposited onto the entire substrate, using SiO_2 pillar arrays as a

mask. They were removed in diluted HF solution, leaving behind a mesh on the Si substrate. The diameter of the pores had a good fidelity to the diameter of the PFS dots. Finally, ordered arrays of Si nanowires were obtained by etching the Si substrate with the Au mesh in an etchant containing HF and H_2O_2. By this approach, diameters of the Si nanowire as small as 19 nm could be realized. The spacing between the nanowires was 10 nm.

As shown the advantages of this fabrication technique are numerous, indeed:

- A good control of etch rates has been achieved;
- The experimental requirements are very simple, safe and low cost;
- It is possible to machine large area substrates;
- it is possible to achieve long vertical etch depth starting from narrow overtures, overcoming the limits of dry etching techniques-

Two drawbacks limit the large diffusion of this fabrication technique: a control of axial orientation of the etched nanostructures and an accurate and simple metal positioning on silicon surfaces.

CHAPTER 2

ELECTROLESS SILVER DEPOSITION ON (100) AND (111) SILICON SUBSTRATES

In this chapter the Electroless Metal Deposition of Ag will be investigated on both (100) and (111) oriented Silicon substrates.
Wafers were processed in two distinct configurations:

a. Simple (100) and (111)Si wafers as starting substrates,
b. Macro-patterned with anisotropic etching in alkaline solution sample, that allows the simultaneous exposure of (111) and (100) contiguous surfaces to the deposition solution.

Silver atoms preferably deposit on surface discontinuities so the electroless metal nuclei density should depend on the surface unsaturated bond density of the exposed areas [59]. This factor varies with crystallographic orientation and with the morphology of the substrates.
It has been shown (chapter 1) that the deposition rate is very fast during the first few seconds and then it levels at a lower value of at least one order magnitude for the (100) oriented wafer. The same trend as it will be reported occurs also for the (111) oriented wafer and the amount of deposited silver is weakly dependent on orientation.
When deposition was performed in configuration b), an inhomogeneous silver distribution was obtained: the metal ions agglomerate preferentially on the convex interplanar transition region between the two exposed

surfaces, rich of kinks and nano-terraces. The metallic cluster density and size decrease with the distance from it. In addition, deposition resulted orientation dependent, being higher on the (100) surface.

2.1 Influence of substrate morphology.

According to the data reported in the literature, surface morphology has a strong influence during electroless metal deposition. Structural modified regions can catalyze metal ions deposition and clustering leading to a self selective mechanism on large area substrates.

It has been demonstrated that metal deposition occurs preferentially on defects sites (patterned by Focused Ion Beam or induced by scratching the Si surface with the tip of an Atomic Force Microscope). In the experiments of Homma et al. nanoscopic patterns were generated on H-terminated (100)Si wafers by nano-indentation technique, using a scanning probe microscope (SPM) with a diamond probe [60].

By controlling the parameters such as the indentation force, nanoscopic patterns with different degrees of defects were obtained. The scanning surface potential microscopy (SPoM) analysis showed that these sites locally possessed negative shift in potential, i.e., higher activity for the reductive deposition of metal ions, which increased with an increase in the degree of defectiveness.

In the work of Chen [61] et al. silicon (100) surfaces have been locally modified by Ar^{+} ion implantation (beam energy 6keV with an incidence angle of 13°, for 10h) and then immersed in an HF based solution contaminated with Cu^{++} concentration of 100ppb. The SEM investigations are reported in fig.2.1. The white droplets are Cu nanoparticles that preferably deposited in the damaged region. A sharp boundary separates the two regions: the damaged (covered with Cu) from the undamaged one.

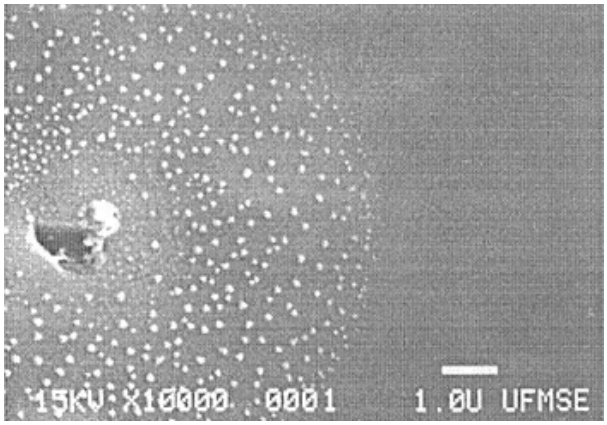

Fig.2. 1 From Chen et al. [61] the damaged ring where it copper deposited according to a self selective mechanism.

Choi et al. [62] demonstrated that self selective electroless plating could be achieved on silicon by simply scratching the surface with an AFM tip, as reported in fig. 2.2. The copper deposition was strongly enhanced in the defective regions and increased with increasing immersion time.

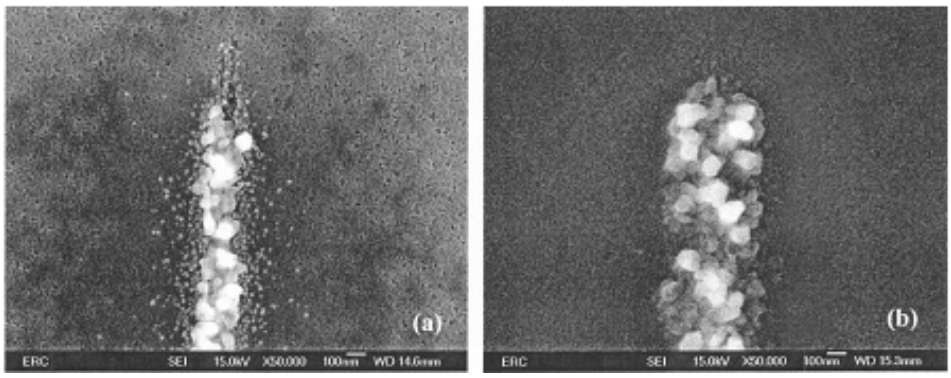

Fig.2. 2 SEM micrographs by Choi et al. [62] of copper selectively deposited on scratches induced with an AFM tip. (a) Cu 5ppm, 10min; (b) Cu 5ppm, 20min; (c) Cu 5ppm, 30min and (d) Cu 2ppm, 30min.

These experiments indicate clearly that some regions in silicon are energetically favorable for metal deposition. They correspond to those in

which crystal lattice is partially or totally destroyed, that is, defect sites or amorphous regions. Dangling bond density in these regions is expected to be higher than in other undamaged regions. They are more chemically active and can be oxidized more easily. Although the dangling bonds are passivated by fluorine or hydrogen in dilute HF solution, they have still a higher energy than a Si-Si bond in bulk silicon crystal.
The detailed explanation for the observed trend is hard to achieve, however the exact positioning of the metal catalyst on silicon surface is essential to obtain ordered arrays of silicon nanostructures.

2.2 Silver deposition on individual Si(100) and Si(111).

2.2.1 Experiments

The Silver Nanoparticles (AgNPs) formation and growth were investigated for both oriented Si substrate and for different time of immersion in a solution containing HF and Ag^+.
Si (100) n-type (P-doped $\rho \cong 3\text{-}5\Omega\cdot cm$) and Si (111) n-type (P-doped $\rho \cong 0.1\text{-}0.16\Omega\cdot cm$) wafers were used as starting materials.
A thick layer of AZ resist was spun coated on the back of each wafer, to prevent silver deposition during the immersion in the solution. It has been found that this resist is a very useful masking material during MAcE [63].
The samples were cut in squares of 0.5cm in side and dipped in Diluited Hydrofluoridric Acid Solution (DHF, Hydrofluoridric Acid and Water 1:7). By this treatment, adopted to remove the native oxide, H-terminated surfaces were obtained.
The electroless silver deposition was achieved by samples immersion in solution I (0.005M $AgNO_3$ and 4.8M HF) for times in the range 5s to 160s to guarantee a detailed investigation on Metal Nanoparticles generation and growth.
It should be pointed that for short deposition times, e.g. 5s, one makes a lot of errors. Immersion and extraction times are significant in respect to the 5

second dip and also the rinsing of the reactants away from the surface is at least on the same time scale. This factor should be considered when a comparison between the (100) and (111) wafers at 5s is done. Nevertheless short times are useful to delineate a trend for nucleation and early stages of growth of silver particles.
The as-deposited samples were analyzed with various techniques: SEM, RBS and cross section TEM.

2.2.2 Results

The SEM investigations performed on the same samples are reported in fig. 2. 3.
They show that after 5s of immersion, in agreement with the data reported in chapter 1, a large amount of silver nuclei are present on both (100) and (111)Si substrates (fig. s 2.3a and 2.3e). Then, for a prolonged immersion duration, the AgNPs grow in size and interconnect in between them, covering partly the silicon surface.

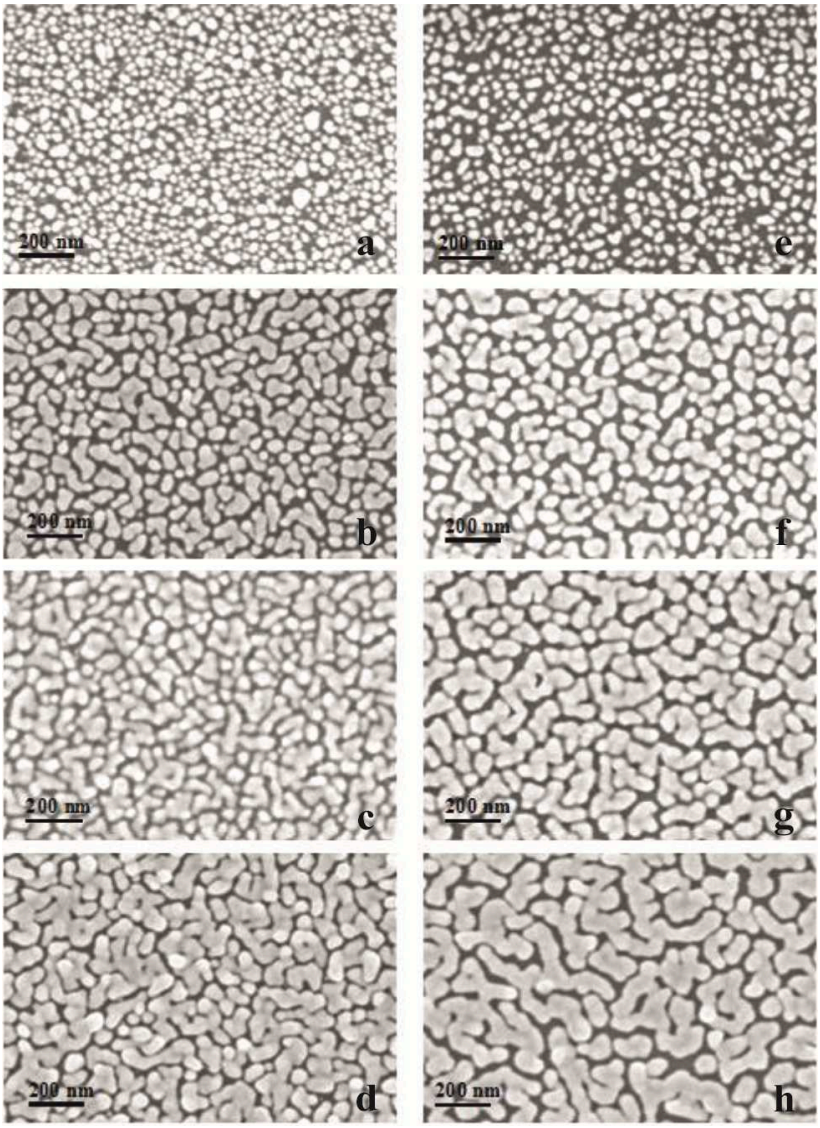

Fig.2. 3: SEM images of (100) and (111) Si substrates after Ag plating for (a) (100) 5s; (b) (100) 40s; (c) (100) 120s; (d) (100) 160s; (e) (111) 5s; (f) (111) 40s; (g) (111) 120s; (h) (111) 160s

It is interesting to observe that even after 160s of immersion a continuous metal film is not achieved, according to the proposed 3D island growth

mode.

The RBS spectra of 2MeV He^+ ions have been recorded for all the samples. They show that the amount of deposited Ag increases with immersion time for both oriented substrates, as reported in fig. 2.4 in terms of atomic density. The AgNPs density instead, obtained with the elaboration of SEM micrographs of fig. 2.3, is reported in fig. 2.5.

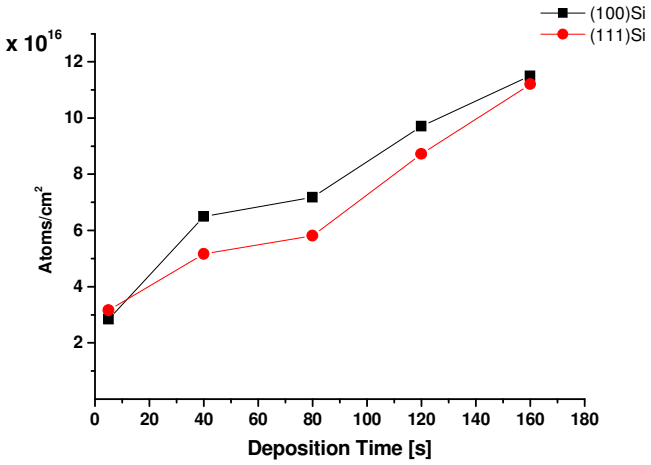

Fig.2. 4 Ag (Atoms/cm^2) from RBS analyses for the (100) and (111) Silicon substrates.

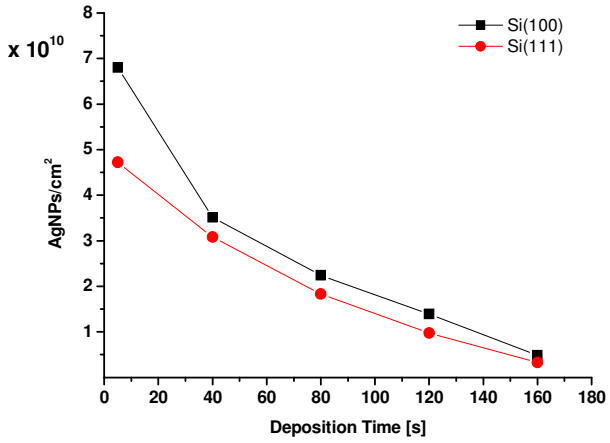

Fig.2. 5: Silver cluster density as a function of the immersed time.

The data reported in fig. 2.4 indicate that for the two oriented substrates, within the experimental uncertainties the deposition rates coincide, even if the silver amount is slightly higher on (100)Si.

Fig. 2.5 shows a higher density of silver clusters, at all the investigated deposition times for (100)Si. The nuclei density calculated at 5s is very high, about $7x10^{10}$ AgNPs/cm^2 for (100) and $5x10^{10}$ AgNPs/cm^2 for (111)Si. Then the particles' density decreases: for the (100) substrate: it is $7x10^{9}$ AgNPs/cm^2 at 160s deposition time and for the (111) substrate is nearly half, $3x10^{9}$ AgNPs/cm^2.

To summarize, the first few seconds of deposition are characterized by a fast rate, during which the amount of silver atoms is 10^{16} atoms/cm^2 (fig. 2.4) with a nuclei density of 10^{10} cm^{-2} (fig. 2.5). For longer times the silver deposition rate is nearly constant for both substrates (it varies of a factor 2 form 40s to 160s as reported in the RBS spectra of fig. 2.4) while the cluster density decreases of one order magnitude due to the coalescence.

However the deposition shows a weak dependence on the substrate's orientation.

The clusters' mean size is reported in fig. 2.6. As expected, with decreasing

clusters' density an increasing mean extension for particles occurs. Indeed it grows of two order magnitude form 5s to 160s. Generally it is the same for both orientations except that at 160s when it is nearly a factor of two higher for the (111) oriented substrate. This is probably the effect of lower particle density on coalescence (i.e. the particles span on a larger area).

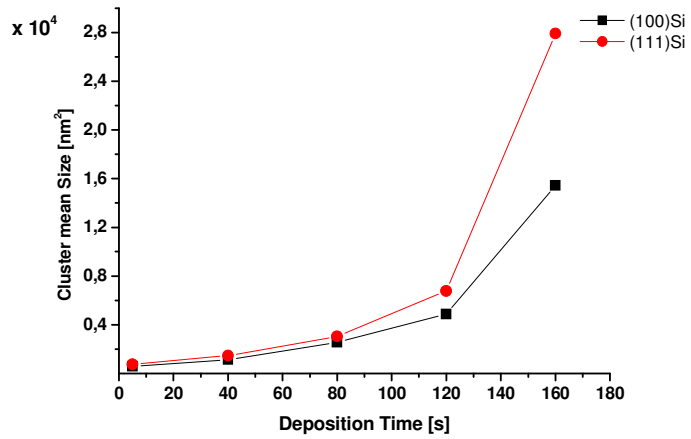

Fig.2. 6: Silver cluster mean size versus deposition time.

The density of the silver clusters is higher on (100)Si, but they are smaller than those more dense found on (111)Si. The amount of deposited silver is nearly the same for both orientations. As a result of these two different trends the covered area is nearly the same for the two substrates as shown by the data reported in fig 2. 7.

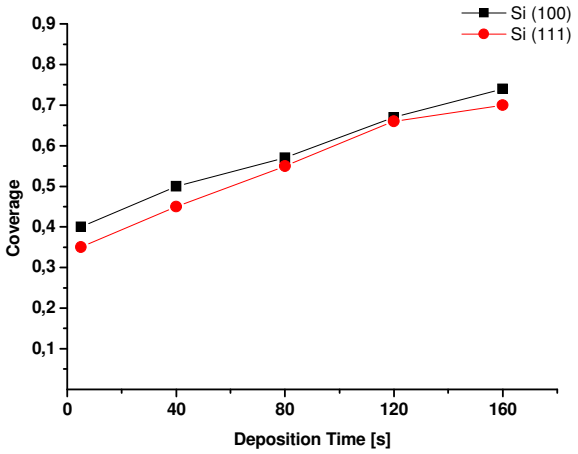

Fig.2. 7 Surface coverage of Ag clusters on (100), (111) Si substrates, for different dipping times.

In the first 5s, the covered area reaches the 40%, then the deposition rate slows down and the measured coverage doubled in 155s of immersion.

Coverage as obtained by SEM images elaboration is weakly orientation dependent, just like Ag amount and the clusters density. It is clear that the adopted method to analyze the SEM images could lead to certain incertitude.

Some samples were analyzed by TEM cross section and typical images are shown in fig. 2.8 for both oriented substrates and for two different deposition times: 40s (fig. 2.8a-b) and 160s (fig. 2.8c-d) respectively.

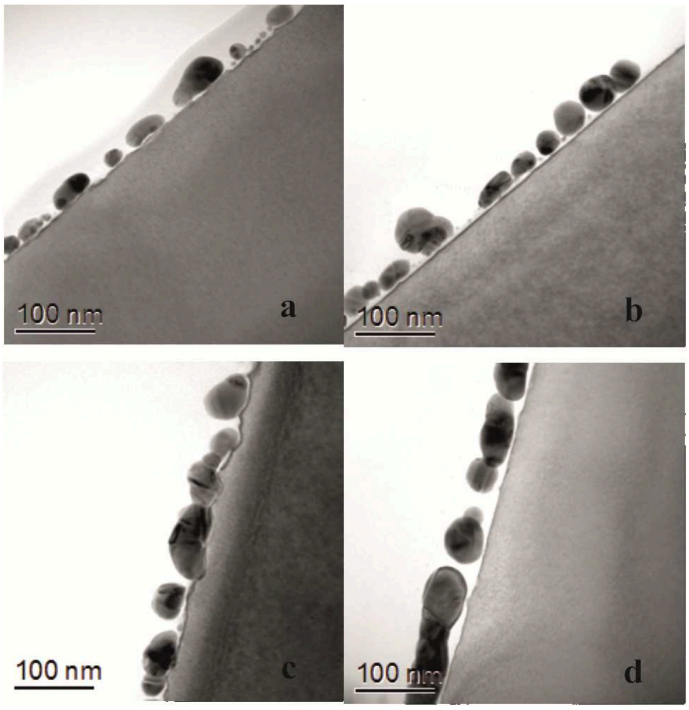

Fig.2. 8: Cross section transmission microscopy images (a) (100)Si 40s, (b) (111)Si 40s for 160s; (c) (100)Si 160s; (d) (111)Si 160s oriented substrates respectively.

The silver clusters increase in size with deposition time not only laterally but also vertically, the mean height is about 22nm at 40s while it is 40nm at 160s. if we compare the thickness variation with the square root of the mean area, plotted in fig.2.6, we could observe that while the height varies of a factor two in 120s, the in plane extension changes of a factor 4, confirming that during this stage of deposition the main effect is particles coalescence. Some grain boundaries could be observed on particles thus supporting the occurrence of coalescence.

A thin oxide layer is visible at the interface Ag/Si, that it is quite rough especially for the (100) substrate. This may be due to a higher reactivity of the (100) surface as kinks and dislocations are present in larger amount. It is known indeed, that Si(100) undergone a (111) faceting in oxidative solution [64]. No intermixing of Ag with Si has been detected [65].

2.2.3 Considerations about the orientation dependence of Electroless Ag Deposition.

The nucleation and growth mechanism of AgNPs on silicon substrates have been exploited elsewhere [66-70]. From the measurements presented in the previous section a fast silver deposition occurs on both oriented substrates during the very first seconds (less than 5s) of immersion in the plating solution reaching a coverage of about 40%, thereafter the rate slows down of a factor ten and it remains constant and uniform for both oriented substrates. At the maximum adopted deposition time, i.e. 160s, the surface coverage reaches 70% in both substrates. This behavior implies a change in the electrical response of the silicon surface. Soon as part of the silicon is covered by silver a Schottky barrier is formed with a depletion layer of 0.12µm for the 3-5 Ω·cm n-type Si (100) and 0.09µm for the 0.1 Ω·cm n-type (111) Si respectively.

The depleted layer extends also laterally and as a result the Ag^{+} ions prefer to deposit onto the preexisting silver clusters than on the uncovered silicon surface. The data indicate moreover that the AgNPs density is higher on Si (100), but their means size is lower in comparison with Si (111). The difference might be attributed to the different reactivity of the two surfaces because of the higher number of surface bonds and of stable H-termination sites in HF treated Si (111) surfaces. In any case the incertitude in times due to the experimental conditions, does not allow a clear detection of orientation dependence for electroless silver deposition.

To elucidate if there is a dependence on the substrate orientation, deposition was performed simultaneously on (100) and (111)Si by means of the apparatus reported in fig.2.9 The deposition time was chosen long enough (30min) to overcome incertitude associated with immersion and extraction of samples.

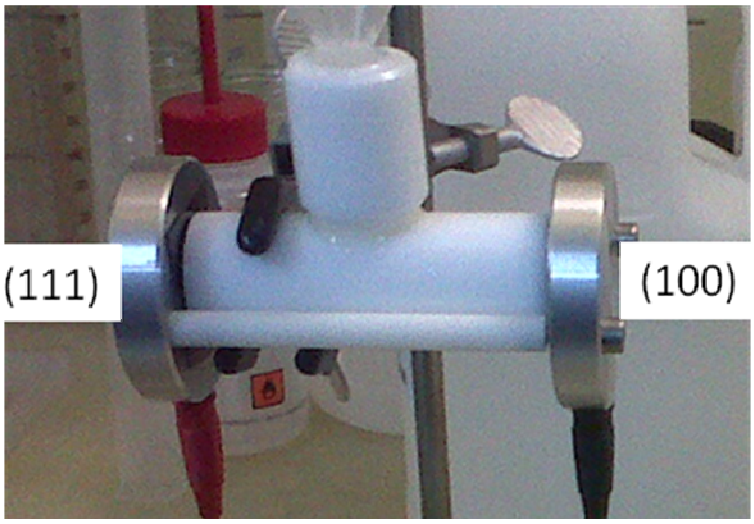

Fig.2. 9:Experimental setup for simultaneous deposition of silver on Si(100) and Si(111)

In fig. 2.10 the SEM plane views of both substrates are depicted. The silicon surface of both substrates is covered with dendritic silver clusters that are more dense on (100)Si.

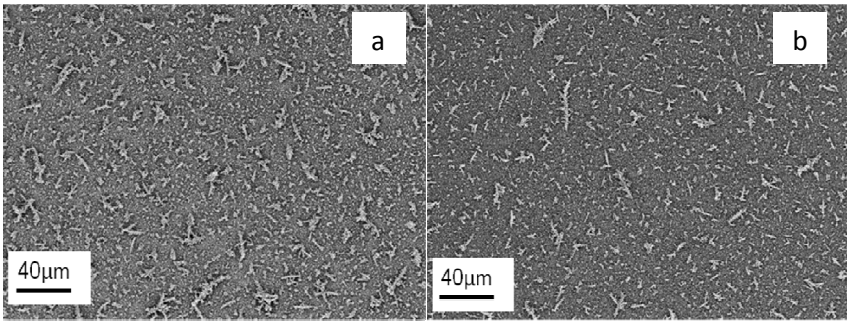

Fig.2. 10:. In plane SEM of(100)Si and (111)Si deposited for 30min

The higher Ag amount on (100)Si was confirmed by cross section SEM, as reported in fig. 2.11.

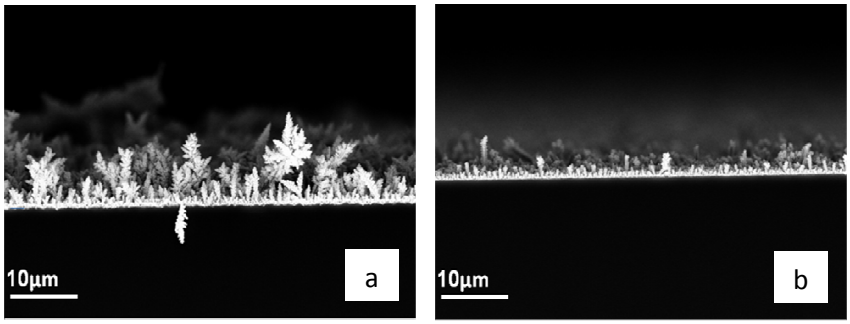

Fig.2. 11: Cross section SEM of samples after 30min deposition (a) Si(100) and b) Si(111).

The analyses confirm that deposition is orientation dependent, being faster on (100)Si. However these dendritic clusters don't allow the fabrication of silicon nanostructures, because, as explained in the previous chapter, they originate from the empty spaces in between metal particles. Nevertheless the experiment shows that orientation dependence for silver deposition could be postulated.

In the next paragraphs, indeed, deposition will be investigated on a substrate that allows the contiguous exposure of (100) and (111) surfaces to the plating solution. In this configuration the incertitude due to the dipping and rinsing in the individual processing was eliminated and the orientation dependent behavior for silver deposition could be investigated also for shorter times.

2.3 Silver deposition on macro-patterned Si wafers: simultaneous exposure of contiguous (100) and (111) surfaces.

2.3.1 Fabrication of macro-patterned Si.

The starting substrate was n-type Si(100) (P-doped ρ = 3-5 Ω·cm) with a 300nm thick thermal SiO_2 overlayer. The mask for the macro pattern was a strip 700µm wide and millimeters long, it was obtained by contact lithography, using a UV flood lamp.

The {100} and {111} Si planes were obtained by means of the anisotropic etching [71] with alkaline solutions (KOH Potassium Hydroxide).
The obtained pattern depends on the mask features while its morphology is strictly related to the adopted experimental parameters, i. e. etching time and temperature.

2.3.2 A brief overview on KOH etching of Si

A schematic representation of etching in KOH solutions on masked (100)Si is reported in fig. 2.12. Etching starts with the fast, vertical removal of (100) atoms. Near the mask, the (100) planes are covered and so etching leaves the (111) atoms exposed. According to the back bond breaking theory an atom on (111) surface is harder to remove than one on (100) and etching will proceed slowly in the [111] directions. As a result the walls of the obtained holes are the four (111) planes, tilted of 54.74° respect to the horizontal direction.

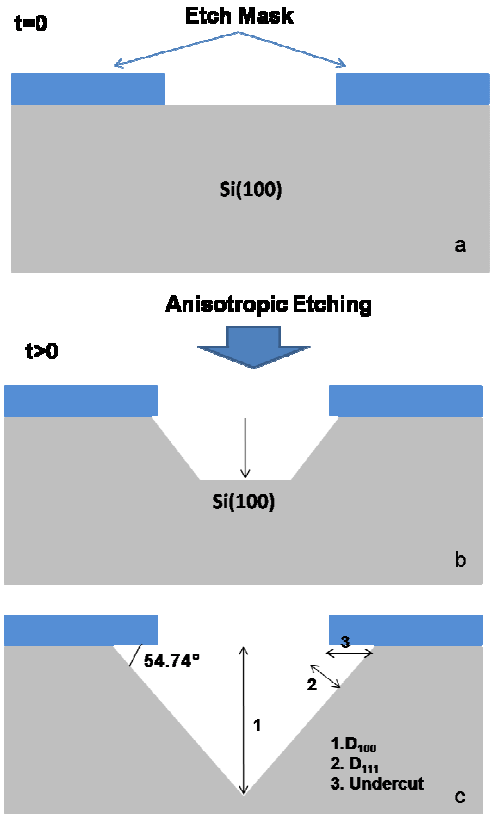

Fig.2. 12: Etching of masked (100)Si (a) t=0; as soon as the atoms of (100) planes are removed along the vertical direction, the exposure of (111) planes at the mask edges takes place (b). (c) Final etching geometry obtained on (100)Si.

The etch depth along the (100) (D_{100}), i. e. the hole's height, is related to the mask size:

$$D_{[100]} = \frac{mask\ \ side}{2} tg\ \ 54.74$$

Eq. 2. 1

While the etching depth along the [111] direction is strictly related to the undercut, i.e, the distance etched under the mask and is given by:

$$D_{[111]} = Undercut\ \ sen54.74°$$

Eq. 2. 2

It is clear that the extension of the obtained surfaces is also strictly related to the etching time.

However during the experimental procedure, etching of mask also occurs. It is well known indeed that SiO_2 is also etched, with a lower rate, in KOH, as reported in fig. 2.13 [71].

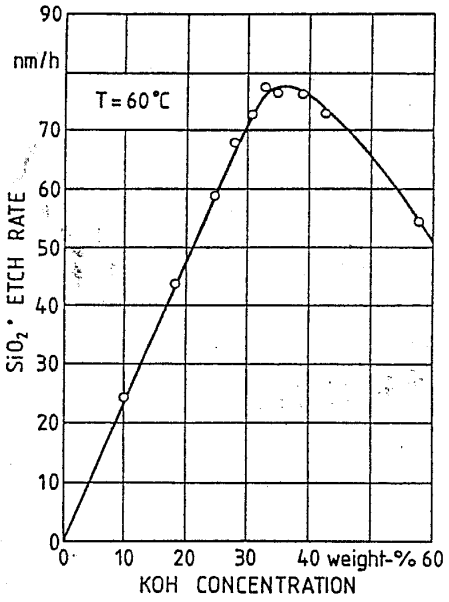

Fig.2. 13 Etch rate of SiO2 at 60°C versus KOH concentration from [71].

The etch rate increases exponentially with temperature, so the mask thickness could limit the etching time. This factor influenced the fabrication of macro-patterned Si.

In our experiments SiO_2 mask was 700µm wide, so according to eq. 2.1, etch depth along the [001] should be about 500µm, in order to obtain the

described pyramidal holes. The adopted solution was KOH 20%wt, while the etching temperature was 80°C to ensure a fast removal of Si atoms. As shown in table 2.1 this combination should ensure suitable etching rate together with good control of experimental conditions (e. g. by preventing evaporation that could change the concentration of solution).

	Temperature [°C]								
% KOH	20°	30°	40°	50°	60°	70°	80°	90°	100°
10	1.49	3.2	6.7	13.3	25.2	46	82	140	233
15	1.56	3.4	7.0	14.0	26.5	49	86	147	245
20	1.57	3.4	7.1	14.0	26.7	49	86	148	246
25	1.53	3.3	6.9	13.6	25.9	47	84	144	239
30	1.44	3.1	6.5	12.8	24.4	45	79	135	225
35	1.32	2.9	5.9	11.8	22.3	41	72	124	206
40	1.17	2.5	5.3	10.5	19.9	36	64	110	184
45	1.01	2.2	4.6	9.0	17.1	31	55	95	158
50	0.84	1.8	3.8	7.5	14.2	26	46	79	131
55	0.66	1.4	3.0	5.9	11.2	21	36	62	104
60	0.50	1.1	2.2	4.4	8.4	15	27	47	78

Table 2. 1: Etch rate [µm/h] for various molarities and temperatures [71]. At 20%wt and about 80°C the expected etch rate is between 50 and 86 µm/h. A slight deviation from the calculated data is expected since for long time it isa variation in the solution molarity and temperature could occur.

Since in this conditions the expected etch speed of SiO_2 is about 100nm/h and the thickness of the macro-patterned mask was 200nm, etching time was limited to 1h40min. Instead of the expected pyramidal hole, a truncated V groove 700µm wide and 70µm deep, as shown in the schematic representation of macro-patterned Si shown in fig.2.14 (not in scale). The lower (100) plateau is due to the survey of (100) plane at the bottom (short etching time compared with the mask width fig. 2.12b).

As shown in the inset of fig. 2.14 the inclined walls consist of two (111) planes. The occurrence of this phenomenon will be explained later.

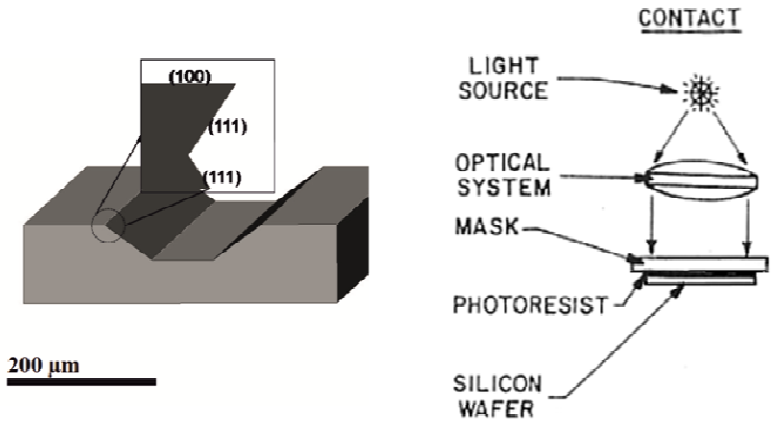

Fig.2. 14 Schematic of macro patterned Si substrate. The strip was about 700µm wide and 70µm deep. The truncated V groove shape is generated by under etching of (100) planes. The horizontal plateax are the (100) planes. The walls are the (111). Fabricated with contact lithography.

2.3.3 Morphological characterization of macro patterned Si

A detailed morphological analysis is required a priori, to investigate the changes induced by the fabrication step, in terms of variations in the surface bond density.

The structured substrate has horizontal (100) plateaux belonging to the original wafer, masked by SiO_2 during etching. It is well known that (100) planes have two dangling bonds per atoms.

The (111) walls, generated by etching, have one dangling bond per atoms. The surface bond density of the two crystallographic planes is reported in the table 2.2 below [72] while in fig.2.15 the dangling bonds configuration is illustrated.

Planes	**Surface bond density ($10^{15}/cm^{-2}$)**
(111)	0.78
(100)	1.36

Table 2. 2 Surface bond density of (100) and (111) Silicon surfaces. From ref [72.]

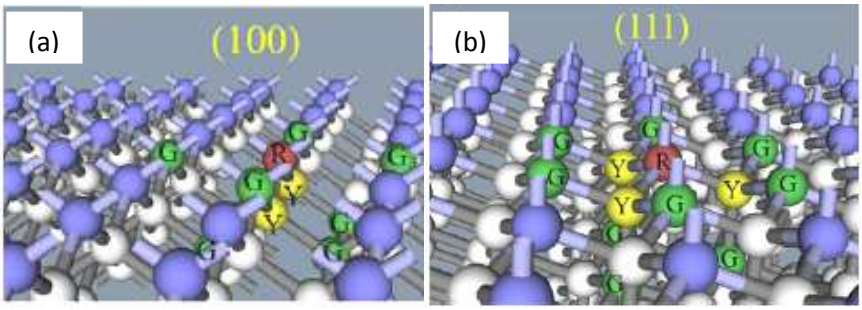

Fig.2. 15 Atomic configuration of (a) (100) (two dangling bonds per atom) and (b) (111) (one dangling bond per atom) silicon surfaces. R denotes a generic atom, while Y (yellow) and G (green) indicate its first and second neighbors respectively

The transition region between the two planes in the upper part is not abrupt (convex angle 306°). For the macro-patterned substrate it is rounded, smoothed and it extends for several hundreds of nanometers, with a curvature radius of a few nm. Morphological details of the atomic arrangement of the transition region have been studied by HRTEM (High Resolution Transmission Electron Microscopy). The HRTEM image of the upper transition region in macro-patterned Si is shown in fig.2.16a The rounded zone includes, as it is well known, several low index planes as {311}, {211} [73], and several terraces and kinks on the (111) and (100). The two planes meet in the lower edge of the macro-patterned silicon at an angle of 128° (fig. 2.16b). The transition region is still rounded; it extends for very few nanometers, with a very low roughness and kink and terraces density.

The micrographs show a strong variation of surface bond density between the upper and the lower transition regions and according to the data reported in paragraph 2.1, the deposition should take place with a different rate being faster on the more damaged regions.

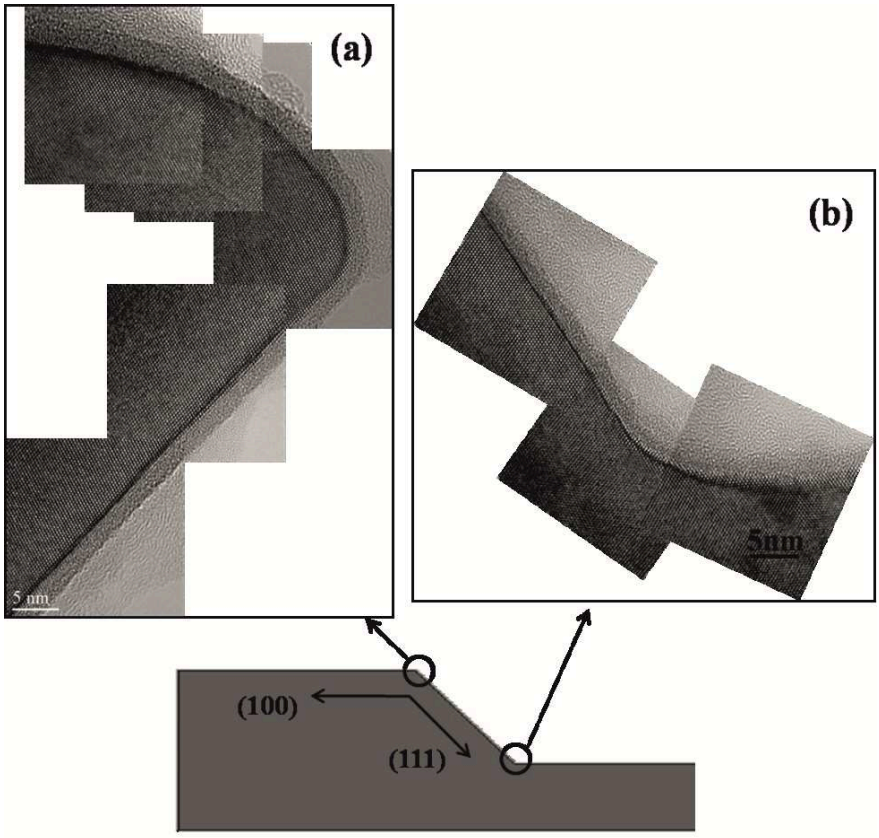

Fig.2. 16: HRTEM micrographs of the upper (a) and the lower (b) transition regions of macro patterned Si. A clear difference in the surface bond density is detectable. In (a) the (100) surface is extremely rough. In addition the different curvatures between (a) and (b) suggest a probable difference in surface reconstruction and in the kind of H-terminations.

The origin of the observed increased surface bond density of the transition regions is due to the KOH etching dynamics.

As soon as etching starts (100) atoms are fast removed, while the (111) appear at the edges of the masked regions. Etching proceeds in both [100] and [111] directions with two different rates, due to the anisotropy. The (111) planes are not uniformly etched because in the upper part they are exposed to the etching action for a longer time than the bottom. The

roughness and morphology of the undercut regions is caused by the prolonged etching of (111). In the macro patterned Si, high temperatures lower the anisotropy degree, resulting in moderately fast etching of (111) planes. If coupled with long etching times, high temperatures produced the observed rhomboidal profile (fig. 2.17).

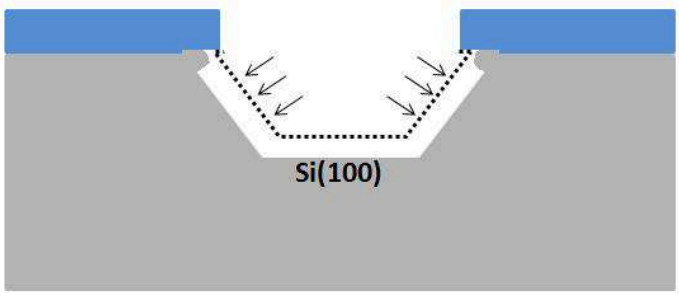

Fig.2. 17: Origins of the upper transition regions roughness during KOH etching

2.3.4 Silver deposition on macro patterned Si

The deposition time in solution I (0.005M $AgNO_3$ 4.8M HF) was 40s. With this condition, as reported in previous paragraphs, the Silver Nanoparticles (AgNPs) distribution on (100) and (111) substrates was low enough to allow the direct observation of an enhanced deposition on the defective areas introduced in the present experiment. The metal deposition was investigated with SEM (Scanning Electron Microscopy) and with XTEM (Cross Section Transmission Electron Microscopy) to evaluate the Silver clusters size distribution on the different exposed Si surfaces to the solution I.

To demonstrate the validity of the proposed model for the deposition dynamic, it was also performed on:

a. Etched macro pits that experienced for shorter time KOH erosion, where the upper transition region is expected to be less rough than that presented for the macro patterned Si;

b. Macro patterned substrate with two different surface conditions: crystalline and amorphized by ion implantation (Ge^+ 30keV 6E14 ions/cm^2), where the lattice periodicity was completely destroyed by ion implantation.

2.3.5 Results

The AgNPs distribution is reported in fig. 2.18. It depends on the surface orientation and also on the distance from the edges. The SEM images were taken at specific distances from the upper edge for both (100) and (111) surfaces. The silver clusters located on the upper transition region between the (100) and (111) surfaces have a dendritic shape (fig. 2.18a). The metal coverage for the (100) decreases with increasing the distance from the edge. It is about 90% in the near edge area (fig. s 2.18a-b) and it decreases to 72% at about 30μm (fig. 2.18c) and to 61% at a distance of 70μm (fig. 2.18d) respectively.

The AgNPs' size and density show the same decreasing trend. They are totally interconnected in the near-upper edge region. The cluster size, on the (100) plateaux, at a distance of 10μm amounts to $5x10^3nm^2$, with a density of $9x10^9cm^{-2}$(fig. 2.18b), it decreases to 10^3nm^2 with a density of $3.6x10^{10}$ cm^{-2} at the distance of 70μm (fig. 2.18d). On the (111) surface the coverage is 72% in the near upper edge region (fig. 2.18e), 20% lower than that on the (100) plateaux (fig.2.18a-b). At a distance of 10μm it is 50% (fig. 2.18f) while in the near-bottom region, where the transition between the (100) and the (111) planes is concave and more abrupt, with a lower amount of surface bonds, the deposition is inhibited and the coverage ranges from 24% (fig. 2.18g) to values less than 10% (fig. 2.18h). The AgNPs density on the walls is $9x10^9cm^{-2}$ in the near upper region (fig. 2.18e) and it increases with distance: it is $5x10^{10}$ cm^{-2} at 10μm (fig. 2.18f) and $7x10^{10}cm^{-2}$ at 30μm (fig. 2.18g). Their size shows a reverse trend: it is $9x10^3nm^2$ in the near upper region, $1x10^3nm^2$ at 10μm and $2x10^2nm^2$ at 30μm, about one order magnitude lower than that of the (100) plateaux.

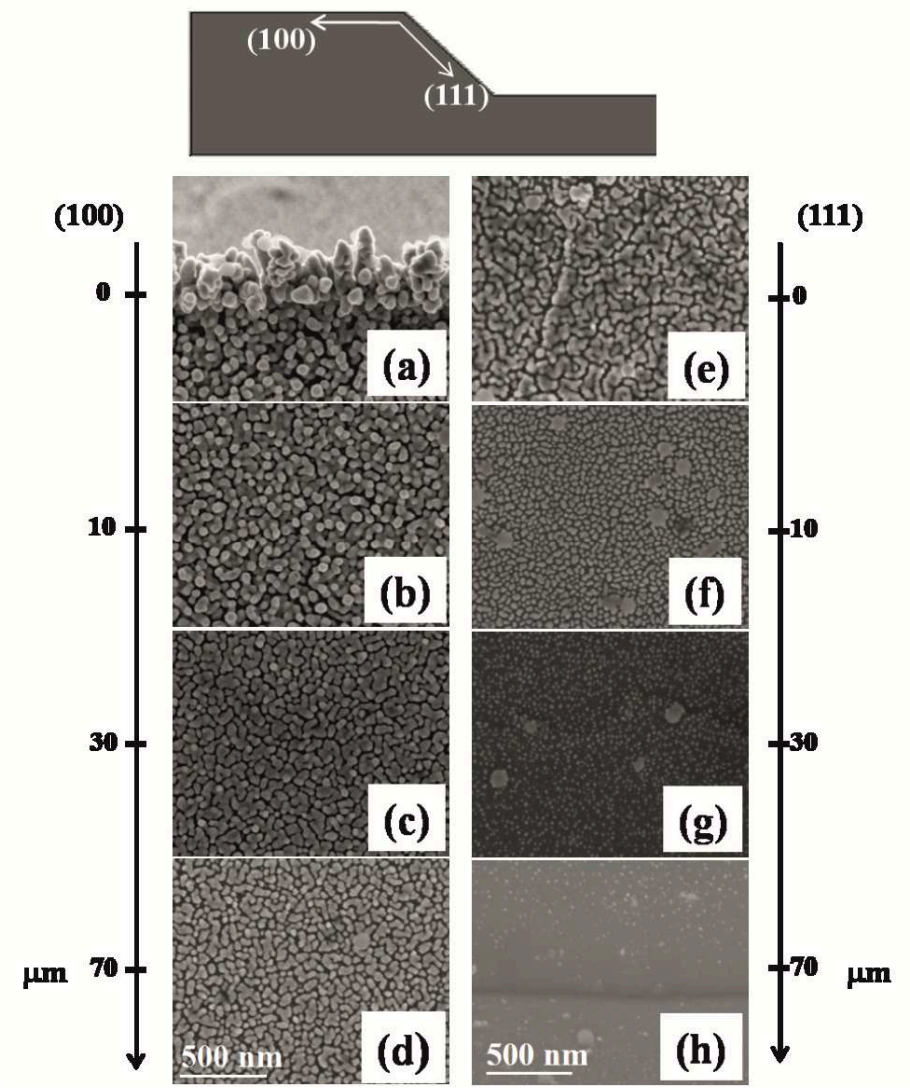

Fig.2. 18: AgNPs distribution on (100) (a-d) and (111) (e-h) planes of macro patterned Si. The origin is taken at the upper transition region. The clusters extension decreases with increasing distance from the edge. (a) Si(100) on the edge; (b) Si(100) at10µm from the edge; (c) at 30µm; (d) at 70µm (e) Si(111) near the edge; (f) Si(111) at 10µm; (g) Si(111) at 30µm; (h) Si(111) at 70µm exactly in the bottom transition region.

The deposition step was also performed by stirring solution I (see fig.2.19).

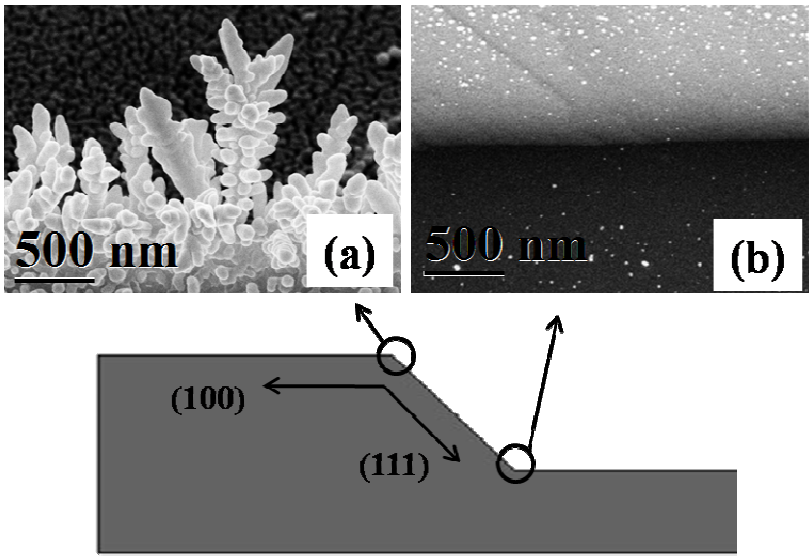

Fig.2. 19: AgNPs distribution on the top (a) and the bottom (b) transition regions of macro patterned Si, obtained by stirring solution I. As shown the same self selective mechanism is observed and the Silver clusters have a dendritic shape in the upper part while the deposition slows down in the bottom.

The process took place in the same self selective way, i.e. it is strongly enhanced in the upper edge region with the formation of dendritic Ag clusters and inhibited in the lower edge region. To further investigate the orientation dependent features, the unstirred samples were analyzed with XTEM. Fig. 2.20 shows the silver nanoparticle distribution on the near upper edge region. Even if the dendritic clusters were destroyed by the specimen preparation, the mean height of the remaining AgNPs is about 80nm on the (100) surface and 30nm on (111) walls showing a clear dependence on orientation.

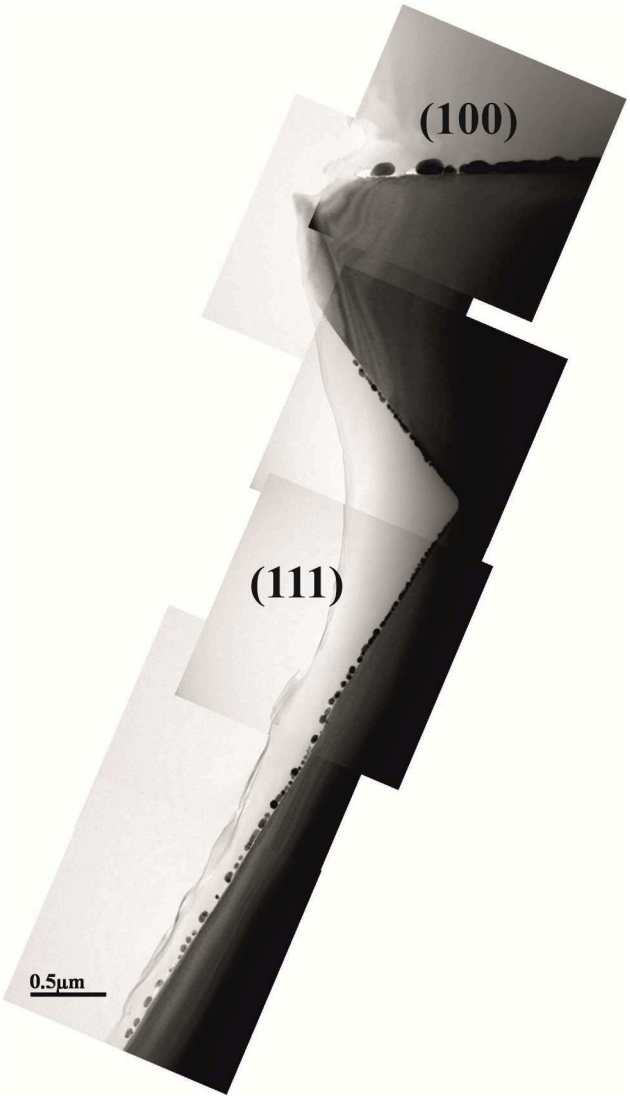

Fig.2. 20 Cross section TEM for silver clusters on macro patterned Si (100) plateau and on (111) in the near upper transition region.

2.4 Discussion

When contiguous (100) and (111) surfaces are simultaneously dipped an orientation dependent distribution of Ag clusters could be detected.
Metallic aggregates are formed preferentially on surface discontinuities, which are thermodynamically favorable sites and might act as catalyst for the subsequent metal ion deposition
The observed silver distribution on macro patterned Si could be understood as a complex combination of substrate morphology, orientation, kind of H-terminations and mass transport during electroless plating.
The non uniform silver cluster density induces also depletion in the adjacent metal ion concentration.

2.4.1 H-Terminations Role

It has been speculated that the Ag atoms readily terminate the surface dangling bonds, replacing less stable Si-H bonds [74, 75].
The atoms of the very first surface layer have unsaturated bonds, the so-called dangling bonds, due to the disruption of the periodicity of the crystal structure at the surface. In particular, the surface cleaned with HF solutions, is known to be hydrogen terminated. The phenomenon of hydrogen termination of silicon surfaces has been extensively investigated. H-termination is essentially complete with immersion time on the order of 1min, it is formed through chemical adsorption yielding a covalent bond having a strength close to that of the Si-Si bond and the surface is passivated by hydrogen termination. Each surface silicon atom can be terminated by one, two, or three hydrogen atoms, depending on its geometric position in the surface lattice. Whether the termination is dominated by mono, di- or trihydride depends on the orientation and roughness of the surface. The ideal (100) surface tends to be terminated by SiH_2 and the (111) by SiH or by SiH_3, due to the difference in the number of dangling bonds. The (111) surface with an almost complete termination by

SiH, has atomic flatness. Predominant SiH_3 termination of flat (111) surface is also reported. The silicon atoms on step, which are terminated by di- and tri-hydrogen, are preferentially attacked, while the atoms, which are terminated by mono-hydrogen, are not directly attacked [76-80].
According to [81, 82], deposition occurs to a much greater extend on H_x-Si(100) surfaces compared to H-Si(111), being smaller the number of di-hydride sites on Si(111) surfaces.

2.4.2 The role of surface microstructure

In addition Silicon microstructure influences the electroless deposition. On mechanically modified or partly amorphized silicon surfaces electroless metal deposition is enhanced because defects sites, thanks to their unsaturated bonds, are more chemically active [60-62].
The electroless silver deposition on both (100) and (111) Si wafers individually treated was only slightly dependent on the orientation of the substrate. Although the initial deposition rates differ between the two substrates, the immersion time will level off any different initial nuclei density. In the present experiment instead, various surface structures are simultaneous exposed to the Ag ion flux. In details: i) the (111) planes with a dangling bond per atom and with a surface bond density of $0.78x10^{15}cm^{-2}$; ii) the (100) plateaux with two dangling bonds per atoms, with a surface bond density of $1.36x10^{15}cm^{-2}$; iii) the upper edge region, made by a series of several orientation planes to join the (100) to the (111), with a high density of kinks and nano-terraces are all simultaneous exposed. A variation in the surface bond density implies also a difference in the kinds of H-terminations and so a change in the surface reactivity. The surface morphology is affected by the adopted KOH etching parameters that results in defective undercut region.
The SEM images of the as deposited macro-patterned Si show that the silver coverage and the sizes of the clusters, with dendritic shape, are highest on the upper edges. The AgNPs density, at the same distance from

the upper transition region, is lower on the (111) surface. It could be speculated that the deposition rate, as previously mentioned, is faster in the highly reactive upper edge where the largest number of Ag nuclei is found and this process will cause locally depletion in the Ag^{+} concentration. Since the ion diffusivity in the solution is about 10^{-4} (cm^2 x s^{-1}) a consistent flux of ions, induced by the concentration gradient, will be directed towards the region where a high number of nuclei is present. As a consequence the decrease in the Ag ions concentration will cause a lower deposition rate in the still bare silicon. On the (100) plateaux the cluster density is lower than that on the edges, but still higher than that on the (111) walls. A qualitative estimation of the influence of surface morphology in nucleation and growth of silver nanoparticles by electroless deposition could be obtained observing metal clusters distribution in the etch pit of in fig. 2.21.

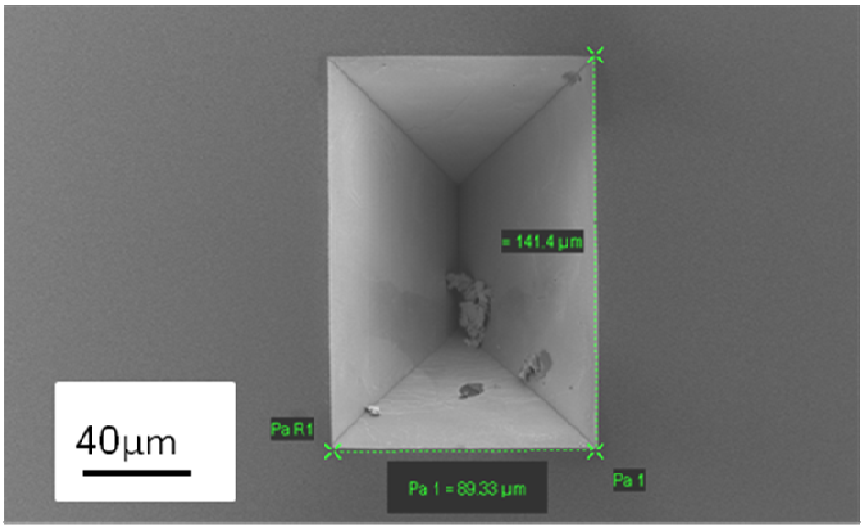

Fig.2. 21 An etch pit caused by a local over etch of the SiO2 mask during etching with KOH.

This pit was generated during etching with KOH of macro patterned Si. As explained in the previous paragraphs etching time was chosen in order to prevent the complete removal of the mask. However a local variation in the

SiO_2 etch rate caused the exposure of (100)Si during the final minutes of etching. The pit indeed is about 30µm deep and experienced the etching solution for a shorter time than the exposed areas of macro patterned silicon. If we accept that the transition region morphology is related to the etching time, in this case we do not expect the occurrence of rhomboidal surfaces here.

These pits were found in a macro patterned sample dipped in deposition solution for 15s and for 30s. fig. 2.22 and fig.2. 23 respectively a comparison between the silver cluster in their transition region and in those of macro patterned Si, which experienced KOH etching for longer times is reported.

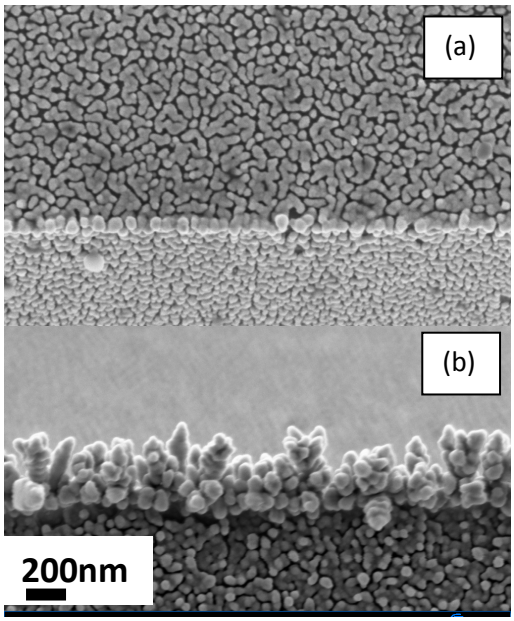

Fig.2. 22 Silver distribution after 15s immersion in solution I on the upper transition regions of (a) the etch pit and (b) the macro patterned structures. The clusters' size is different because it is affected by surface morphology.

A clear variation in cluster density is detected. This trend is maintained also for longer deposition times, as reported in fig. 2.23.

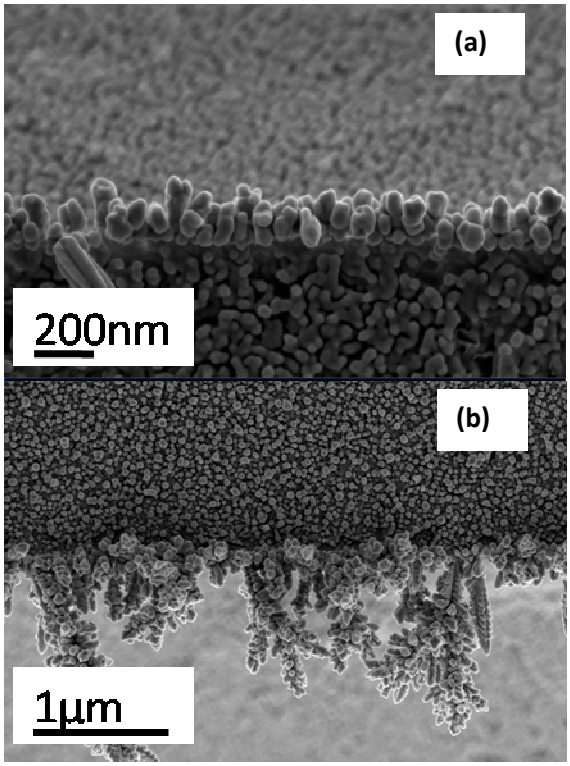

Fig.2. 23: Silver distribution Silver after 30s immersion in solution I on the upper transition regions of (a) the etch pit and (b) the macro patterned structures.

The observed differences could be seen as a demonstration of the influence of the surface microstructure on cluster nucleation and growth. Since the etching times for the two cases were different a lower damage occurred in the pits, with a lower amount of surface bond density and or a short extension for the upper transition region. This will cause a lower Ag nuclei generation and so a slower growth rate.

2.4.3 The Mass Transport Influence

From a dynamical point of view it could be speculated that the mass transport could influence the clusters distribution. Indeed it is enhanced on

convex surfaces and observing the SEM micrographs of fig. 2.18 it is plausible to admit that it could influence the silver distribution. To investigate its relevance, the deposition was also performed on a new macro patterned silicon (etched with KOH at 60°C for 1h to prevent the generation of the etch notch) after an ion implantation process that destroyed the difference in the surface bond density, and so the variation in the kind of H-terminations, among the three exposed areas (i.e. (111), (100) and the transition region). In this sample every site is equivalent to the others and it is useful to investigate the effect of mass transport on the metal distribution. Deposition was also performed on the sample before ion implantation. The comparison between the AgNPs on the crystalline and on the amorphous macro patterned sample is reported in fig. 2.24.

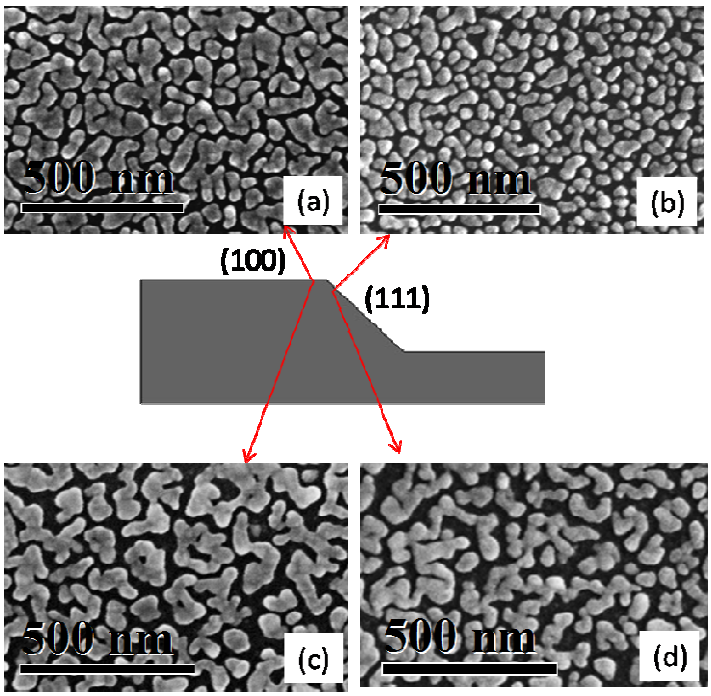

Fig.2. 24 AgNPs distribution in the near upper region for: crystalline (a) Si(100) and (b) Si(111) and amorphized (c) Si(100) and (b) Si(111).

The SEM micrographs of fig. 2.24 refer to the near upper transition region. The coverage on the crystalline sample is orientation dependent. On the (100) (fig. 2.24a) surfaces is 66% in near of the transition region then it decreases to 45% at 10μm and to 35% at 40μm (fig. 2.25 a and b). On the (111) a lower value is found. It is 55% near the upper edge, then it decreases to 34% at 10μm. The total length of (111) surface is 20μm and at this distance from the upper edge, coverage is less than 10%. As a result the covered area varies of 10% between (100) and (111) crystalline surfaces. The corresponding variation for amorphized sample is <2%.

For (100) crystalline sample, coverage is sensitive to the distance from the edge (fig. 2.25 a-b). On amorphized (100) surface, the covered area at 10μm and 40μm from the upper edge is the same (fig. 3.25c-d).

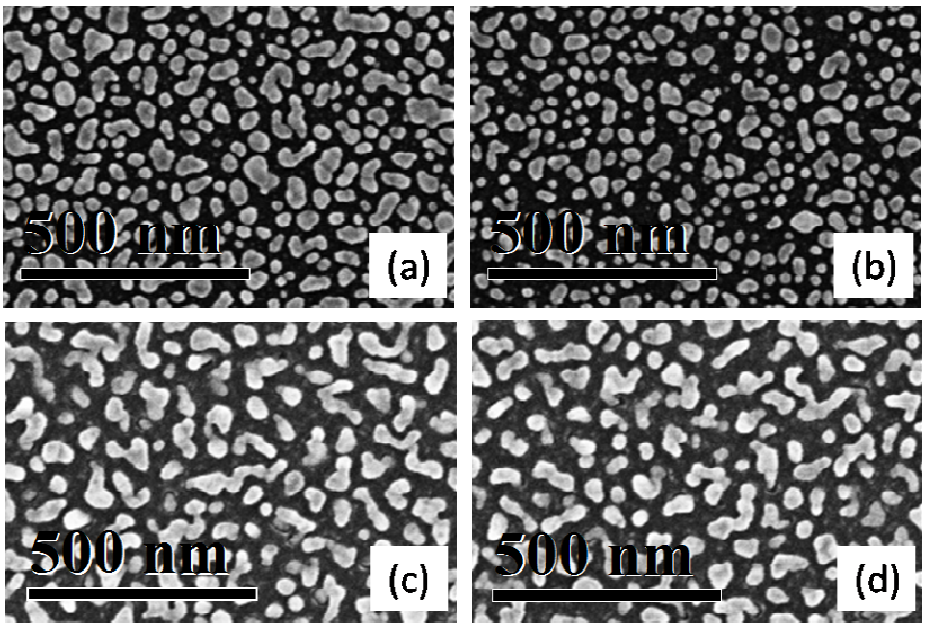

Fig.2. 25 AgNPs on crystalline (100) surface at (a) 10μm and (b) 40μm from the upper edge. (c) and (d) the same as for (a) and (b) but for amorphized (100) surface.

So mass transport enhances deposition on the convex surface, but the influence of contiguous areas with varying surface reactivities (in terms of unsaturated bonds and kind of H-terminations) could be neglected.

Summary

The silver deposition on (100) and (111) oriented silicon substrates has been carried out in two distinct configurations:

- Individually by immersing distinct Si(100) and (111) wafers in the solution;
- Simultaneously through the macro patterned Si with (100) and (111) surface on the same sample.

When samples underwent short individual depositions only a slight dependence on surface orientation was detected. On the other side, from the experiment performed for prolonged times that influence could be postulated. The macro patterned Si was fabricated *ad hoc* to investigate the aforementioned dependence.
With etching in the KOH solution an inhomogeneous surface bond density was produced.
The kind of introduced H-terminations, and so the surface reactivity, changed too, being related to the number of unsaturated bond per atom.
They influenced the deposition step leading to an increased metal coverage with the bond density of the exposed surfaces. Indeed the number of generated silver nuclei is related to the number of unsaturated and Hydrogen terminated bonds that are preferred nucleation sites. For this reason the convex upper edge region between the (100) and (111) planes is characterized by the highest silver clusters density.
The existing nuclei grow fast then into larger subtracting ions from the solution and so slowing down the deposition rate in the surrounding areas with low surface bond density. In this way a self selective mechanism takes

place for silver electroless deposition on patterned silicon surfaces.
When deposition is performed on amorphized macro patterned samples, silver distribution loses its orientation and site dependent properties. So The observed mechanism is due to a complex combination of increased surface bond density, kind of H-terminations and mass transport influence.

CHAPTER 3

INFLUENCE OF METAL MORPHOLOGY ON THE ETCHING DIRECTION AND APPLICATION IN SiNPS FABRICATION

The etching direction during MAcE is influenced by the ratio between the HF and H_2O_2 concentrations in the adopted solution (named **ε=[HF]/[H_2O_2]**) [83, 84]. An explanation for this dependence will be given in section 3.1. In addition there are some reports that deal about the influence of the metal morphology: if the ratio between its thickness and its in plane extension is low, etching proceeds always along the normal to the substrate. In the aforementioned studies etching conditions normal to the surface were achieved through lithographic metal patterns, while for isolated particles etching directions were the [001].
In chapter 2, the shape evolution of silver nanoclusters showed that extended and interconnected silver clusters could be obtained in two ways:

a) Prolonging the deposition time (e.g. 160s) as observed on (100) and (111) samples that underwent an individual immersion step;
b) Exploiting the dependence on the surface bond density and the influence of mass transport on convex surfaces, as observed in the near upper transition region of macro-patterned Si, for both (100) and (111) contiguous areas.

In this chapter a systematic study of silver-catalyzed etching of the as deposited Silicon substrates presented in chapter 2 is carried out. The

results show that etching directions depend on metal morphology.
In detail, for the (100)Si substrate partially covered with small silver clusters the etching proceeds both in vertical and horizontal [100] directions. For larger coverage (70%) the Ag nanoparticles sink all together along the vertical direction. For the (111) Si substrate, when the Ag nanoparticles are isolated, they sink in all the equivalent [100] directions with an irregular path; when they begin to coalesce, uniform domains of Si nanowires aligned along the [100] directions are formed. When the silver clusters are well interconnected (70% of coverage), the etching is vertical.
This dependence was confirmed when MAcE was performed on the as deposited macro-patterned Si: the inhomogeneous coverage, achieved with the proposed self selective mechanism, allowed the generation of porous layers due to the low silver coverage in the less damaged regions. Aligned nanowires were instead obtained by etching the large and interconnected silver clusters located on the near upper transition region.
Silver coverage is then another experimental parameter to induce a preferred orientation of the etched Si nanowires.
The obtained results for silver positioning and etching direction where applied to a micro-patterned silicon substrate, with (100) and (111) surfaces of few hundred nanometers length. It was observed an enhancement of the self selective metal cluster's nucleation and growth. The larger particles were found on the (100) areas. During the subsequent etching, silver aggregates experienced various paths, uniform and normal to the surface, if large and well interconnected, inhomogeneous and [001] oriented, if small and separated, leading to the fabrication of an ordered array of Si Nanopillars, 10μm long and 600nm wide.

3.1 The orientation dependent behavior of MAcE

Metal-Assisted chemical Etching on Silicon is achieved by partly covering the substrate with metal nanoparticles (MeNPs) which act as catalysts, promoting, in the presence of an oxidative agent (e.g. H_2O_2) and in HF-

based solutions, a fast removal of silicon atoms underneath them. This mechanism, with increasing the etching time, leads to the fabrication of nanostructures, due to the conglomeration of nanoholes (produced by Silicon etching), over the entire silicon wafer. No electrochemical cell assembly or any external applied electric current is needed. In chapter I, the factors that influence the etching mechanism have been illustrated, underlining the role of temperature, illumination, doping type. Their impact on the etch rate has been elucidated: temperature and strong illumination lead to an increase of the etch depth, while the doping level affects the morphology of the obtained nanowires (porous, non porous). There are two other elements that strongly influence the MAcE of silicon: orientation of the starting substrate and metal morphology. In MAcE of silicon wafers, the direction of etching determines the axial crystal orientation of the resulting SiNWs.

The substrate orientation strongly influences the process: the Metal Assisted chemical Etching of Silicon is intrinsically anisotropic with a preferred crystallographic [100] direction.

The SiNWS in (100) oriented Si substrates are generally perpendicular to the wafer surface even if a change from the [001] to the [110] directions was observed by Kim et al. with highly oxidative solutions [83] (high [H_2O_2]).

The same dependence on the oxidant concentration has been observed for SiNWs in non (100) oriented surfaces. As already mentioned this is not the only factor influencing etching directions: the metal shape plays a relevant role as pointed out in recent publications.

In this section an overview on the phenomenological explanations to clarify these dependencies is provided.

3.1.1 Dependence on the etching solution composition

In general, the anisotropic dissolution of silicon is explained recalling the back bond breaking theory: the removal rates of Si atoms are associated with the number of back bonds that F atoms have to break to remove a

silicon atom. Si(100) surfaces with two bonds symmetrically directed into the solution are the easiest to etch. This configuration is depicted in fig.3.1 where the diagrams show a two-dimensional Fisher projection with the dashed line indicating an arbitrary demarcation between solution and silicon [85].

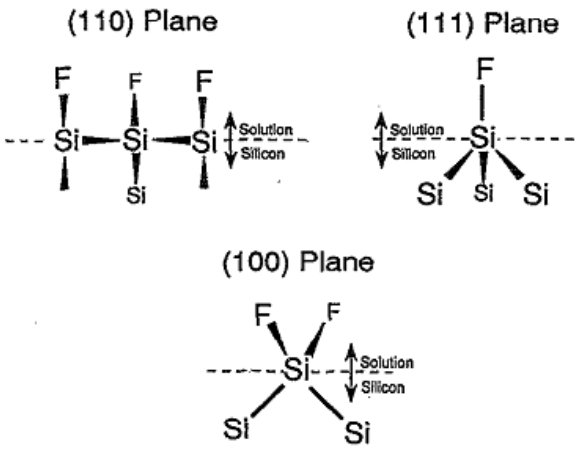

Fig.3. 1 Atomic configuration of silicon surfaces during etching in fluorine solutions. (a) Si(110), (b) Si(111) and (c) Si(100).

(a) Etching of (100)Si: the dependence on the ratio ε=[HF]/[H_2/O_2]

Deviations from [001] etching directions occur also for (100) oriented substrates. In ref [83] the role of HF and H_2O_2 (the ratio **ε=[HF]/[H_2/O_2])** concentrations has been elucidated, together with the induced changes in the etching rate, direction and morphology (solid nonporous or porous) of the obtained SiNWs. The results are reported in the ternary diagram of fig. 3.2. In the cited experiments, etching always proceeds along the [100] directions but the wires' morphology is related to the value ε being solid for ε > 1.15 (yellow region) and porous for 0.3 < ε < 1.15 (green region).

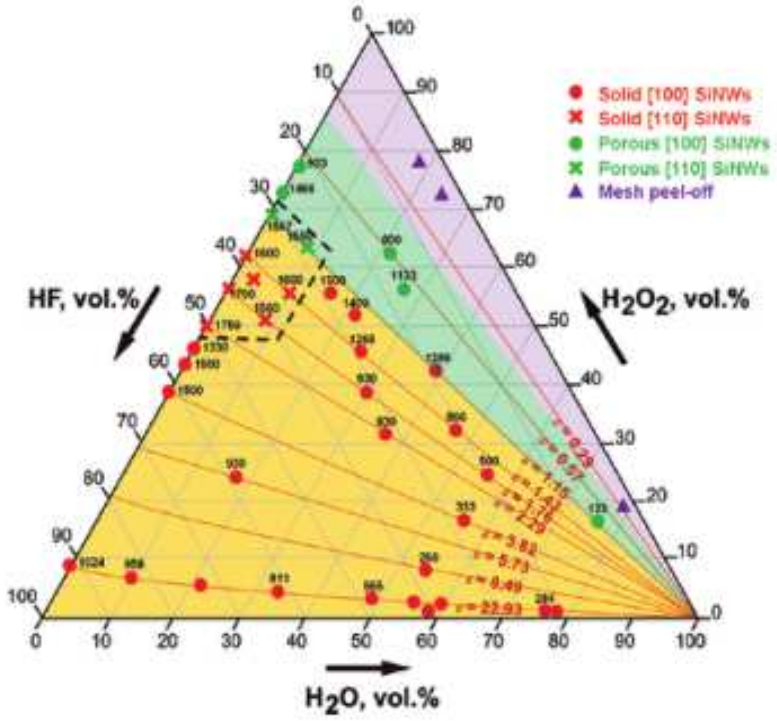

Fig.3. 2: The evolution of the etch rate [nm/min](number on symbols), nanowire axial orientation and morphology (porous or solid) during MacE of Si(100) in ternary mixtures of 46%wt HF, 35%wt H_2O_2 and H_2O at room temperature by Lee et al. The region enclosed by dashed line corresponds to the etchant composition window where etching proceeds along slated [110] directions.

The basic idea is that in MAcE of Silicon, the movement of the etching front is a net consequence of two competing events: the injection of positive holes into bulk silicon through the metal-silicon quasi-Schottky interface and removal of oxidized silicon by HF from underneath the catalyst metal. The generation of holes is related to the catalytic decomposition of H_2O_2 at the interface between the bulk electrolyte and the catalyst metal surface, so the amount of holes injected into silicon is proportional to the H_2O_2 concentration or its decomposition activity.

Porous nanowires are obtained in highly oxidative solutions ($0.3 < \varepsilon < 1.15$) because removal of oxidized silicon will take place slowly due to the limited amount of HF and the excess holes (due to the high [H_2O_2]) can diffuse away from the etching front to lattice defects and dopant sites on the surface of already formed SiNWs.
The dominant etching direction is the [001] according to the back bond breaking theory except that in the region enclosed with the dashed line in fig. 3.2 where slanted nanowires on (100)Si (along [110] directions) were obtained. This condition is achieved in highly concentrated solution, (for $\varepsilon \cong 1$) when oxidation and removal of silicon atoms would occur with great rapidity and also the planes with more silicon back bonds to polarize will be etched.

(b) Etching directions of non (100) Si

If the etching direction of (100)Si is generally normal to the surface, that of non (100) substrates, e.g. (110) and (111), is still unclear, the data reported in the literature are sometimes contrasting because of the lack of a detailed understanding.
The etching of non (100) substrates is affected by several factors: the metal catalyst distribution, the metal thickness, the doping level of substrates etc. As a result, the orientation of the SiNWs in non (100) oriented substrates ranges between the inclined and the normal to the surface directions, according to the adopted chemical-physical experimental parameters.
The etching direction of (111) Si depends also on the oxidant [H_2O_2] concentration in the solution. The experiments so far reported in the literature are all performed with $\varepsilon >> 1$, and solid nanowires are obtained. The oxidant concentration varies between 0.1M and 0.001M (while the [HF] is about 5M]. In the latter case, the usual crystallographic preferred [001] etching directions prevails, and the etching proceeds along inclined directions with respect to the surface normal whereas it gradually moves

towards the normal to the surface with increasing the oxidant concentration till 0.1M.

The change in the etching direction with oxidant concentration has been explained by a combination of the surface state of Si in different solutions and the back bond strength.

It has been proposed that, by analogy to the anodic electrochemical etching of Si, there are two competing dissolution processes [86]. The first one is the direct dissolution (1) of silicon and the second one is Si oxide formation, followed by the dissolution of oxide (2, 3).

$$Si + 4HF_2^- \rightarrow SiF_6^{2-} + 2HF + H_2 + 2e^- \qquad (1)$$

$$Si + 2H_2O \rightarrow SiO_2 + 4H^+ + 4e^- \qquad (2)$$

$$SiO_2 + 6HF \rightarrow H_2SiF_6 + 2H_2O \qquad (3)$$

If the concentration of H_2O_2 is very low, the etching is limited by holes generation, and the direct dissolution of Si by HF proceeds (1), according to the model proposed for porous silicon generation. Consequently the etching direction of Si should be discussed by considering the back bond strength [ref Smith and Collins]. As a result the [001] etching directions prevail in non-(100) substrate.

In contrast, (2, 3) prevail if the concentration of H_2O_2 is sufficiently high so that the rate of Si oxide removal by HF is slower than the formation rate. In this case the etching front is completely covered by Si oxide, the etching of Si proceeds through the dissolution of the Si oxide layer by HF which is a well-known isotropic process.

In synthesis, in the aforementioned models, the tuning in the etching directions is related to the interplay of the rate of oxidant consumption with that of oxidant supply. When the last is the limiting factor the etching takes place along the preferred crystallographic orientation, i.e. along the [001] [87].

3.1.2 The influence of metal morphology

It has been found that the etching mechanism for non (100) oriented substrates is also related to the deposited metal morphology.
The results presented in this paragraph have been obtained in etching solution with ε >>1 with constant oxidant content for each solution, to allow the direct observation of catalyst shape influence.
Lee et al. studied the sinking behavior during MAcE of Au particles. Experiments demonstrated that there is a strong correlation between the metal amount and the morphology of the etched holes. The results are showed in fig. 3.3 [88-90].
In contrast to the pores formed with isolated Au particles of few µm size (straightly oriented along the [001]) (fig. 3.3a), those formed with Au deposits consisting of a few Au particles (fig. 3.3b), were crooked. When the deposits consisted of an aggregation of a large number of Au particles (fig. 3.3c), more than 10, the pores again grew along the [001] direction. A different etch rate was also observed between the first two cases and the latter (30% etched length between fig.s 3.3 (a-b) and fig. 3.3c). It was speculated that the faster boring speed for the aggregates is attributable to the large surface area of the 3-dimensionality aggregated structures that allowed the reduction of H_2O_2 in a larger amount per unit area. In the etching experiments with non-spherical Au particles (fig. 3.4a), the pores formed showed different shapes (fig. 3.4 a-b). The irregular surface morphology of the Au particle induced probably spatial variations in the supply of positive holes to Si, leading to the different etching rate on a particle. As a result of these fluctuations the etched holes have an irregular profile.

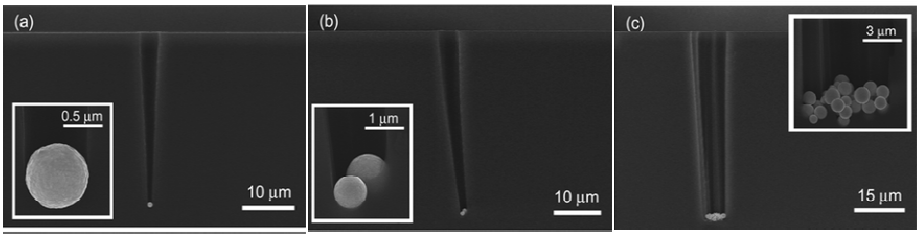

Fig.3. 3: Sinking behavior for Au particles during MacE of Si(100). (a) Isolated cluster etched silicon along [100]; (b) etch pits generated from aggregates of few clusters were crooked; (c) etch pits generated from aggregates of large number of clusters were again along the [100].

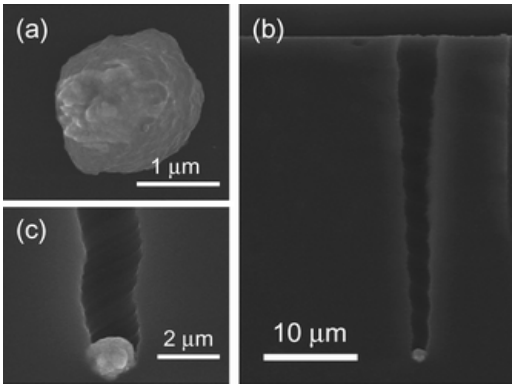

Fig.3. 4: Etch pit from a metal particle with irregular shape. [90]

The HRTEM (High Resolution Transmission Electron Microscopy) performed by Sharma et al. [91] on the AgNP/Si interface after sinking in silicon (see fig. 3.5) revealed a thin oxide layer in Si of varying thickness between the points 1 and 2 of fig. 3.5b. The corresponding EDX (Energy-dispersive X-ray spectroscopy) spectra confirmed the different Oxygen content between the two analyzed areas.

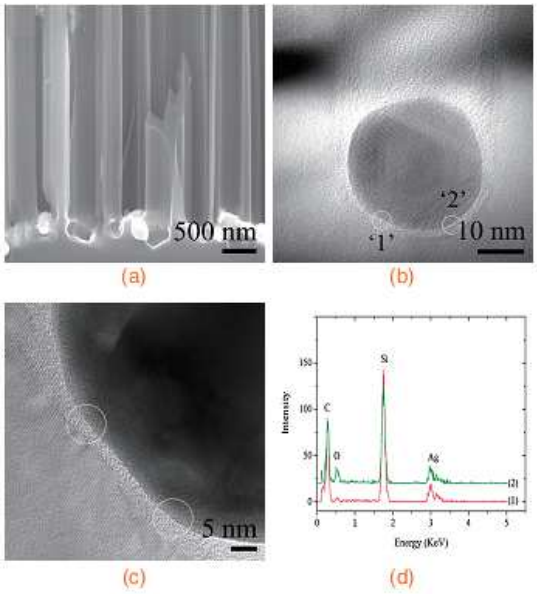

Fig.3. 5: (a) Cross section SEM of SiNWs obtained with etching in aqueous solution with 4.8M HF and 0.3M H2O2 of (100)Si loaded with a 5nm thick silver film; (b) HRTEM of a single Ag particle at the bottom of the etched pit; (c) enlarged view of (b) showing a variation in the oxide thickness and (d) TEM-EDX spectra at locations 1 and 2 of (b) showing the different oxygen content.

The observed variation in the oxide thickness means that the holes injection and also the associated electric field generated at the metal/semiconductor contact, are not uniform along the whole interface.

In the experiments performed by Hildreth et al. [92] it was shown that silver nanorods randomly distributed on silicon substrates had a cycloid path during MAcE of Si(100)(fig. 3.6).

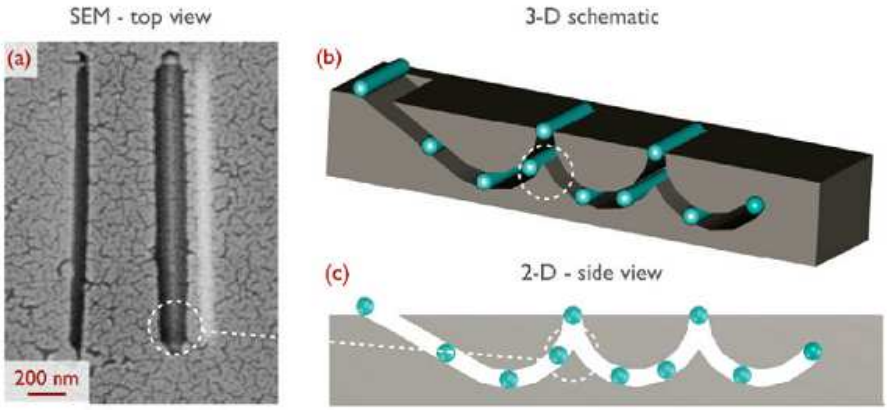

Fig.3. 6: Cycloid path for silver nanorods from the experiments of Hildreth et al.

Chang et al. [93] found that the etching direction in non (100)Si could be related to the ratio between the metal thickness and its in-plane extension. Their results are shown in fig. 3.7.

They demonstrated that it is possible to tune the etching direction of non (100) substrates by simply changing the features of the metal pattern employed as catalyst. In their experiments the etching behavior of Si(100), (110) and (111) with three different metal distributions was treated:

1. Au nanoparticles deposited with e-beam evaporation, 2nm thick;
2. Pattern of circular nanoholes with 22nm diameter and a pitch of 13nm, 12nm thick (obtained with Block Copolymer Lithography);
3. Pattern of circular nanoholes with 140nm diameter and a pitch of 260nm, 12nm thick (obtained with Interference Lithography).

The etching proceeded always along the normal to the surface for the (100) substrate (fig. 3.7 a-d-g). For the two other orientations under investigation a change in the etching direction occurred with the features of metal pattern. It was [001] for configurations 1 and 2 (see fig. 3.7 b-e for Si(110) and fig. 3.7 c-f for Si(111)). The substrates etched with metal catalyst of

configuration 3 showed instead vertical nanostructures (fig. 3.7d for (110)Si and fig. 3.7g for (111)Si).

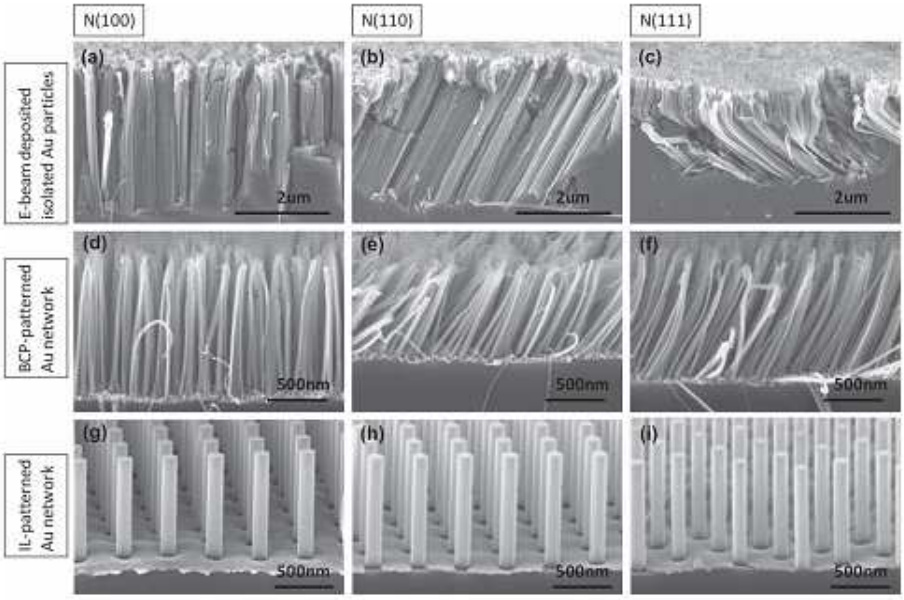

Fig.3. 7: SEM images after MacE of silicon substrates with three different crystallographic orientations and Au catalyst of three different morphology. (a,b,c) Si (100), (110) and (111) respectively loaded with isolated clusters. (d,e,f) the same as (a,b,c) but with a metal mesh with small holes spacing and (g,h,i) with large holes spacing.

The ratio between the film thickness and its in plane extension is about 1 and 20 for configurations 2 and 3, respectively. For morphology 1 this ratio is >10 but the influence of their irregular shape and non uniformity size distribution could affect the etching direction.

From the reported data presented in this section it is clear that there is a strict correlation between the metal morphology and the etching direction.

3.2 Experiments

The samples obtained after the deposition step on bare Si(100), Si(111) wafers and macro-patterned Si, as deposited in chapter 2, were dipped in an etching solution (named II) with 0.1M H_2O_2, 4.8M HF.
The ratio ε is about 50, in order to obtain solid nanowires. The oxidant concentration, instead should guarantee vertical etching on both orientation, as speculated in paragraph 3.1.1 (b).
Immersion time was for 30min for all the samples, to allow also the observation of possible changes in the etch rate.
The samples were analyzed with SEM to have a global vision on the etch depths and uniformity of the obtained nanoholes. Some samples (Si(100) and Si(111)) were also analyzed with cross section TEM, to elucidate the etching directions and the depth at which silver nanoparticles stopped their sinking in silicon. As it will be shown later, it is not the same for all of them.

3.3 *Etching of Si(100) and Si(111)*

The SEM cross section investigations showed that different etching regimes could be identified. For the (100)Si two sinking behaviors have been detected:

i(a). For deposition times varying from 5 to 120s, the silver nanoparticles during etching follow inhomogeneous paths in all the [001] directions;

ii(a). For 160s deposition time, they sink uniformly in silicon along the normal to the surface.

Etching of (111)Si shows other interesting features, indeed:

i(b). For deposition times ranging from 5 to 80s, etching occurs along the [001] directions, as for (100)Si in i(a);

ii(b). For 120s deposition time, etching still occurs along the [001] directions, but the sinking behavior becomes locally correlated and uniform etched domains could be detected;

iii(b). For 160s deposition time, etching of loses its anisotropic nature and proceeds along the normal to the surface.

3.3.1 Morphological characterization of etched (100) and (111)Si.

The SEM cross section of (100) Si substrate, treated in solution I for 5s and in solution II for 30min is shown in fig. 3.8. The depth of nanoholes produced by AgNPs motion is not uniform. The etching trajectory for most of them changes suddenly from vertical to horizontal direction, still along the [100] axes, as shown by the XSEM enlarged magnification. The silicon surface is covered with a porous layer, 1µm thick, generated by the uncorrelated paths of nanoparticles. Some clusters instead, etch silicon along the normal. As a result, the global thickness of the etched layer is about 11µm.

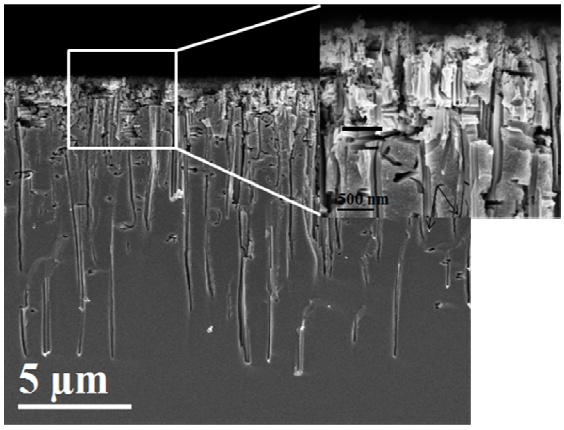

Fig.3. 8: SEM cross section along the (110) plane of (100)Si dipped for 5s in the silver based solution and etched for 30min. Two regions could be clearly detected: a thin porous layer 1µm thick (as reported in the enlarged magnification) and well defined pores that reach the bottom of the etched region, whose thickness is about 10µm.

A detailed XTEM investigation was performed on the same sample. As explained, these analyses allowed the silver clusters' localization in silicon after etching in silicon. They are reported in fig.3.9. Many AgNPs (black dots) do not sink deep in the bulk silicon but remain confined in the surface porous layer while others are located at the bottom of the etched region.

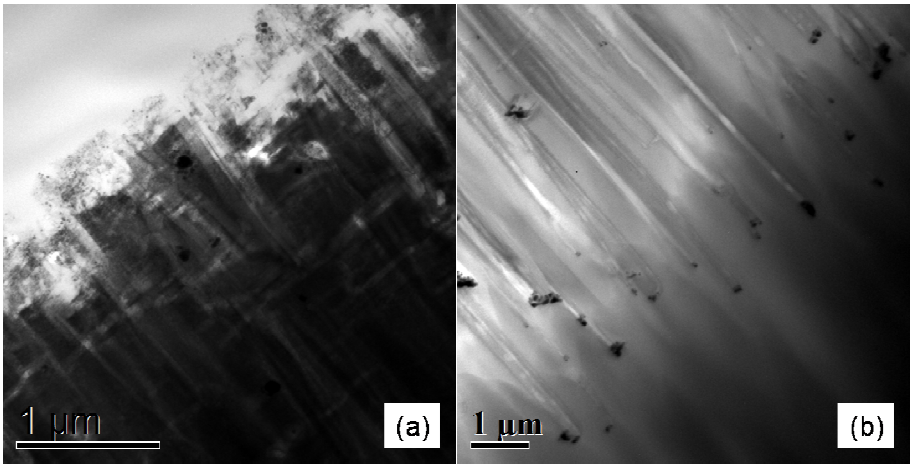

Fig.3. 9: TEM cross section of sample reported in fig. 2.3a(silver deposition) and 3.8 (SEM cross section after etching). The analysis is useful to detect the etch depth of single silver cluster (black dots). Some of them are confined in the porous layer in the upper part (a) while others reach the bottom of the etched region (b).

In the case of (111) Si substrate the dominant etching direction is still the [100] with uncorrelated etching trajectories. The XSEM images of the sample are shown in fig.3.10.

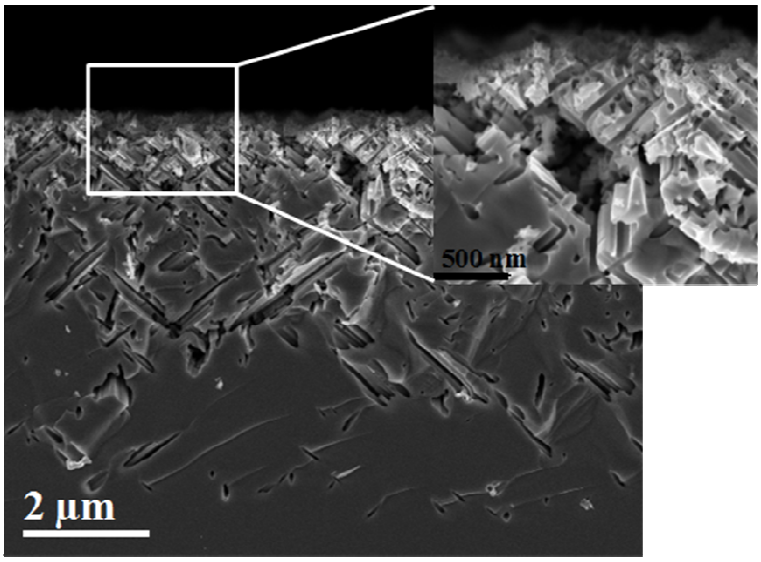

Fig.3. 10: SEM cross section of (111)Si (dipped for 5s in the silver based solution) etched for 30min. Two regions could be clearly detected: a thin porous layer, 1µm thick (as reported in the enlarged magnification) and well defined pores that reach the bottom of the etched region, whose thickness is about 6µm.The length of pores is about 10µm.

As for (100)Si the silicon surface is covered with a porous layer, 1µm thick, while the global thickness of the etched region is about 6µm. But, if we consider that particles moved along inclined directions, i.e. the [001], we could estimate that the total length of the path is again about 10µm, as for (100)Si. The cross section TEM, reported in fig.3.11, confirm that some Ag clusters (black dots) are located in the porous layer, while other in the bottom of the global etched region.

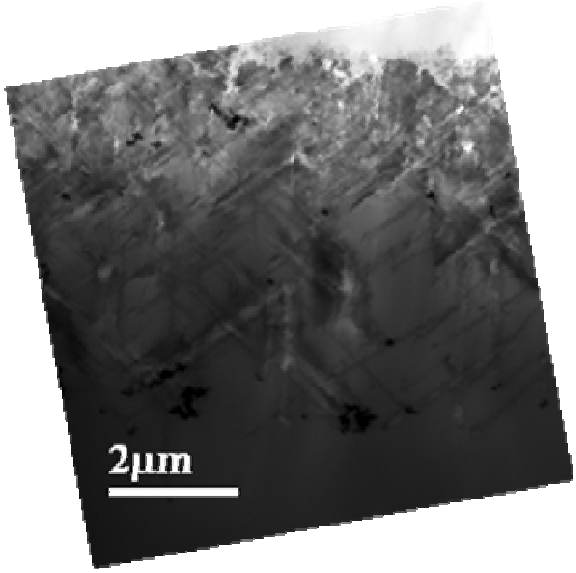

Fig.3. 11: TEM cross section of sample reported in fig. 3.10 showing silver clusters located at various distances from the top surface.

The morphology and structure of the SiNWs after etching the samples previously dipped in solution I for 40s and 80s (not shown), are quite similar to those illustrated by fig. 3.8 and fig. 3.10 respectively.

With increasing the coverage and the mean area of AgNPs (for 120s deposition time), the etching behavior of (100)Si is still in the regime described by i(a). The cross sections SEM and cross sections TEM are shown in fig 3.12 a and b respectively

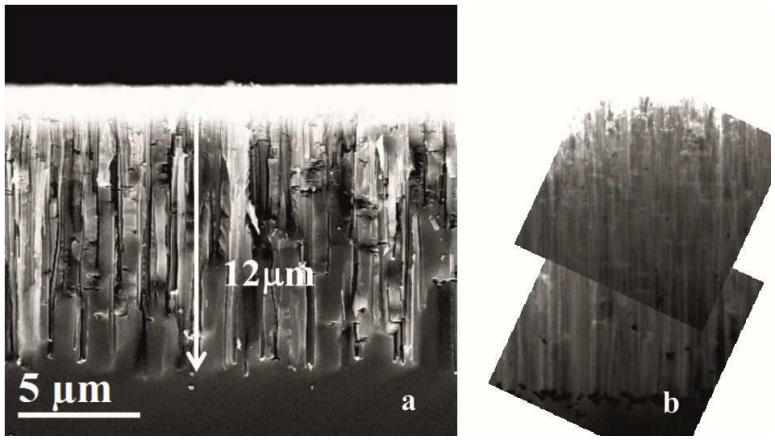

Fig.3. 12: (a) SEM cross section and (b) TEM cross section (see the AgNPs at the bottom of the etched region) of Si (100) substrate previously immersed for 120s.

The porosity of the surface layer decreases, while more particles reach the bottom of the global etched region that extends always for about 12μm. In these conditions only few particles stayed (see the AgNPs at the bottom of the etched region of fig. 3.12b) in the upper part and their etching paths show an increased degree of correlation.

A particular behavior is detected for the (111)Si treated for 120s in the deposition solution. The cross section SEM is reported in fig.3.13a , the cross section TEM in fig 3.13b.

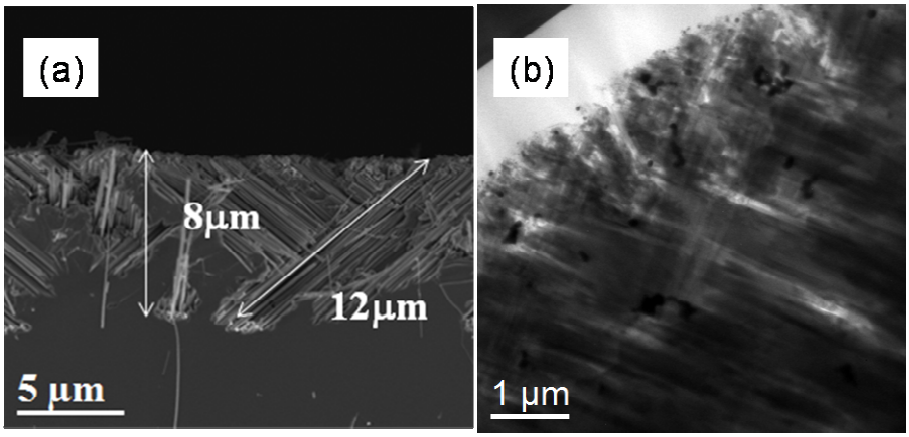

Fig.3. 13: (a) cross section SEM of (111)Si dipped for 120s in the Ag based solution and etched for 30min. Well defined domains of SiNWs aligned along the [001] are detectable. The cross section TEM (b)shows the Ag clusters in the etched layer.

The etching direction is still the [100] or an equivalent but a collective sinking motion is taking place on (111) Si oriented substrate. Well defined domains of several microns in extension with SiNWs aligned along the [001] directions are seen in the XSEM of fig 3.13a. The zig zag movement occurs along the [100] direction and the length of the etched straight lines is also of few microns. In this case, the XTEM analyses showed the presence of the porous top layer and the AgNPs located in this region.

As a matter of fact the total length of the etched material, in all the analyzed cases, ranges between 11 and 12 microns with a rate of about 370nm/min in agreement with literature data [27] for the same experimental conditions.

The suppression of lateral path (case ii (a) and iii(b) respectively)is achieved for the samples dipped for 160s in solution I, i.e. for a coverage of about 70%. The sinking takes place only in the vertical direction as clearly shown by the cross section SEM and cross section TEM of SiNWs on (100)Si reported in fig.3.14a and b respectively. All the silver clusters are located at the same distance from the top surface. The same behavior characterizes the etching of (111) Si as shown in fig. 3.14c and d respectively. The SiNWs

are perfectly aligned along the vertical direction and the sinking is uniform and correlated. No AgNP is found on silicon surface.

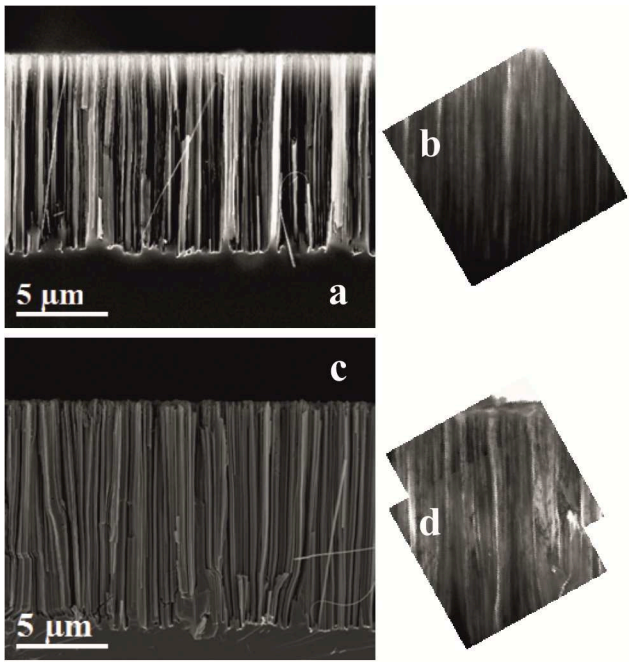

Fig.3. 14: (a) SEM cross section of Si (100) dipped for 160s in the silver based solution and etched for 30min; the inset (b) shows the TEM cross section; (c) same as (a) but for Si (111) oriented substrate, the inset (d) shows the TEM cross section.

As already mentioned the etch rate is the same in all the investigated cases, it is independent on the substrate orientation and on the silver clusters coverage. The latter influences then the etching direction but not the rate, the nanowires' length is unchanged.

3.3.2 Morphological characterization of etched macro-patterned Si

A same coverage dependent etching is obtained on macro-patterned Si.
The etched surfaces are reported in the cross section SEM of fig. s 3.15a-d

for the (100) plateau and of fig. s 3.16a-c for the (111) walls respectively. Near the upper transition region, where the AgNPs are large and interconnected, etching direction is normal to the surface, no matters the crystallographic orientation of the treated areas is. This is clearly shown in the enlarged magnification XSEM image of fig. 3.15b and in the dashed region of fig. 3.16a, where SiNWs are perfectly aligned and no horizontal etching is detected. With decreasing Ag amount, the NPs' motion becomes uncorrelated and the etching trajectory for most of them changes suddenly from vertical to horizontal directions, still along the [100] axes as shown in fig. s 3.15(c-d) where the pits on the SiNWs walls are due to the horizontal motion of AgNPs.

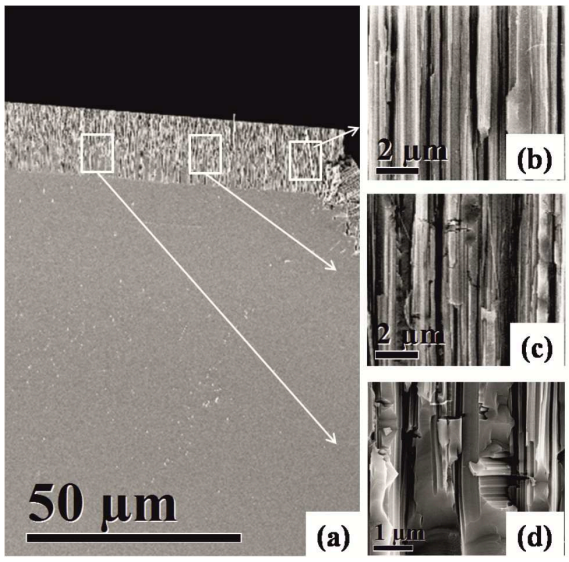

Fig.3. 15: The SiNWs obtained from silver distribution on (100) plateaux of macro patterned Si. The etching direction depends on silver coverage and is normal to the surface for high coverage as in (b) at about 10µm from the upper transition region; with decreasing silver coverage and cluster extension, the sinking behavior becomes uncorrelated and horizontal etching occurs. The holes of (c) and (d) are due to the horizontal path of particles.

For the (111) surface with decreasing silver, etching starts in the normal

direction and then moves towards the [100] (fig. 3.16b). In the near bottom transition region where Ag amount was very low, some particles move along the [001], others only generate a porous layer on the etched surface (fig. 3.16c).

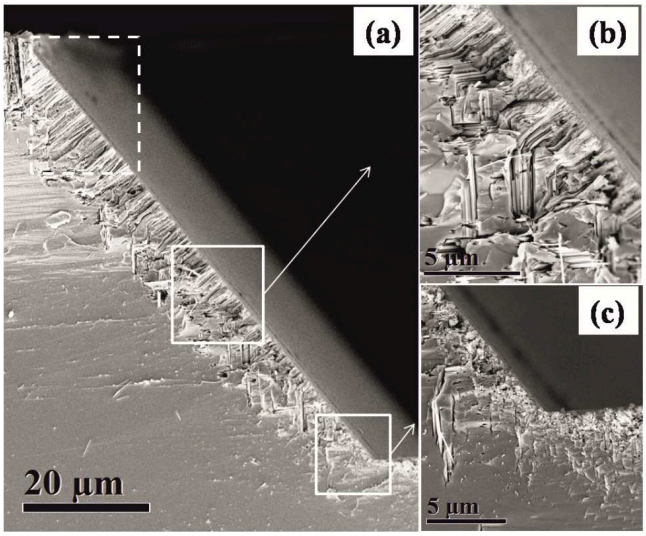

Fig.3. 16: SiNWs obtained on the (111) wall of macro patterned Si. the etching direction for (111) oriented substrate depends strongly on silver coverage. It's normal to the surface for high coverage an extension of clusters, while it turns toward the [001] with decreasing silver amount.

In the macro-patterned Si the etched depths on the (100) and (111) surfaces differ. This could be related to the strong variation of silver coverage and to its influence on the mass transport illustrated in chapter I. In fig. 3.16c, the lower transition region after etching is reported. The thickness of the etched porous layer is the same for (111) (tilted) and (100) (horizontal) surfaces.

3.4 Discussion

As explained in the previous sections, metal assisted etching starts with the

reduction of oxidant at the AgNP electrolyte interface; the holes, here generated, diffuse through the metal and are injected into the Si in contact with Ag. So Si is oxidized in the contact area with silver and then removed by HF. The AgNPs gradually sink into the silicon forming pores and etching may occur as a localized electrochemical process. Microscopically local anode (silicon) and cathode (metal) sites form on the etched surface with local cell currents flowing between them during etching. This current is due to holes injected into the silicon valence band from the metal particle to silicon. Since the holes are provided by the reaction of oxidant with the metal particle, the etching depends on the rate at which the oxidant can generate holes under the metal particles.

The etching proceeds slowly on the uncovered silicon surface because the oxidizing agent preferentially captures electrons from the Ag particles, thanks to their strong catalytic activity for the cathodic reaction, so the silver role is to increase the current density, accelerating the dissolution of silicon. The details about the chemical reaction are reported elsewhere [see chapter 1].

The experiments indicate that the sinking directions depend on surface orientation and silver coverage.

According to literature the etching direction is determined by the relation between holes generation and oxidized silicon removal (see paragraph 3.1).

In our experiments, the variation in the etching direction could not be related to the oxidant concentration, since the [H_2O_2] and [HF] chosen guarantee fast holes generation and removal rates. The etching solutions the same for all the analyzed samples, consequently the etch rate is constant, as measured from the XSEM images reported in the previous section. The oxidant concentration does not determine the change of etching direction from the [001] to the normal to the surface.

By crossing the analyses on the Ag particle distribution reported in chapter 2 with the etching directions shown in the previous paragraph, one may affirm that the change in the etching direction is related to the surface coverage and to mean size of particles.

In spite of the high H_2O_2 concentration adopted, for low coverages the AgNPs' sinking is anisotropic for both oriented substrates.
In the (100) Si substrate at small clusters' size and low coverage the etching proceeds both in vertical and horizontal [100] directions. With increasing Ag amount and coverage (70%) the nanoparticles sink all together along the vertical direction. In the (111) Si substrate isolated nanoparticles sink alongl the equivalent [100] directions following an irregular path; when they begin to coalesce, domains of Si nanowires, all aligned along the [100] directions, are formed. For silver clusters well interconnected (70% coverage), the etching proceeds along the vertical direction.
This dependence on metal morphology is confirmed by the experiments performed with the macro-patterned Si. Indeed, thanks to the self selective deposition mechanism, areas with decreasing silver amount were obtained. When the coverage is high and the AgNPs are well interconnected, etching occurs along the normal to the surfaces, for both analyzed orientations. With decreasing particle's size, trajectories become uncorrelated and etching along the [001] directions occurs. The etching directions were maintained also lowering the oxidant concentration to 0.002M. With this value [001] etching for (111) surfaces was expected. Instead the only observed effect was an obvious decrease of the etch depth (see fig. 3.17).

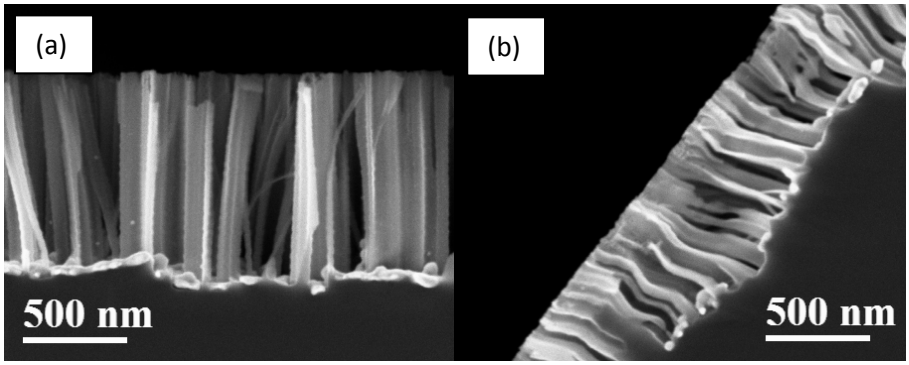

Fig.3. 17: (a) (100) Plateau and (b) (111) walls in the near upper edge region, etched for low oxidant concentration, 0.002M H_2O_2. The etching directions are normal to the surfaces.

According to the phase diagram, the Ag-Si system is a binary eutectic system, with negligible mutual solubilities of Ag and Si in the solid state, with no solid reaction and no stable phase at the interface [94].
To explain the influence of silver nanoparticles on the morphology of nanowires some other factors should be considered [23, 95-97]:

- An interaction between particles responsible for the collective motion;
- The size of the particle is responsible for the suppression of lateral path (also in terms of ratio between film thickness and in plane extension);
- The interaction between silver and H_2O_2 that might modify the silver nanoparticle shape during etching.

It has been assumed that a distance dependent interaction between Ag particles is present. This makes them cooperatively move in the same direction. The origin of such interaction is not understood. Possible reasons might be image force between silver particles, or and the influence of band bending at the Silver /Si interface from neighboring silver particles which affects carrier transfer through the Silver /Si interface. The range of influenced domains can be larger than 100µm [23].
Each single Ag nanoparticle could catalyze the etching of the contacted silicon freely in random downward directions, not only vertically, because a single particle is not restricted by its surroundings. This unrestricted configuration is depicted in fig. 3.18.

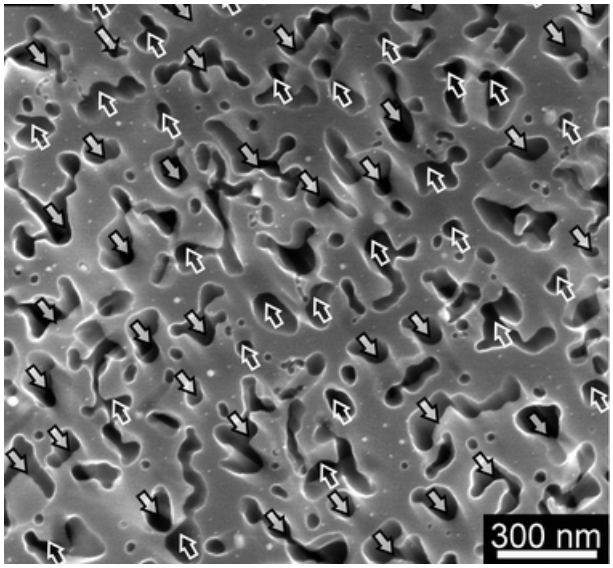

Fig.3. 18: Motion tracks of unrestricted silver particles. In absence of a geometrical constraint they sink along the [001] directions.

Different parts of the discontinuous metal film tend to move along the [001] directions at random, depending on the defects site on the surface of the substrate, the shape or profile at the edge of the silver pores or the silver mesh, and the interaction between the substrate and the silver particles.

However, in the net-like structure of 160s Ag nanoclusters, the interaction among clusters reduces the ability of each cluster to move freely, resulting in the collective sinking of Ag clusters vertically.

It can also be found that while maintaining the network structure, some Ag clusters become slightly smaller during etching, and some particles are detached from the big clusters. In fig.3.19 a single AgNP detected at the bottom of the etched layer is shown. The surface of metal cluster is rough and porous. Silver in fact easily oxidize and dissolve in H_2O_2 solution.

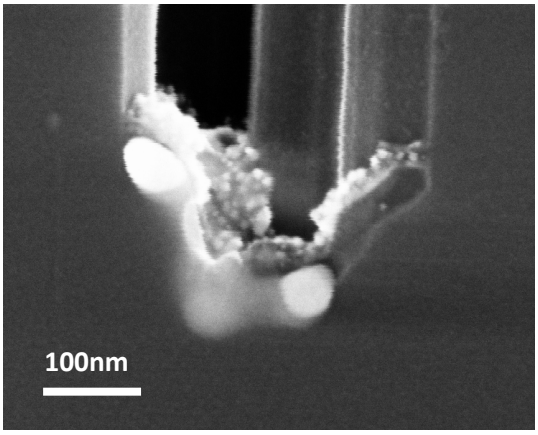

Fig.3. 19: A silver nanoparticle after etching in H_2O_2 based solution. Its surface is not smooth because silver oxidized in H_2O_2

Along with the etching process, these variations in the roughness of Ag result in the change in morphology of Si nanostructures, from an irregular shape at the early stage of etching to a regular shape after etching. However, what exactly causes these changes is yet not clear.

3.5 Application of the achieved metal positioning for the fabrication of SiNPs: MAcE on micro-patterned Si.

The experiments on macro-patterned Si have shown that accurate metal positioning could be achieved by exploiting the self selective deposition mechanism on contiguous different orientation substrate.
The change in the etching directions with metal distribution instead, showed that lowering the silver coverage a thin surface porous layer is formed.
These two findings have been exploited performing MAcE on a micro-patterned substrate, fabricated with anisotropic etching in alkaline solutions, where the extension of (100) and (111) surfaces were strongly reduced, in order to enhance the different metal cluster density and the strong reduction of etch rate on the less covered areas.

An ordered metal mesh has been achieved on Si wafer that resulted, after the subsequent etching, in the formation of ordered nano-pillars.

3.5.1 Fabrication of micro-patterned Si

The micro-patterned Si was fabricated with projection lithography (Canon 5X Stepper I-line, λ=365nm), the mask (SiO_2 85nm thick) was made of square windows, 0.6µm wide and with a pitch of 1µm.
Pyramidal holes, 0.9µm wide, and 0.7µm deep, (with a pitch of 1µm) were realized by KOH (20%wt, 50°C for 45min) etching. The walls are {111} planes, while the horizontal plateaux (0.1µm wide), are {100} planes.
A schematic picture of micro-patterned Si is given in fig.3.20.

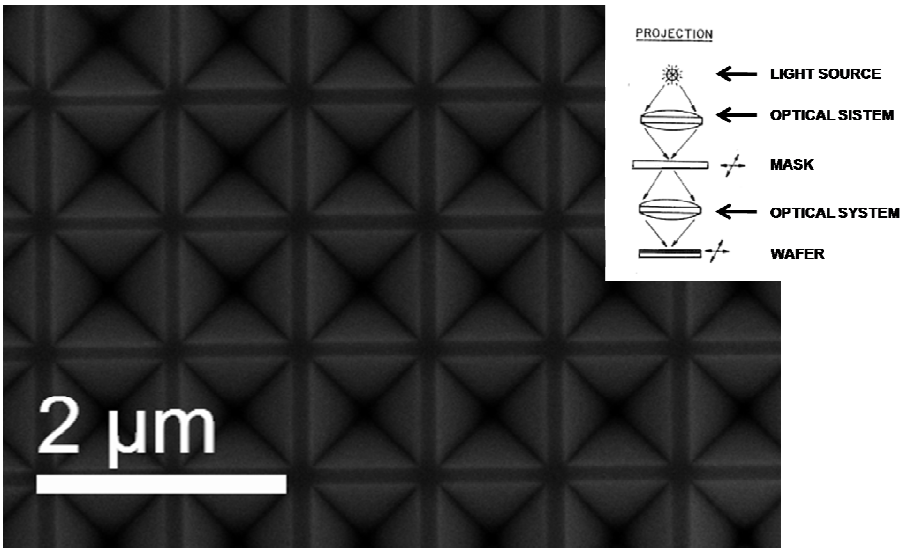

Fig.3. 20: Micro patterned Si obtained with projection lithography (see the inset). The pyramidal holes are 0.9µm wide and 0.7µm deep. The (100) horizontal plateaux are 0.1µm wide. The inclined walls are the (111).

3.5.2 Morphological characterization of micro-patterned Si

Since metal deposition is achieved also by controlling the surface bond

density, a detailed morphological description is required to understand the expected metal distribution. In the micro-patterned silicon substrate the upper notch is absent. As explained in chapter 2 indeed, the roughness of the undercut regions after etching with KOH is related to the adopted experimental parameters. In this case, etching conditions were “soft”, i. e. low temperature and short time.
The transition region spans few tens of nanometers, with a curvature radius of 10nm about. As for the macro patterned Si, it is characterized by a higher density of surface bonds, as depicted in the HRTEM of fig.3.21a.

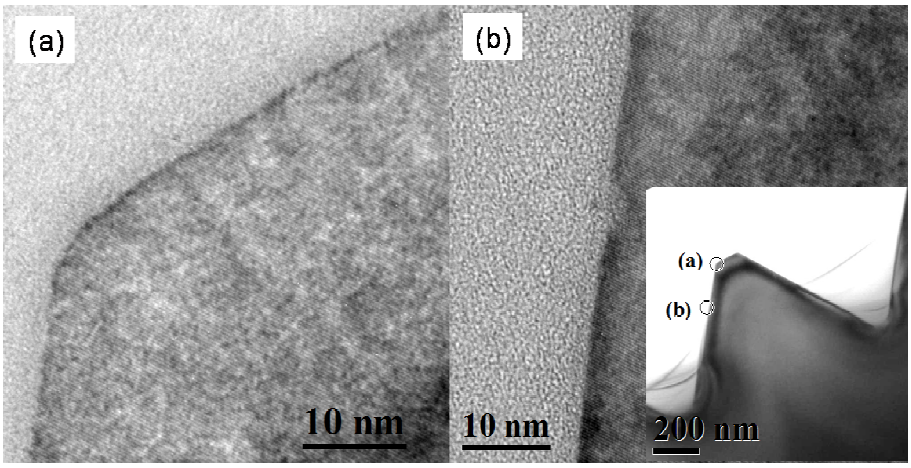

Fig.3. 21: HRTEM micrographs of (see the circles the inset) (a) transition region of micro patterned Si and (b) (111) walls . The variation in terms of surface bond density and roughness between (a) and (b) is marked.

For comparison the smooth (111) plane of pyramidal holes is reported in fig 3.21b. As clearly shown the surface roughness is very high in the transition region, also for the micro patterned Si. On the same substrate another region of interest could be found: the joint lines among the four {111}. It is reasonable to expect a low surface bond density here.

3.5.3 Experiments

The Silver deposition on micro-patterned Si (fig. 3.20), square edge 900nm and 700nm depth, (solution I with 0.005M $AgNO_3$ and 4.8M HF) was performed for different times (10, 40 and 120s) to investigate the AgNPs evolution.

The AgNPs distribution is reported in fig. 3.22. The samples were dipped in solution I for 15s (fig.3.22a), 40s (fig. 3.22b) and 120s (fig. 3.22c) respectively. The (100) plateaux of 100nm width in between the two contiguous edges are fully covered with large silver clusters for all the adopted deposition times. The figures clearly show that metal deposition occurs preferentially at the two lateral edges. In between them the density of AgNPs is reduced in spite of the small width of the plateaux.

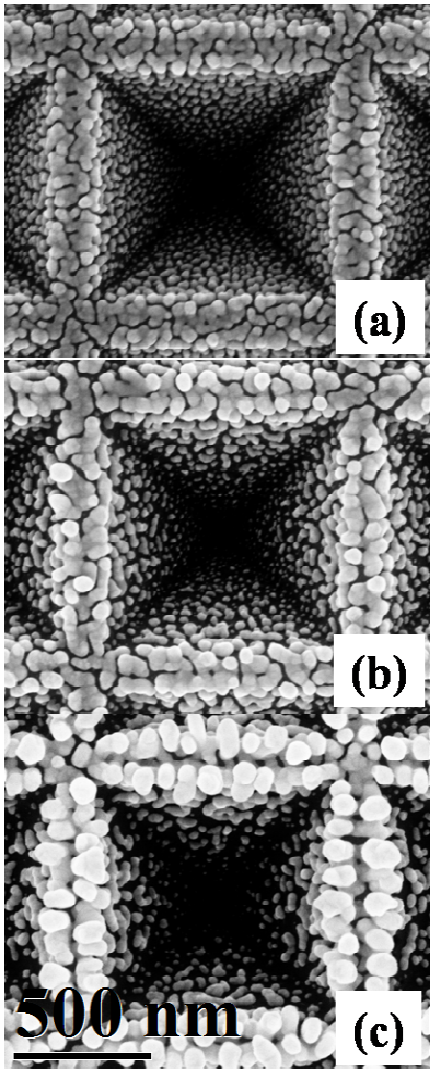

Fig.3. 22: AgNPs distribution on micro patterned Si for 15s (a); 40s (b) and 120s (c) deposition in solution I

The metal deposition is also in this case orientation dependent, it is faster on the [001] planes and on convex surfaces where a large number of surface bonds is present. On the bottom of the pyramidal holes and on the joint lines of the four (111) lateral faces it is inhibited, as in the case of the

concave area of macro-patterned Si.
A much lower number of surface bonds is in the latter case required to match the transition region for geometrical reasons.
The deposition step was also performed in a stirred solution, the same spatial trend was found for the distribution of Ag clusters (see fig.3.23). A reduced immersion time was required.

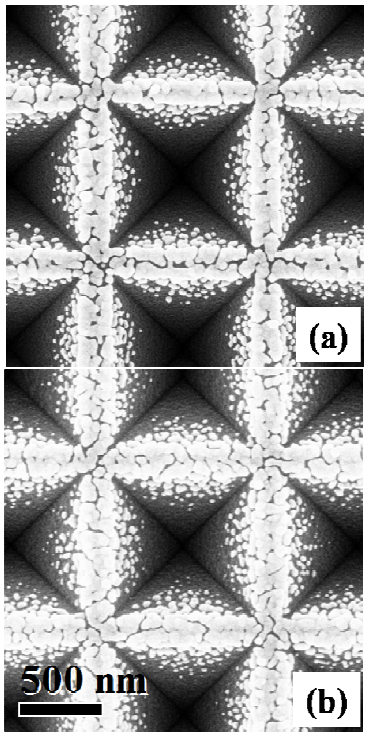

Fig.3. 23: AgNPs distribution on micro patterned Si obtained by immersion in stirred solution I for (a) 15s and (b) 30s. The same trend of fig. 3.22 for metal positioning could be observed.

Etching of the substrate loaded with AgNPS (120s deposition time) occurred in the usual solution (0.1M H_2O_2 and 4.8M HF) for 30min. A SEM investigation was carried out to evaluate the morphology of the obtained structures. Some samples were also analyzed with XTEM, to establish the

position of AgNPs after sinking in Si The [100] plateaux, fully covered with the silver clusters were completely etched, leading to the fabrication of an ordered array of Si nanopillars uniformly distributed over the entire substrate (fig. 3.24a). To investigate the etching trajectory of Silver clusters on the pyramids' walls the top view cross sections of nanopillars were analyzed by TEM (fig. s 3.24b-c). The XTEM images in the near top (fig. 3.24b) and in the near bottom (fig. 3.24c) section of pillars respectively were recorded. The analyses show that the sinking took place along the vertical, i.e. the [001] directions, since the AgNPs coverage and in plane extension were low on the lateral (111) planes. The number of etched holes observed in fig. s 3.24b (top) and 3.24c (bottom), due to the AgNPs that sink in Si, decreases with the distance from the tip. This means that the AgNPs sinking trajectories are uncorrelated. The etched silicon depth is at least one order of magnitude higher than the height of the pyramidal holes (about 10μm versus 0.7μm). The size of the edge of the nanopillars is about 0.6μm.

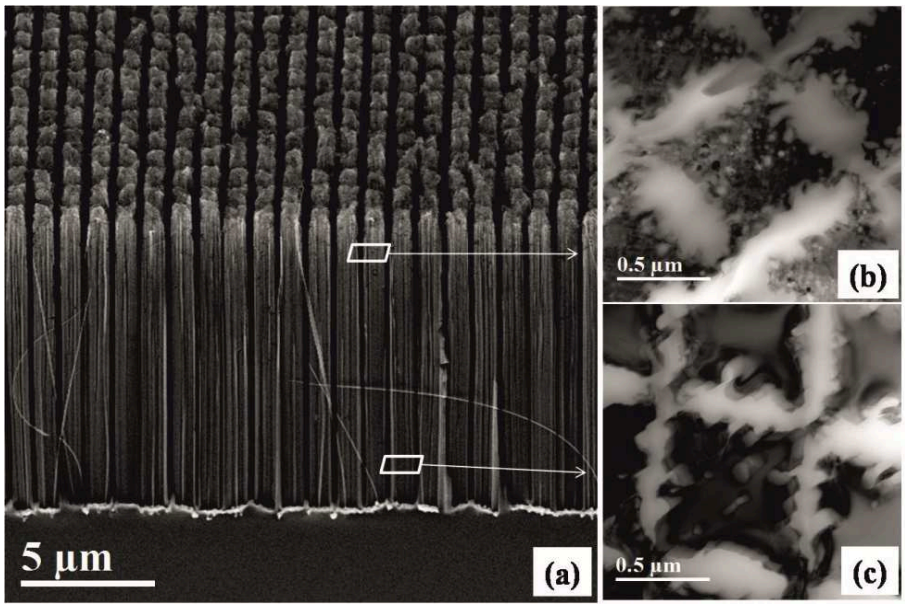

Fig.3. 24 (a) Si nano structures obtained after etching in solution II of the micro patterned Si. The ordered metal distribution, resulting from the self selective mechanism, produced an ordered array of silicon nanopillars thanks to the dependence of the etch rate and trajectory from the metal distribution; TEM top view of the upper (b) and lower (c) sections showing a decreasing porosity for pillar due to the uncorrelated trajectories of small particles on (111) planes.

Summary

MAcE has been performed on the silver loaded substrates of chapter 2. The concentration of etching solution (0.1M H_2O_2 and 4.8M HF) was enough to ensure a fast oxidation and removal of the Si underlying the silver particles. The results show that the etching direction is strictly related to the metal morphology. For both (100) and (111) substrates it has been found that when silver particles are small and isolated, they sink is silicon along the [001] directions with uncorrelated trajectories. When the silver coverage exceeds the 70% and the mean distance between the metallic particles is less than 10nm, the etching direction changes from the preferred (100) to the normal to the surface. An intermediate sinking behavior was found for

(111)Si: the sample treated with deposition solution for 120s showed uniform domains of nanowires aligned along the [001].

The experiments demonstrate that when the substrate is covered with interconnected AgNPs and their in-plane extension is larger than their average thickness, the etching direction is normal to the surface, since in these conditions their lateral movement is suppressed, they lose the degrees of freedom for motion in silicon and etching is restricted, thanks to the balance of the forces acting on the AgNPs' network [21]. [41, 46-47]. So the crystallographic preferred etching direction can be suppressed simply by introducing a morphological constraint.

In addition, the observed site selective mechanism for metal deposition observed in chapter 2 was strongly enhanced when the size of the exposed areas was reduced, as for micro-patterned Si where the deposition occurred mainly on the upper edges. The (100) plateaux were indeed totally covered with AgNPs while on the lateral (111) surfaces the nucleation and growth processes were considerably reduced. By etching the silver plated micro patterned Si, it was observed that the large clusters totally covering the (100) plateaux, induced correlated etching of silicon underneath them, leading to the fabrication of an ordered array nanopillars. The metal clusters on (111) surfaces, due to their low extension, produced a thin porous layer on the top surface and sank with uncorrelated trajectories along the [001].

As a result some reached the bottom while others stayed confined in the porous layer at the top of the pillar.

Electroless metal deposition is a simple method used when there is not strict demand on metal positioning and morphology. In this chapter it has been demonstrated that instead it could be applied allowing high levels of selectivity, by simply exploiting the effects of a complex combination of substrate morphology, orientation, kind of H-terminations and mass transport limitations during electroless plating. So the convex areas, thanks to high density of surface bonds and to the enhanced mass transport on convex surfaces, will capture Ag^+ ions quickly, preventing deposition on the

smoothest and concave surfaces. The method, based on Metal Assisted chemical Etching, requires and a simple lithographic step, followed by a short dipping in alkaline solutions for the anisotropic etching. On the basis of the observed changes of the AgNPs' distribution with the scaling of the exposed areas size, it should be possible to inhibit the silver deposition on the lateral (111) walls by further reducing their extension. This experimental procedure will allow the formation of SiNPs without the presence of porous region. These features allow the fabrication on the same silicon wafers of nanopillars with 600nm size.

CONCLUSION AND FUTURE PROSPECTIVE

In this work a study on the Silver Electroless Deposition (from a solution containing Ag^+ ions and Hydrofluoridric Acid, HF) and on subsequent metal assisted etching (in a solution containing an oxidative agent; Hydrogen Peroxide, and HF) on Silicon has been carried out.

It has been demonstrated that deposition is characterized by a fast initial step. The experiments confirm that in the first 2s, nucleation has been accomplished and growth and coalescence of clusters occur.

Deposition was studied for both (100) and (111) Silicon wafers, showing a weak dependence on the substrate orientation if it is performed in an individual configuration (i. e. by single immersion of each sample).

On the other side, when the two orientations are contiguous, silver ions could be driven in a self selective way.

This mechanism occurs when areas with varying surface bond density and kind of H-terminations are contiguous, as for the (100) and (111) planes of macro patterned. A large number of clusters is found on (100) planes. The mass transport then, influence will enhance deposition on the convex interplanar regions. The self selective deposition was enhanced by scaling the size of the exposed surfaces, as for the micro patterned Si.

The subsequent etching performed on the silver loaded samples showed a dependence on metal morphology for the sinking direction.

When silver is in the form of isolated particle, it sinks along the [001] directions in silicon, no matters the crystallographic orientation of the starting substrates.

On the other side, for large and interconnected clusters the preferred etching direction is the normal to the substrate.

This trend has been explained with a change in the geometrical factors of the particles and a reduction of the degrees of freedom for sinking with the growth of their in plane extension. Effects due to the dynamics of mass transport for reactants and by-product can't be neglected.

The inhomogeneous silver distribution achieved on micro patterned Si, produced an ordered array of Si Nanopillars.

Electroless metal deposition is a simple method used when there is not strict demand on metal positioning and morphology. In this thesis it has been demonstrated that instead it could be applied allowing high levels of selectivity.

The proposed method requires a simple lithographic step, followed by a dipping in alkaline solutions for the exposure of contiguous (100) and (111) Si surfaces. On the basis of the observed changes of the AgNPs' distribution with the scaling of the size of the exposed areas, as for the micro patterned Si, it should be possible to inhibit the silver deposition on the (111) surfaces by further reducing their extension, generating solid silicon nanostructures with high aspect ratio. These features allow the fabrication on the same silicon wafers of nanopillars with size in the range of 50nm to 1μm.

According to the data reported in the literature, the very dense SiNWs arrays with high aspect ratio show a small optical loss of the incoming light, thanks to multiple reflections. Silicon nanostructures fabricated with MAcE have received wide interest in the field of batteries because of their capability of accommodating a large volume change. This technique can be used to fabricate large area oriented SiNW p-n junction diodes starting from planar materials with a p-n junction.

So the results presented in this work could contribute to assemble the difficult but intriguing and promising scenario of Metal Assisted chemical Etching of Silicon.

• REFERENCES

[1] G. Cao, Y. Wang *Nanostructures and Nanomaterials: Synthesis, Properties and Applications,* World Scientific in Nanoscience and Nanotechnology, Vol.2, 2011;

[2] D. D. D. Ma, C. S. Lee, F. C. K. Au, S. Y. Tong, S. T. Lee, Science, 299, 1874, 2003;

[3] F. Rahman *Nanostructures in Electronics and Photonics* Pan Stanford Publishing Pte. Ltd. 2008;

[4] R. Q. Zhang, A. De Sarkar, T. A. Niehaus, T. Frauenheim Phys. Status Solidi B, 249, 401–412, 2012;

[5] J. Heitmann, F. Muller; M. Zacharias and U. Gosele Adv. Mater. 17, 2005;

[6] H. Foll, M. Christophersen, J. Carstensen, G. Hasse Materials Science and Engineering R 280 2002;

[7] M. S. Schmidt, J. Hubner, A. Boisen Adv. Mater. 24, 2012;

[8] J. L. Liu, Y. Lu, Y. Shi, S. L. Gu, R. L. Jiang, F. Wang, Y. D. Zheng Appl. Phys. A 66, 539-541 (1998);

[9] V. Schimdt, J. Wittemann; S. Senz, U. Gosele Adv. Mater. 21, Issue 25-26 pp 2681-2702, 2009;

[10] V. Sivakov , G. Andra , A. Gawlik , A. Berger , J. Plentz , F. Falk , S. H. Christiansen , Nano Lett., 9, 1549 2009;

[11] C. K. Chan , H. L. Peng , G. Liu , K. McIlwrath , X. F. Zhang , R. A. Huggins , Y. Cui , Nat. Nanotechnol. 3, 31 2008;

[12] Y. Cui , Q. Wei , H. Park , C. M. Lieber , Science, 293, 1289, 2001;

[13] H. Fang, X. Li, S. Song, Y. XU, J. Zhu, Nanotechnology 19, 255703 (2008);

[14] B. Ozdemir, M. Kulakci, R. Turan, HE Unalan, Nanotechnology **22** 155606 (2011);

[15] L. Tsakalakos, J. Balch, J. Fronheiser, B. A. Korevaar; O. Sulima, J. Rand Appl. Phys. Lett. 91, 233117 (2007);

[16] R. S. Wagner, W. C. Ellis Appl. Phys. Lett. 4, 89, 1964; 1960;

[17] X. Li, P. W. Bohn Appl. Phys. Lett. 77, 2572 (2000);

[18] J. M. Heck et al. "High Aspect Ratio Polysilicon-Germanium Microstructures" presented at Proc. 10th Int. Conf. on Solid State Sensors and Actuators, Sendai Japan 1999;

[19] Y. Yasukawa , H. Asoh , S. Ono , Electrochem. Commun., 10, 757 2008;

[20] D. Dimova Malinovska , M. Sendova Vassileva , N. Tzenov , M. Kamenova , Thin Solid Films, 297, 9 1997;

[21] J. Diaz et al. Appl. Phys. 2003, 94, 7526;

[22] T. L. Rittenhouse et al. Solid State Commun 2003, 126, 245

[23] Z. Huang, N. Geyer, P. Werner, j. de Boor, U. Gosele Adv. Mat. **23**, 285-308 (2011);

[24] M. L. Zhang, K. Q. Peng, X. Fan J. Phys. Chem. 4444-4450, 112, 2008;

[25] S. Toda, T. Oishi, T. Yoshioka, T. Okuno, Japanese journal of Applied Physics 49, 2010;

[26] S. Yae, N. Nasu, K. Matsumoto, T. Hagigara, N. Fukumuro, H. Matsuda Electrochimica Acta, 53, 35-41 (2007);

[27] G. Oskam, J. G. Long, A. Natarajan, P. C. Searson J. Phys. D: Appl. Phys. 31, 1927-1949, 1998;

[28] C. Carraro, R. Maboudian, L. Magagnin Surface Science Reports 62, 499-525, 2007;

[29] K. Peng, Y. Yan, S. Gao, J. Zhu Adv. Funct. Mater., 13, 2003;

[30] K. Peng, J. Hu, Y. Yan, Y. Wu, H. Fang, Y. Xu, S. Lee, J. Zhu Adv. Funct. Mater. 16, 387-394 2006;

[31] K. Peng, H. Fang, J. Hu, Y. Wu, J. Zhu, Y. Yan, S. Lee Chem. Eur. J. 12, 7942-7947, 2006;

[32] P.R. Brejna, P. R. Griffiths Appl. Spectrosc. 64, 493-9, 2010;
[33] H. Tong, L. Zhu, M. Li, C. Wang Electrochimica Acta 48, 2473-2477, 2003; n
[34] M. A. Lachiheb, N. Nafie, M. Bouaicha Nanoscale Res. Lett. 7, 455 (2012);
[35] X. Wan, Q. K. Wang, P. H. Wangyang J. Nanopart. Res. 14, 784, 2012;
[36] J. N. Crain, K. N. Altmann, C. Bromberger, F. Himpsel Phys. Rev, B 66, 205302, 2002;
[37] F. M. Liu, M. Green J. Mater. Chem. 14, 1526-1532, 2004;
[38] C. Ye Chun, C. MA Chuan, C. Wang, F. Zhou Trans. Nonferrous Met. Soc. China 19, 1474-1478, 2009;
[39] W. Ye, C. Shen, J. Tian, C. Wang, C. Hui, H. Gao Solid State Sciences 11, 1088-1093, (2009);
[40] T. Qiu, X. L. Wu, Y. F. Mei, P. K. Chu, G. G. Siu Appl. Phys. A 81, 669-671, 2005;
[41] K. W. Kolasinski J. Phys. Chem. C 114, 22098-22105 2010;
[42] Z. P. Huang, N. Geyer, L. F. Liu, M. Y. Li, P. Zhong Nanotech 21, 465301, 2010;
[43] K. Tsujino, M. Matsumura Electrochimica Acta 53, 28-34, 2007;
[44] K. Peng, A. Lu, R. Zhang, S. T. Lee Adv. Funct. Mater. 18, 3026-3035, 2008;
[45] Lehmann, V. Electrochemistry of Silicon: Instrumentation, Science, Materials, and Applications; Wiley-VCH: New York, 2002;
[46] N. Geyer, B. Fuhrmann, Z. Huang, J. de Boor, H. S. Leipner, P. Werner J. Phys. Chem. C, 116, 2012;
[47] C. L. Lee , K. Tsujino , Y. Kanda , S. Ikeda , M. Matsumura , J. Mater. Chem., 18, 1015 2008;
[48] S. L. Cheng , C. H. Chung , H. C. Lee , J. Electrochem. Soc. 2008, 155, D711 2008;
[49] V. A. Sivakov, G. Bronstrup, B. Pecz, A. Berger, G. Z. Radnoczi, M. Krause, S. Christiansen J. Phys. Chem. C, 114, 3798-3803, 2010;

[50] Y. QU, L. Liao, Y. Li, H. Zhang, Y. Huang, X. Duan Nano Letters, 9, 4539-4543, 2009;
[51] S. Cruz , A. Honig-dOrville , J. Muller , J. Electrochem. Soc. 2005, 152, C418
[52] C. L. Haynes, R. P. Van Duyne J. Phys. Chem. B, 105, 5599-5611, 2001;
[53] Z. P. Huang , H. Fang , J. Zhu , Adv. Mater. 2007, 19, 744;
[54] H. Masuda , K. Fukuda , Science, 268, 1466 1995;
[55] Z. P. Huang , X. X. Zhang , M. Reiche , L. F. Liu , W. Lee , T. Shimizu ,
[56] S. Senz , U. Gosele , Nano Lett. 2008, 8, 3046
[57] W. K. Choi , T. H. Liew , M. K. Dawood , Nano Lett. 2008, 8, 3799;
[58] S. W. Chang , V. P. Chuang , S. T. Boles , C. A. Ross , C. V. Thompson , Adv. Funct. Mater., 19, 2495, 2009;
[59] L. Santinacci, T. Djenizian, P. Schmuki, J. of Electrochem. Soc. 148, C640-C646, 2001;
[60] T. Homma, N. Kubo, T. Osaka Electrochimica Acta, 48, 3115-3122, 2003;
[61] Z. Chen, S. M. Lee, R. Singh J. Electrochem.Soc. 147, 3889-3891, 2000;
[62] J. Choi, Z. Chen, R. Singh J. Electrochem. Soc. 150, C563-C565 2003;
[63] A. G. Nassiopoulou, V. Gianneta, C. Katsogridakis Nanoscale Research Letters, 6, 2011;
[64] D, Graf, S. BauerMayer, A. Schnegg J. Appl. Phys. 74, 1679, 1993;
[65] A. Samavar, T. Miller, T. C. Chiang Physical Review B, 38, 14, 1988;
[66] Y. Sheng, M. Li, Z. Wang, Y. Liu Chinese J. Struct. Chem. 27, 326-334, 2008;
[67] Y. Ogata, K. Kobayashi, M. Motoyama Current Opinion in Solid State and Materials Science 10, 163-172, 2006;
[68] P. Gorostiza, J. Servat, J. R. Morante, F. Sanz Thin Solid Films 275, 12-17, 1996;
[69] V. M. Arutyunyan Sov. Phys. Usp. 32, 1989;

[70] P. M.Hoffmann, G. Oskam, P. C. Searson Journal of Applied Physics, 83, 8, 1998;
[71] R. Memming, G. Schwandt Surface Science, 5, 1, 97-110, 1966;
[72] H. Seidel, L. Csepregi, A. Heuberger, H. Baumgartel J. Electrochem. Soc. 137(11) (1990);
[73] J. Hesketh, C. Ju, S. Gowda, E. Zanoria, S. Danyluk J. Electrochem. Soc. 140, 4, 1080-1085 (1993);
[74] D. Resnik, D. Vrtacnik, S. Amon J. Micromech. Microeng. 10, 430-439 (2000);
[75] M. Sakurai, C. Thirstrup, M. Aono Phys. Rev. B, 66, 23, 16167-16174 (2000);
[76] M. J. Butcher, F. H. Jones, P. H. Beton J. Vac. Sci. Technol. B18, 2000;
[77] R. G. Mertens, R. G. Blair, K. B. Sundaram Journal of Solid State and Technology 1, P40-P45, 2012;
[78] X. G. Zhang Electrochemistry of Silicon and its Oxide Kluwer Academic (2001) p.p.55-60;
[79] T. Qiu, P. K. Chun Mater. Sci. Eng. R 61, 59-77 (2008);
[80] R. M. Stiger, S. Gorer, B. Craft, R. M. Penner Langmuir, 15 (3), 790-798 (1999);
[81] J. Sun, Y. W. Lu, X. W. Du, S. A. Kulinich Appl. Phys. Lett. 86, 17 (2005);
[82] S. W. Lim, R. T. Mo, P. A. Pianetta, C. E. Chidsey J. Electrochem. Soc. 148, C16-C20 (2001);
[83] J. Kim, H. Han, Y. H. Kim, S. Choi, J. C. Kim, W. Lee ACS Nano 5, 3222-3229, 2011;
[84] C. Chartier, S. Bastide, C. Levy-Clement Electrochimica Acta 53, 17, 5509-5516, 2008;
[85] R. L. Smith, S. D. Collins J. Appl. Phys. 71, R1, 1992;

[86] Z. Huang, T. Shimizu, S. Senz, Z. zhang, N. Geyer, U. Gosele J. Phys. Chem. C 114, 10683-10690, 2010;

[87] J. Kim, Y. H. Kim, S. H. Choi, W. Lee ACS Nano, accepted May 10, 2011;

[88] C. Lee, K. Tsujino, Y. Kanda, S. Ikeda, M. Matsumura J. Mater. Chem., 18, 1015-1020, 2008;

[89] K. Tsujimino, M. Matsumura Electrochimica Acta 53, 28-34, 2007

[90] Y.M. yang et al. Applied Surface Science, 254, 3061-3066, 2008;

[91] P. Sharma, Y. L. Wang Applied Physics Express, 4, 2011;

[92] O. J. Hildreth, W. Lin, C. P. Wong ACS Nano, 3, 12, 4033-4042, 2009;

[93] S. W. Chang, V. P. Chuang, S. T. Boles, C. V. Thompson Adv. Funct. Mater. 20, 4364-4370, 2010;

[94] H. Fang, Y. Wui, J. Zhao, J. Zhu Nanotechnology, 17, 3768, 3774, 2006;

[95] S. You, M. Choi, Aerosol Science 38, 1140-1149, 2007;

[96] R. R. Rossi, M. X. tan, N. S. Lewis Applied Physics Letters 77, 17, 2000;

[97] J. P. Sullivan, R. T. Tung, M. R. Pinto, W. R. Graham J. Appl. Phys. 70, 7403, 1991.

RINGRAZIAMENTI

Questa tesi rappresenta la conclusione del mio lungo percorso di studi e numerose sono le persone che hanno contribuito al raggiungimento di questo importante traguardo.

Un grazie di cuore va alla mia meravigliosa famiglia, a mia nonna Michela che mi ha sempre incoraggiato, a mia sorella Viviana, con con il suo appoggio mi ha aiutato a sdrammatizzare i momenti di tensione che ho vissuto, ai miei genitori, che si sono sempre prodigati senza remore per garantirmi un'istruzione, assecondando le mie inclinazioni e sopportando con amore il mio stato d'animo altanelante. Questo tesi è dedicata a loro, nella speranza di riuscire, almeno in parte, a ricompensarli per tutto quello che mi hanno dato.

La realizzazione di questo lavoro non sarebbe stata possibile senza il prezioso contributo di professionisti che si dedicano con amore al proprio lavoro e dai quali sono stata supportata.

Infiniti ringraziamenti vanno al Prof. E. Rimini per l'impegno e la dedizione con cui mi ha seguito. Spero di fare tesoro di tutti gli insegnamenti professionali e di vita che, con entusiasmo e professionalita, ha cercato di trasmettermi. Lo ringrazio anche per tutta l'attenzione rivolta all'interpretazione dei dati sperimentali.

La mia sincera gratitudine va al Dott. G. D'Arrigo. Non avrei mai raggiunto questo traguardo se, ormai tre anni fa, non mi avesse incoraggiato a concorrere per l'ammissione al corso. Desidero ringraziarlo anche per aver

condiviso con me il suo ingegno e le sue conoscenze.

Sinceri ringraziamenti vanno alla Prof. ssa Grimaldi, per il suo competente contributo all'interpretazione dei risultati sperimentali e per avermi messo a disposizione la strumentazione necessaria per eseguire gli impianti ionici e le misure RBS.

Un grazie sentito va al Dott. C. Spinella, per avermi dato la possibilità di scoprire l'affascinante mondo dell'attacco chimico assistito da metallo, per le sue delucidazioni e per avermi permesso di svolgere la mia attività all'interno dell' Istituto per la Microelettronica e i Microsistemi (IMM) di Catania da lui diretto.

Infinita gratitudine va a tutto il personale tecnico dell'IMM di Catania, ai microscopisti, S. Pannitteri, C. Bongiorno e M. Italia, al responsabile della clean room, S. Di Franco, a S. Tatì, C. Percolla e A. Marino per gli impianti.

Grazie anche a M. Torrisi di STMicroelectronics Catania per le analisi SEM.

Sentiti ringraziamenti vanno anche al Dott. F. Giannazzo, alla Dott.ssa E. Bruno, alla Dott.ssa L. Romano, al Dott. G. Nicotra, alla Dott.ssa S. Scalese, al Dott. A. Mio e alla Dott. ssa G. Impellizzeri per avermi assistito con gli impianti, le SEM, le RBS e le iniziali osservazioni in situ TEM. Grazie anche alla Dott.ssa S. Libertino per avermi messo a disposizione parte della strumentazione del suo laboratorio.

Un ringraziamento di cuore va a tutti i miei colleghi ormai amici: Alessia, Antonio, Cristina, Peppe, Rosa, Ruggero per aver condiviso con me straordinari momenti di ilarità e spensieratezza. Questi tre anni non sarebbero stati così belli se non avessi avuto loro a farmi compagnia.

Il mio affetto e la mia gratitudine sincera vanno infine alle mie amiche di sempre, Concy, Eleonora, Ilenia, Maria, Marilena, Samantha e Valeria che mi sono rimaste sempre accanto, non facendomi mancare il loro sostegno, neanche nelle condizioni più avverse.

LIST OF PUBLICATIONS AND CONFERENCES

- R. G. Milazzo, G. D'Arrigo, C. Spinella, M. G. Grimaldi, E. Rimini ***"Ag-Assisted Chemical Etching of (100) and (111) n-type Silicon Substrates by Varying the Amount of Deposited Metal"*** J. Electrochem. Soc. Volume 159, issue 9, D521-D525, 2012;

- R. G. Milazzo, G. D'Arrigo, C. Spinella, M. G. Grimaldi, E. Rimini ***"Simultaneous Formation Of Silicon Nanopillars And Nanowires By Silver Deposition And Chemical Etching"*** submitted to Journal of Electrochemical Society;

- A. M. Mio, G. D'Arrigo, R. G. Milazzo, E. Rimini, C. Spinella, L. Peto, A. Nadzeyka, S. Bauerdick **"Maskless Implants of 20keV Ga+ in Thin Crystalline Silicon on Insulator"** accepted on Journal of Applied Physics (minor revisions);

- R. G. Milazzo, G. D'Arrigo, C. Spinella, M. G. Grimaldi, E. Rimini **"Early Stages of Silver Electroless Deposition on Silicon Substrates"** submitted to Journal of Applied Physics;

- E-MRS Spring meeting 2011 Nice France 9-13 maggio 2011

Poster:

“Crystallization of Silicon Nanostructures amorphized by Ge+ ion irradiation”

R. Milazzo, G. D’Arrigo, C. Bongiorno, C. Spinella, E. Rimini.